# MANY-BODY APPROACHES
# TO QUANTUM DOT

by

PATRICK MERLOT

## *THESIS*

*for the degree of*

## *MASTER OF SCIENCE*

*(Master in Computational Physics)*



*Faculty of Mathematics and Natural Sciences*
*Department of Physics*
*University of Oslo*

*Sept. 2009*

# Acknowledgements

I would like to acknowledge the people who helped me in completing this thesis. From Sigurd for getting me started and his assistance when I was struggling with the C++ coding as well as with some abstract concepts of quantum mechanics, to Lene, Islen, Rune and Johannes for the interesting discussions we had in the office. Also, many thanks to Simen Kvaal for helping me out of some critical questions and feeding me with a lot of new ideas. Thanks again to Rune and Simen for teaching me how to use their simulators. Most importantly, thanks to Morten Hjorth-Jensen for his support all along the master, for providing this interesting topic and also for his constant good mood. Finally many thanks to Nolwenn for pushing me and helping me in any possible ways.

*"The underlying physical laws necessary for the mathematical theory of a large part of physics and the whole of chemistry are thus completely known, and the difficulty is only that the exact application of these laws leads to equations much too complicated to be soluble."*
*P. A. M. Dirac, 1929*

# Abstract

In this thesis, we studied numerically systems consisting of several interacting electrons in two-dimensions, confined to small regions between layers of semiconductors. These artificially fabricated electron systems are dubbed quantum dots in the literature. Quantum dots provide a new challenge to theoretical calculations of their properties using many-body methods. The size of these "artificial atoms" is several orders of magnitude larger than that of atoms, leading to a much greater sensitivity to magnetic fields. The full many-body problem of quantum dots is truly complex and simulating a quantum dot constrained by a magnetic field may be even more complicated.

Of particular interest is the reliability of the Hartree-Fock (HF) method for studies of quantum dots in two-dimensions as a function of the external magnetic field. In order to achieve this goal, we developed a Hartree-Fock code for electrons trapped in a single harmonic oscillator potential in two-dimensions. We also developed a code implementing many-body perturbation theory (MBPT) up to third order either directly applied to the harmonic oscillator basis or as a correction to the Hartree-Fock energy. A discussion of the results compared with large-scale diagonalisation methods indicated a quadractic error growth of HF and MBPT as the interaction strength increases. We tested also the reliability of a single Slater determinant approximation for the ground state of closed shell systems as a function of varying interaction strength. We found that the Hartree-Fock method, compared with large-scale diagonalization methods, has a limited range of applicability as function of the interaction strength and increasing number of eletrons in the dot, indicating a break of the computational technique before entering the limit of validity of the closed-shell model. Our study also showed that the HF approximation might become less accurate compared to MBPT as the number of electrons in the dot increases.

# Contents

# Chapter 1

# Introduction

Following their recent successes in describing and predicting properties of materials, electronic structure calculations using numerical computation have become increasingly important in the fields of physics and chemistry over the past decade, especially with the development of supercomputers. From the basic constituents of a system of particles and their interactions, a computational approach enables to derive the electronic structure and the properties of the system.

A system of particles that is currently considered with attention is the quantum dot: it is an artificial system consisting of several interacting electrons confined to small regions between layers of semiconductors. The whole system can be seen as a nanoscopic box of semiconductor with exceptional electrical and optical properties. Applications based on quantum dots are developed in numerous fields of medicine and modern electronics.

## Overview

This thesis describes a computional study of a quantum dot in two dimensions. It presents the methods used in numerical simulations and some many-body techniques with various levels of sophistication: Hartree-Fock method (HF), many-body perturbation theory (MBPT), variational Monte-Carlo (VMC) and full configuration interaction (FCI) (e.g. large scale diagonalisation) methods. It focuses on the restricted Hartree-Fock method, one of the fastest and cheapest techniques but also one of the less accurate. The aim of the study is to assess the appropriateness of this method to study quantum dots in two-dimensions confined by a spherical potential and squeezed by an external magnetic field.

## Literature review

Similar Hartree-Fock studies were performed by Johnson and Reina in 1992 [25] and Pfannkuche in 1993 [45].

Johnson and Reina derived an analytical expression for the exact ground state and the HF energy of a N-particle quantum dot [25]. They managed to derive it by approximating the electron interactions with a cut-off to first order of the Coulomb interaction. They found that the HF approximation becomes less accurate with an

increasing number of electrons, a decreasing magnetic field, an increasing dot size and increasing electron-electron interaction strength. Our model which includes the complete Coulomb interaction leads to the same conclusion regarding the accuracy of the Hartree-Fock method.

Pfannkuche computed the open-shell Hartree-Fock method and compared the results to exact diagonalization. They also remarked that the usefulness of the Hartree-Fock method would be greatly enhanced if its reliability was properly understood [45]. Compared to their study, our closed-shell model implementation cannot give insights on the electronic structure responsible for the inaccuracy of the correlation effects, but it gives more information about the convergence of HF.

Waltersson analysed quantum dots using open-shell Hartree-Fock and second-order perturbation theory [59]. Their results are used to validate our own implementation of the second order perturbation correction in the basis of Hartree-Fock orbitals.

Simen Kvaal developed a large-scale diagonalization code [32] for computing the approximated ground state using the full configuration interaction method. We use his results as reference for the "exact" ground state in the analysis of our results. We also use his simulator to validate the two-body interaction matrix in the harmonic oscillator basis.

Rune Albrigtsen studied quantum dots using closed-shell variational Monte-Carlo (VMC) method [2]. His simulator is used for few configurations to compare the accuracy against HF and MBPT.

## A guide to the reader

This thesis is organized as follows.

Chapter 2 gives a general presentation of the quantum dot and of computational studies.

Chapter 3 describes the phenomenological aspects and properties of quantum dots.

Chapter 4 reviews some models for the quantum dot and introduces the theoretical approximations used in this thesis: the electrons are trapped in a single harmonic oscillator potential and repel each other according to the bare Coulomb interaction.

When it comes to the treatment of the quantum dot model for numerical simulation, chapter 5 introduces some possible many-body techniques, and more particularly the Hartree-Fock theory. The iterative procedure is reviewed and its description is adapted to our implementation.

Chapter 6 describes our computational implementation of the Hartree-Fock method in two-dimensions for closed shell systems. We also describe the implementation of the many-body perturbation corrections up to third order both as an improvement of the Hartree-Fock energy or as an independent technique.

Results are provided in chapter 7 and compared to large-scale diagonalization. A numerical analysis provides information on the convergence, on the stability and on the efficiency of the Hartree-Fock method and the many-body perturbation theory. We test the reliability of a single Slater determinant approximation for the ground

state of closed shell systems as function of the interaction strength (7.2.1). A discussion of the results (7.3) shows that the complexity of the Hartree-Fock method grows exponentially with the size of the basis set and that parallelization improves the efficiency almost linearly with respect to the number of processors (7.4). When compared to large-scale diagonalisation taken as reference, we observed a quadractic error growth of HF and MBPT as the interaction strength increases (7.3.1). We find that the Hartree-Fock method, compared with large-scale diagonalization methods, has a limited range of applicability as function of the interaction strength and increasing number of electrons in the dot, indicating a breakdown of the validity of the ansatz for the ground state wave function used in the Hartree-Fock calculations. In our case this ansatz is based on a single Slater determinant constructed by filling all single-particle levels below the chosen Fermi surface, the so-called closed-shell approach. Our study also shows that the HF approximation becomes less accurate compared to MBPT as the number of electrons in the dot increases (7.5.2). Concluding remarks and suggestions for future work are given in the chapter 8.

# Chapter 2

# General presentation

In our current understanding of nanotechnology, quantum dots are the most functional and reproducible nanostructures available to researchers. Common shapes include pyramids, cylinders, lens shapes, and spheres. Different synthesis routes create different kinds of quantum dots. They are very small by nature, the smallest objects that we can synthesize on the nanoscale. From this fact, they are assimilated to dots, though one quantum dot can be made out of roughly thousands of atoms. All the atoms pool their electrons to "sing with one voice", that is, the electrons are shared and coordinated as if there was only one atomic nucleus setting up an attraction at the centre. That property enables numerous revolutionary schemes for electronic devices and quantum dots are often referred to as artificial atoms.

Depending on its application, the total diameter of a quantum dot varies between 2-10 nm, corresponding to 10-50 atoms, to sizes of hundreds of nanometers that can contain a total of $100 - 100,000$ atoms within the quantum dot volume [46], with an equivalent number of electrons. Almost all electrons are tightly bound to the nuclei of these atoms, however the number of "free electrons" in the dot can be very small: between one and a few hundreds [1]. The reason why 'quantum' prefixes the name is because the dots exhibit quantum confinement properties in all three dimensions. This means that electrons within the dot cannot move freely around in any direction leading to quantization as we will show in 3. The only thing that behaves like this in nature is the atom. Compared to an atom, a quantum dot is at least ten times bigger and above all tunable. This has a lot of important consequences for researchers. For example they exhibit quantized energy levels like an atom. For a given energy of excitation, for instance, a quantum dot will only emit specific spectra of light. Quantum theory predicts that if their diameter is decreased there will be a corresponding increase in frequency (e.g. in energy) of the emitted light, and this property is now used in many applications.

This element of control over quantum dots' emission properties has huge implications for both electronic devices and medical applications. Due to their excellent confinement properties not seen in nanowires or quantum wells, quantum dots are extremely efficient at emitting light. They have been the source of some of the world's most powerful lasers produced to date, though the practicality of a quantum dot laser is still being improved. In medical studies, quantum dots are already used as

tags that can be inserted into patients. These tags can be seen under most medical scanning technologies and can help pinpoint biological processes as they occur.

## 2.1 History of Quantum Dots

In the late 50's began the first studies of artificial quantum systems, mostly theoretical due to the lack of funds. In the 60's, the technique of epitaxial depositions was developed and with it, the possibility to build ultra-clean composite layers of semiconductor material sandwiched between two other layers of another semiconductor. The first optical properties were discovered and the two-dimensional character of the sample was observed. At the beginning of the 80's, rapid progress in technology was made with accurate lithography technics (the first quasi one-dimensional quantum wire was done based on these advances) [20].

Colloïdal quantum dots were discovered in 1981, during the development of materials for the photo-cleavage of water. Bulk cadmium sulfide (CdS) is known to be an ideal electrode material; however it experiences photocorrosion upon irradiation. It was believed that colloidal particles of cadmium sulfide, coated with a protective agent (i.e. $RuO_2$), would be more resistant to corrosion. Therefore, a synthesis method was developed to produce colloidal CdS through aqueous precipitation. The resulting particles displayed unique properties not found in the bulk, including fluorescent emission. These properties were determined to be the result of quantum size effects [26], and were found to be tunable by altering the size of the particle [50]. This provided a method for selecting excitation and emission wavelengths and particle band gaps.

In the middle of the 80's, the first quantum dot based on etching techniques was developed [Reed et al.;1986]. As a consequence, a complete quantization of the electron free motion was possible.

At the end of the 80's and in the 90's, the methods evolved: lithography and etching are still in use, but electron or ion-lithography have replaced light-lithography resulting in an increased precision [20].

Lent predicted in 1993 the need for building quantum cellular automata (QCA) cells of 2 nm in order to work at room temperature, where quantum cellular automata refers to any models of quantum computation.

"Ultimately, temperature effects are the principal problem to be overcome in physically realizing the QCA computing paradigm. The critical energy is the energy difference between the ground state and the first excited state of the array. If this is sufficiently large compared with $k_B T$, the system will be reliably in the ground state after a characteristic relaxation time. Fortunately, this energy difference increases quadratically as the cell dimensions shrink. If the cell size could be made a few Ångstroms, the energy differences would be comparable to atomic energy levels (i.e. several electron-Volts!)".

"As technology advances to smaller and smaller dimensions on the few-nanometer scale, the temperature of operation will be allowed to increase. Perhaps our envisioned QCA will find its first room temperature implementation in molecular elec-
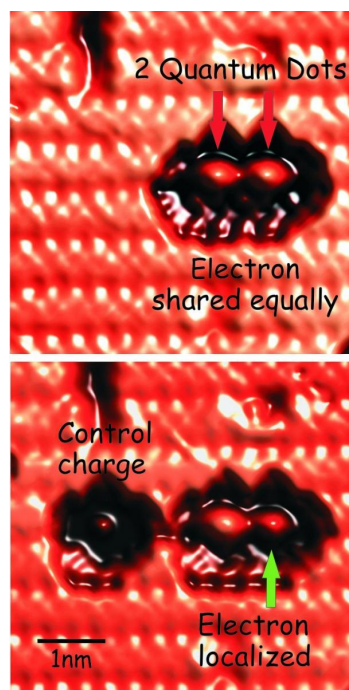
**Figure 2.1:** Two coupled atomic quantum dots are shown in this room temperature scanning tunneling microscopy image. In the top frame the dots share one electron. The electron moves freely between the dots just like an electron in a chemical bond within a molecule. The lower frame demonstrates control over that single electron and the potential to do computations in a new way. The electric field from the control charge pushes the electron to prefer staying on only one of the quantum dots. (Image courtesy of University of Alberta/Prof. Robert A. Wolkow)

tronics." [35]

Interest in the use of quantum dots in biomedicine began in 1998. Coupling the quantum dots directly to biorecognition molecules (e.g. antibodies, proteins), the particles could be targeted to particular parts of the cell, producing a fluorescent indicator [7, 8].

Early this year (Jan. 2009), the four-quantum dot cell dreamed by Lent to build his "quantum cellular automata" as a replacement for classical computation using *CMOS* technology has been achieved with the fabrication and control of a 1 nm-scale assembly of a four coupled silicon dangling bond (In condensed matter physics, a dangling bond occurs when an atom is missing a neighbour to which it would be able to bind. Such dangling bonds are defects that disrupt the flow of electrons and that are able to collect the electrons). Indeed single-atom quantum dots make possible a new level of control over individual electrons, a development that suddenly brings quantum dot-based devices within reach [17]. Composed of a single atom of silicon and measuring less than one nanometre in diameter, these are the smallest quantum dots ever created. Until now, quantum dots have been useable only at impractically low temperatures, but the new atom-sized quantum dots work at room temperature. And because they operate at room temperature and exist on the familiar silicon crystals used in today's computers, researchers expect these single atom quantum dots to transform theoretical plans into real devices. Figure 2.1 shows how atom-sized quantum dots can be manipulated at room temperature. The single-atom quantum dots have also demonstrated another advantage: significant control over individual electrons by using very little energy. This low energy control is seen as the key to quantum dot application in entirely new forms of silicon-based electronic devices, such as ultra low power computers.

## 2.2   Some applications of QD

Exceptional electrical and optical properties make quantum dots attractive components for integration into electronic devices. One significant asset of quantum dots over traditional optoelectronic materials is that they exist in the solid state. Solids tend to be more compact, easily cooled, and allow for direct charge injection. Additionally, quantum dots can interconvert light and electricity in a tunable manner dependent on crystal size, allowing for easy wavelength selection. This is a significant improvement over silicon-based materials, which require modification of their chemical composition (i.e. doping) to alter optical properties [60]. As a result researchers have experimented with quantum dots in lasers, LEDS, photovoltaics and also for new generations of transistors, prototypes of spin devices, logic gates with quantum computers as the ultimate goal. Most of these applications are still in early development; however the benefits of quantum dot components are evident, and could lead to a complete revolution of the way of building electronic components at atomic scale.

Another application of quantum dots and one of the fastest moving and most exciting interfaces of nanotechnology is the use of (colloïdal) quantum dots in biology. Again their unique optical properties make them appealing as *in vitro* and *in vivo* fluorophores in a variety of biological investigations, in which traditional fluorescent labels based on organic molecules fall short of providing long-term stability and simultaneous detection of multiple signals [39]. The ability to make quantum dots water soluble and target them to specific biomolecules has led to promising applications in cellular labelling, thus improving diagnostic methods (ex. tracking cancer cells *in vivo* during metastasis [15, 23, 58], as shown in figure 2.2) and in developing better drug delivery systems to improve disease therapy [29]. It is even currently studied as neuroelectronic interface for converting optical energy into electrical signal responding to the need for prosthetic devices that can repair or replace nerve function [63]. However there are still many open questions about the toxicity of inorganic QD. The size and charge of most nanoparticles preclude their efficient clearance from the body as intact nanoparticles. Without such clearance or their biodegradation into biologically benign components, toxicity is potentially amplified and radiological imaging is hindered. Some neutral organic coatings prevents adsorption of serum proteins (which otherwise increase the total diameter by more than $15nm$ and prevent renal clearance). A final hydrodynamic diameter of less than $5.5nm$ resulted in rapid and efficient urinary excretion and elimination of quantum dots from the body [52].

These achievements, even in their premises, have laid the **foundations for theoretical investigations** to enable advances in the understanding of the fundamental structure, stability and aqueous assembly of nanoparticle architectures. A physical systems consisting of between $10s - 1000s$ of atoms is already too complex to be studied otherwise than using numerical methods for a reliable description. The concept of artificial atom can even be generalized to artificial molecules.

Moreover QDs appear as good tools for studying atomic spectra of many-body systems on a theoretical point of view using computational techniques. Thanks to the possibility to build our own artificial atoms without considering the complexity
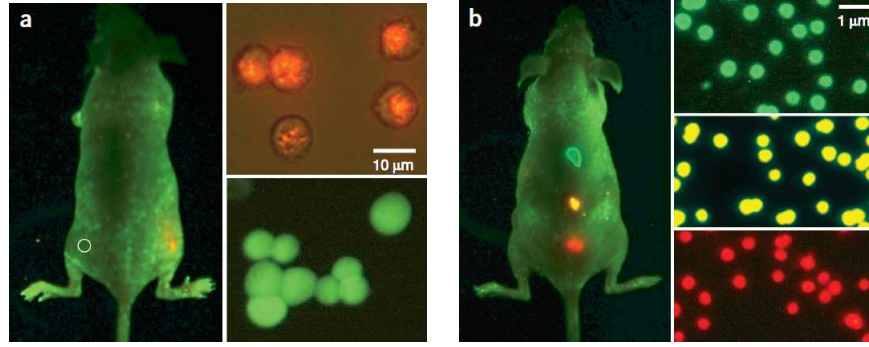
**Figure 2.2:** Sensitivity and multicolor capability of quantum dot (QD) imaging in live animals compared to classical organic fluorescent dyes.
(a) About a thousand QD-tagged cancers cells (orange,upper) and organic fluorescent dye (green, lower). (b) Simultaneous *in vivo* imaging of multicolor QD-encoded microbeads. Approximately 1-2 millions beads in each color were injected subcutaneously at three adjacent locations on a host animal (Image courtesy of X. Gao [15]).

of the nucleus, it becomes simpler to confront numerical and experimental results.

## 2.3 Clarifications about computational studies

The usefulness of numerical simulation is more and more recognized and today it is used in many domains of research and development: mechanics, fluid mechanics, solid state physics, astrophysics, nuclear physics, climatology, quantum mechanics, biology, chemistry... More than being limited to scientific subjects numerical simulation is also used in human sciences (demography, sociology) as well as in finance or economy.

In physics, beside the importance for our basic understanding of quantal systems, the capability to develop and study stable numerical quantum mechanical systems with many degrees of freedom is of great importance, as analytic solutions are rare or impossible to obtain.

Some definitions:

A numerical simulation reproduces the fundamental behaviour of a complex system in order to study its properties and predict its evolution. It is based on the implementation of theoretical models, i.e. it is an adaptation of mathematical models to numerical tools. Data mining and virtual reality are different from numerical simulation and should not be mistaken with it.

A numerical simulation is performed in several steps:

*The model* describes the system analysed by listing its essential parameters and by writing the physical laws that rule its behaviour (and link the parameters) as mathematical equations.

*The simulation* itself is the translation of the equations into computer language, associated with the discretization of the physical domain to make it finite (select a time step, a finite number of points, an acceptable level of accuracy, etc).

*Computational techniques* The resolution of the equations leads to the determination of the numerical values of all the parameters of the system in every points, i.e. the state of the system is known. Various computational techniques can be used to solve the equations, they can be grouped into two main approaches: the deterministic and the statistical (or probabilistic) methods.

In the first approach, an algorithm will solve predictably the equations. For example the object (or the domain) is discretized and the parameters of each element are linked to its neighbours through algebraic equations. It is up to the computer to solve the system that links all the equations. A deterministic method will always produce the same output when given the same input, and the underlying machine will always go through the same sequence of states (which is why it is called "deterministic"). The Hartree-Fock method used in this thesis belongs to this category as well as the Finite element method or the large scale diagonalisation.

The second approach, which groups the "Monte-Carlo" methods, is particularly suited to phenomena characterized by a sequence of steps in which each element of the object can be affected by different "a priori" possible events. From step to step, the evolution of the sample will be determined through a random draw (the name of the method comes from this idea).

*Validation of the results:* the theoretical model and its translation into computer programming must be validated by comparing with experimental data, or by testing a very simple case for which an analytical solution can be found.

Numerical simulations, once validated, can explore more cases or unused configurations that were not tested by experiments, sometimes predicting unexpected behaviours, leading to a greater knowledge of the physical behaviour of the system. Therefore numerical simulation is the third form of study of phenomena, after theory and experiment.

# Chapter 3

# Physics of Quantum Dots: the artificial atoms

As described previously, a quantum dot is a semiconductor whose charge-carriers are confined in all three spatial dimensions, so much confined that quantum effects become visible in many ways: fluorescent effect, quantized conductance, quantized energy spectrum, etc.

The physics behind it involves the electronic structure of the material (here mainly semiconductors) and some basic quantum mechanical effects such as size quantization, quantum tunneling or Coulomb blockade.

This chapter reviews the basic quantum mechanical effects that explain the properties of quantum dots. First it explains what size quantization is and how it happens for a confined particle. Then it presents the properties of semiconductors and the specific features of semiconductors quantum dots, and how it enables the size quantization to occur at larger scale. It then explains the consequences of size quantization on the optical and electronic properties of quantum dots. Finally, it presents the quantum dots in a magnetic field.

## 3.1 Size quantization

Before applying quantum theory to quantum dots, we will explain how quantization arises and why it is not always noticeable in everyday life.

*The particle in a box*  We consider the well-known example of a particle in a one-dimensional box of size $a$ trapped by an infinite potential (see figure 3.1a). The potential $V(x)$ is given below:

$$V(x) = 0, \qquad for \ 0 < x < a,$$
$$V(x) = \infty, \qquad for \ x \leq 0, x \geq a. \tag{3.1}$$

How do these boundary conditions affect the particle? Due to the wave-particle

duality we can write the time-independent Schrödinger equation for this system:

$$\frac{d^2\Psi(x)}{dx^2} = \frac{2m}{\hbar^2}\left[V(x) - E\right]\Psi(x). \tag{3.2}$$

If we write the solutions of the Schrödinger equation under the form $\Psi(x) = Asin(kx) + Bcos(kx)$, we can find the constants A and B by using the boundary conditions: at the boundaries of the box $\Psi$ is null ie $\Psi(0) = \Psi(a) = 0$

$$\Psi(0) = 0 + B = 0, \tag{3.3}$$
$$\Psi(a) = Asin(ka) = 0,$$

This can only be satisfied by $B = 0$ and if either $A = 0$ or if $ka = n\pi$. Setting $A = 0$ would mean that the wave function is always zero, which is unacceptable, we conclude that:

$$\Psi_n(x) = Asin(\frac{n\pi x}{a}), \qquad for\ n = 1, 2, 3, 4, \dots \tag{3.4}$$

The constant $A$ can be determined by normalization, by saying that $\Psi_n(x)^*\Psi_n(x)dx$ is the probability density, ie the probability of finding the particle in the interval of width $dx$ centered on $x$. The probability density at any given point is shown in figure 3.1c. Because the probability of finding the particle somewhere in the entire interval $[0, a]$ is one,

$$\int_0^a \Psi_n(x)^*\Psi_n(x) = 1.$$

From that we obtain the normalized eigenfunctions plotted in figure 3.1b

$$\Psi_n(x) = \sqrt{\frac{2}{a}}\, sin\left(\frac{n\pi x}{a}\right). \tag{3.5}$$

Now that we have the eigenfunctions, we can re-introduce them into the Schrödinger equation to find the eigenvalues (i.e. eigen-energies of the system):

$$E_n\Psi_n(x) = -\frac{\hbar^2}{2m}\frac{d^2\Psi_n(x)}{dx^2} \tag{3.6}$$

$$= \frac{\hbar^2}{2m}\left(\frac{n\pi}{a}\right)^2\sqrt{\frac{2}{a}}\, sin\left(\frac{n\pi x}{a}\right). \tag{3.7}$$

It leads to the following expression for the eigenvalues, which are also the possible energies of the system:

$$E_n = \frac{\hbar^2}{2m}\left(\frac{n\pi}{a}\right)^2 = \frac{\hbar^2 n^2}{8ma^2}, \qquad for\ n = 1, 2, 3, \dots \tag{3.8}$$

Compared to a free particle, we see that the energy for a particle in a box is discrete: this is called quantization and the integer $n$ is a quantum number. Another important result of the calculation is that the lowest energy allowed is greater than zero. The particle has a non zero minimum energy compared to a free particle, known as a zero point energy.

**(a)** The potential



**(b)** First eigenfunctions



**(c)** Probability densities
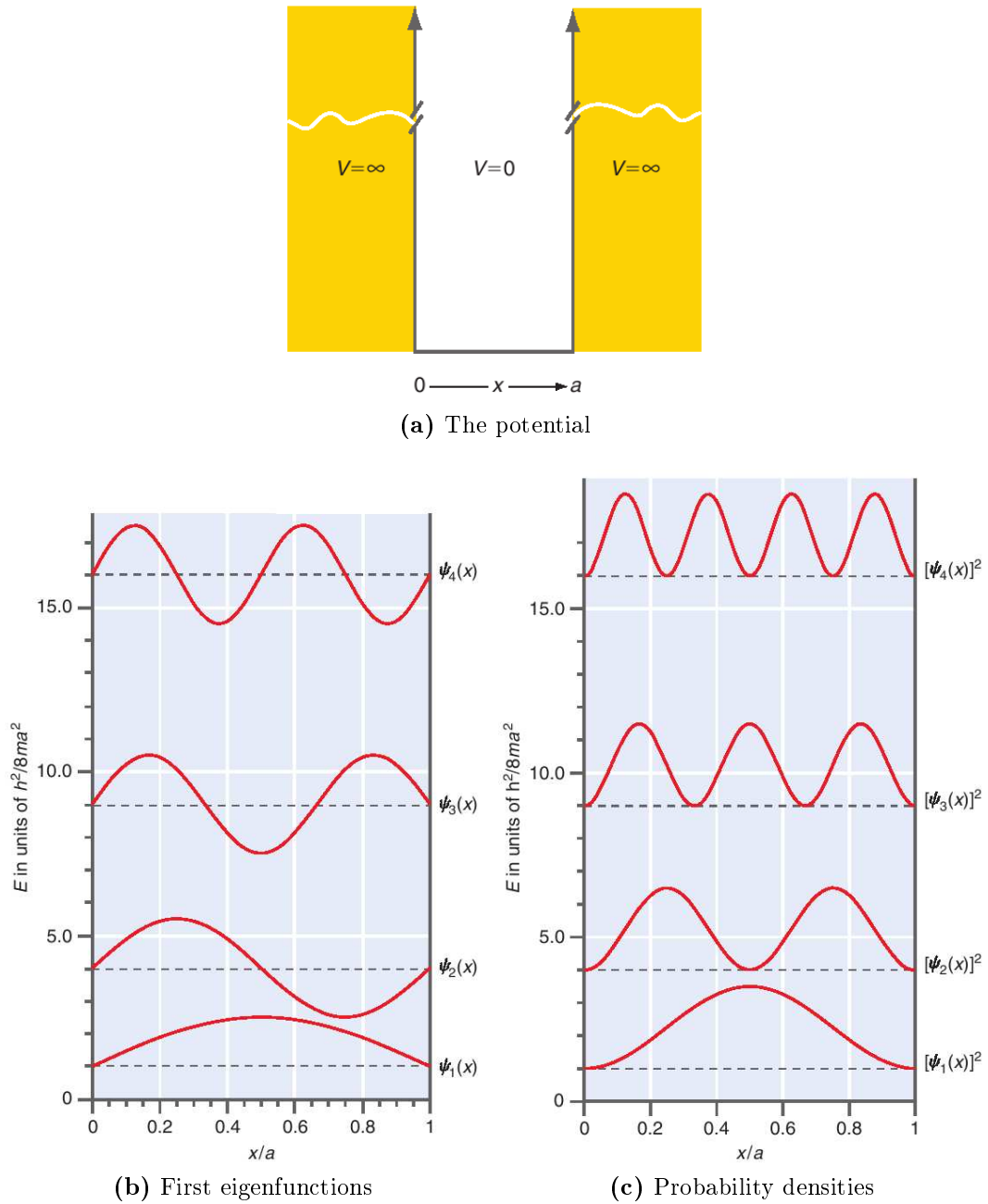
**Figure 3.1:** (a) The potential described by equation (3.1). As the particle is confined to the range $0 \leq x \leq a$, we say that it is confined to a one-dimensional box.
(b) The first few eigenfunctions for the particle in a box are shown together with the corresponding energy eigenvalues. The energy scale is shown on the right with the zero for each level indicated by the dashed line.
(c) The square of the magnitude of the wavefunction, or probability density, is shown as a function of distance together with the corresponding energy eigenvalues. The energy scale is shown on the left. The square of the wave function amplitude is shown on the right with the zero for each level indicated by the dashed line.

Therefore quantization is simply a result of the confinement of the particle and provides new properties to the particle. By making the box size $a$ tend to infinity, the confinement condition is removed and the discrete energy spectrum becomes continous in this limit. More generally, it means that any particle trapped with some boundaries will experience quantization effect, like the particles trapped in the quantum dots.

One way to see quantization effects is to look for observables. The total energy is one example of an observable that can be calculated once the eigenfunctions of the time-independent Schrödinger equation are known. Another observable that comes directly from solving this equation is the probability density, which is the quantum mechanical analogue of position.

*Observation of size quantization depending on temperature*  What is the limit size of the confinement so that such quantization effects are observable at our scale? We consider for example that the particle is an electron trapped in a box. The answer will come from the very small constants we have from the Schrödinger equation: the reduced Planck constant $\hbar = h/\pi = 1.05 \times 10^{-34}$ *J.s* $(kg.m^2.s^{-1})$ and the mass of the electron $m = 9.11 \times 10^{-16}$ *kg*. To be noticeable, the energy should be much greater than the thermal energy which is in the order of magnitude of $k_B T$, where $k_B = 1.38 \times 10^{-34}$ *J.K*$^{-1}$ is the Boltzmann constant and $T$ the temperature, otherwise thermal fluctuations will disturb the motion of electrons and will smear out the quantization effects.

At room temperature (i.e. 20°C $\simeq$ 293K), $k_B T \simeq 4.045 \times 10^{-21}$ *J*. The gap between the first two energy levels should be greater than this value:

$$\Delta E = E_2 - E_1 = \frac{3\hbar^2}{8ma^2} = \frac{4.54 \times 10^{-54}}{a^2} \gtrsim k_B T, \qquad (3.9)$$
$$\Rightarrow a \lesssim 1.06 \times 10^{-11} m = 0.0106. \ nm$$

At dilution refrigerator temperatures (i.e. $\sim 100 \ mK$), $k_B T \simeq 1.380 \times 10^{-35}$ *J*. The gap between the first two energy levels doesn't need to be so big this time:

$$\Delta E = E_2 - E_1 = \frac{3\hbar^2}{8ma^2} = \frac{4.54 \times 10^{-54}}{a^2} \gtrsim k_B T, \qquad (3.10)$$
$$\Rightarrow a \lesssim 5.734 \times 10^{-10} m = 0.573 \ nm.$$

We notice here that it is impossible to observe quantum effect with such a "free electron" at room temperature, since the box should be roughly the size of an atom, but it could be done at very low temperature.

We could therefore deduce the same for quantum dots, that are made of one or several electrons confined in a semiconductor. From what we saw above it is not possible to create a quantum dot small enough to observe size quantization at room temperature. However we will see in the following section that the mass of the charge carriers, which influences the limit size of the confinement, is not the same when the material is a semiconductor.
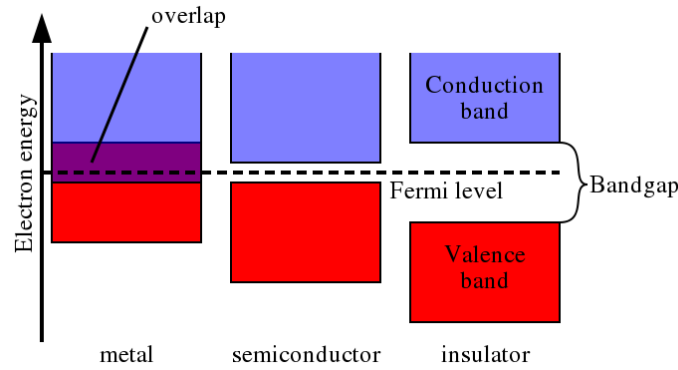
**Figure 3.2:** Simplified diagram of the electronic band structure of metals, semiconductors and insulators. (Image courtesy of P. Kuiper)

## 3.2  Quantum dots made of semiconductors

A semiconductor is a material that has a resistivity value between that of a conductor and an insulator. The conductivity of a semiconductor material can be varied under an external electrical field.

Most semiconductors on the market are made of silicon (Si). Dozens of other materials are used like germanium (Ge) or gallium arsenide (GaAs). Semiconductor materials are the basic constituants of modern electronic devices (radio, computers, telephones, and many others). Semiconductor devices include the transistor, solar cells, many kinds of diodes including the light-emitting diode, the silicon controlled rectifier, and digital and analog integrated circuits. Solar photovoltaic panels are large semiconductor devices that directly convert light energy into electrical energy.

*Energy bands in semiconductors*   In a metallic conductor, current is carried by the flow of electrons, but in semiconductors, current can be carried either by the flow of electrons or by the flow of positively-charged "holes" in the electron structure of the material. As shown in the previous section 3.1 electrons trapped in matter will experience discretized energies. However compared to the particle in a box, electrons in semiconductors as in other solids will not have narrow discrete energy levels but tickher allowed bands of energy separated by forbidden gaps between them. Therefore electrons trapped in matter can have energies only within certain **energy bands**; the lowest energy is the **ground state**, corresponding to electrons tightly bound to the atomic nuclei of the material, and the highest energy is the free electron energy, which is the energy required for an electron to escape entirely from the material. The energy bands each correspond to a large number of discrete quantum states of the electrons. Most of the states with low energy (closer to the nucleus) are full, up to a particular band called the **valence band**. Semiconductors and insulators are different from metals because the valence band in the semiconductor materials is very nearly full under usual operating conditions, thus causing more electrons to be available in the **conduction band**, which is the band immediately above the valence band as shown in figure 3.2. The ease with which electrons in a

semiconductor can be excited from the valence band to the conduction band depends on the band gap between the bands, and it is the size of this energy bandgap that serves as an arbitrary dividing line between semiconductors and insulators.

In the picture of delocalized states, for example in one dimension that is in a wire, for every energy band there is a state with electrons flowing in one direction and one state for the electrons flowing in the other. For a net current to flow, electrons must occupy more states corresponding to the flow in one direction than they occupy states for the flow in the other direction, and for this they need energy. For a metal this can be a very small energy. In the semiconductor the next higher states lie above the band gap. However, as the temperature of a semiconductor rises above absolute zero, there is more energy in the semiconductor to spend on lattice vibration and on lifting some electrons into an energy states of the conduction band. The current-carrying electrons in the conduction band are known as "**free electrons**", although they are often simply called "electrons" if context allows this usage to be clear.

Electrons excited to the conduction band leave behind electron holes, or unoccupied states in the valence band. Both the conduction band electrons and the valence band holes (**excitons**) contribute to electrical conductivity. The holes themselves don't actually move, but a neighboring electron can move to fill the hole, leaving a hole at the place it has just come from, and in this way the holes appear to move, and the holes behave as if they were actual positively charged particles.

One covalent bond between neighboring atoms in the solid is ten times stronger than the binding of the single electron to the atom, so freeing the electron does not imply destruction of the crystal structure.

In semiconductors, the dielectric constant is generally large, and as a result, screening tends to reduce the Coulomb interaction between electrons and holes. The result is a Mott-Wannier exciton, which has a radius much larger than the lattice spacing. As a result, the effect of the lattice potential can be incorporated into the **effective masses** of the electron and hole (see table 3.1 for typical values), and because of the lower masses and the screened Coulomb interaction, the binding energy is usually much less than a hydrogen atom, typically the order of 0.1 *eV* (Wannier excitons are found in semiconductor crystals with small energy gaps and high dielectric constant).

In quantum mechanics, the positions of electrons and holes are described as wavefunctions or probability distributions. The exciton has a certain size, determined by the combined probability distribution functions, and if this size exceeds the particle diameter, quantum confinement occurs. The size limit for quantum confinement can be approximated from the modified version of the De Broglie wavelength equation considering its effective mass $m^*$:

$$\lambda_B = \frac{h}{p} = \frac{\hbar}{m^*\omega}, \tag{3.11}$$

where $\lambda_B$ is the de Broglie wavelength (the wavelength associated to a particle with momentum $p$), $\hbar$ the reduced Planck constant and $\omega$ the angular frequency of the particle.

Nanocrystals contain much fewer atoms than the bulk, therefore charge screening effects are reduced. The effective mass declines and the de Broglie wavelength can

| Semiconductor material | $\epsilon_r$ | $m_e^*$ | $m_h^*$ |
|---|---|---|---|
| (Free electron mass $m_e = 9.11 \times 10^{-16}\ kg$) | | | |
| (Dielectric constant of vaccuum $\epsilon_0 \simeq 8.854 \times 10^{-12}\ A^2s^4kg^{-1}m^{-3}$) | | | |
| Silicon (Si) (4.2 $K$) | 11.7 | 1.08 $m_e$ | 0.56 $m_e$ |
| Germanium (Ge) | 16.4 | 0.55 $m_e$ | 0.37 $m_e$ |
| Gallium arsenide (GaAs) | $11.1 - 12.4$ | 0.067 $m_e$ | 0.45 $m_e$ |
| Indium antimonide (InSb) | 15.9 (at $77K$) | 0.013 $m_e$ | 0.6 $m_e$ |
| Zinc oxide (ZnO) | $-$ | 0.19 $m_e$ | 1.21 $m_e$ |
| Zinc selenide (ZnSe) | $-$ | 0.17 $m_e$ | 1.44 $m_e$ |

**Table 3.1:** Relative dielectric constant ($\epsilon_r$) measured at $290K$ [62] and effective mass of charge-carriers for some common semiconductors [18], $m_e^*$ and $m_h^*$ respectively for the electron and hole effective mass

become extremely large, up to several nanometers and make the nanocrystal excited with much less energy than an atom. For cadmium sulfide (CdS) and cadmium telluride (CdTe), these wavelengths are 5.5 $nm$ and 7.5 $nm$ [63]. For particles that are confined within sizes smaller than this wavelength, the excitons "feel" restricted. Thus the nanocrystal will display a band gap and associated (optical and electrical) quantum effects inversely proportional to its size.

*Energy spectrum of semiconductor quantum dots* An additional feature to the transition from bulk crystals to nanocrystals is a radical change in the energy spectrum of the free carriers. It changes when the diameter $d$ of the crystal becomes comparable to the de Broglie wavelength of electrons in the crystal. Motion in the direction accross the nanocrystal can be assumed bounded, and the energy spectrum in this direction becomes discrete.

Figure 3.3 illustrates the different energy spectra of bulk materials, molecules and quantum dots.

Bulk semiconductor materials are characterized by bands of allowed potential energy values. For an electron to be excited, it must absorb an energy higher than the band gap. Any value greater than the band gap will produce an excited state.

When we examine a system consisting of only two atoms, the molecular orbitals formed create discrete potential energy states. Electrons will only be excited if the energy absorbed corresponds to specific discrete quantities. Other values are not permitted and will not produce excited states.

Quantum Dots are an intermediate between discrete and continuous energy levels. As the number of atoms in the particle is reduced, the energy bands split and shrink but not to the point of being exactly discrete. Thus electrons in quantum dots may be excited by energies in discrete intervals.
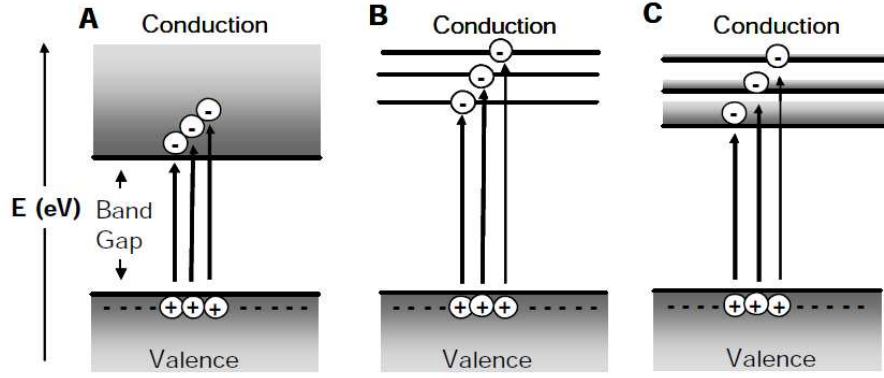
**Figure 3.3:** Possible energy states as a function of the particle size.
(**A**) **Bulk materials** have continuous energy bands and absorb energy at a value greater than the band gap. (**B**) **Molecular materials** possess discrete energy levels and only absorb energy with certain values. Moreover the band gap is greater than the one of a bulk material as a result of shrinking and splitting of the energy bands. (**C**) **Quantum dots** lie between the extremes (A,B). They possess discrete energy bands and absorb energy in discrete intervals. The band gap is between the one of bulk material and the one of a molecular material. (Image courtesy of J. Winter [63])

## 3.3   Optical properties

A lot of applications rely on the optical properties of quantum dots which result from quantum confinement.

The electrical and optical energy of the band gap are equivalent through the following conversion:

$$\Delta E = \hbar\omega = \frac{hc}{\lambda}, \tag{3.12}$$

where $\Delta E$ is the band gap difference (figure 3.4), $\hbar$ is the reduced Planck's constant, $c$ is the speed of light, $\lambda$ and $\omega$ respectively the wavelength and the angular frequency of the incident light. Thus the energy difference of the band gap is inversely proportional to the wavelength of the incident light. Nanoparticles will only absorb light of wavelengths shorter than the one determined by the band gap value.

For example, CdS (bulk) has a band gap of 2.42 $eV$, which corresponds to a wavelength of 512 $nm$. So CdS (bulk) begins to absorb light at 512 $nm$ and absorbs continuously into the UV (e.g. shorter wavelengths/higher energies). As particle size declines, the band gap increases and the absorbance starts at shorter wavelengths (Figure 3.4).

The influence of particle size on optical properties is not limited to absorbance. Particle fluorescence is also a function of the band gap. After an electron is excited, some of its energy is lost to atomic vibrations, satisfying the second law of thermodynamics. Typically, this energy is converted to heat. When the electron decays into the ground state it will emit light at a longer wavelength because of this energy loss (Figure 3.5a). As the band gap decreases, a smaller amount of energy is dissipated through fluorescent emission to return to the ground state, and the
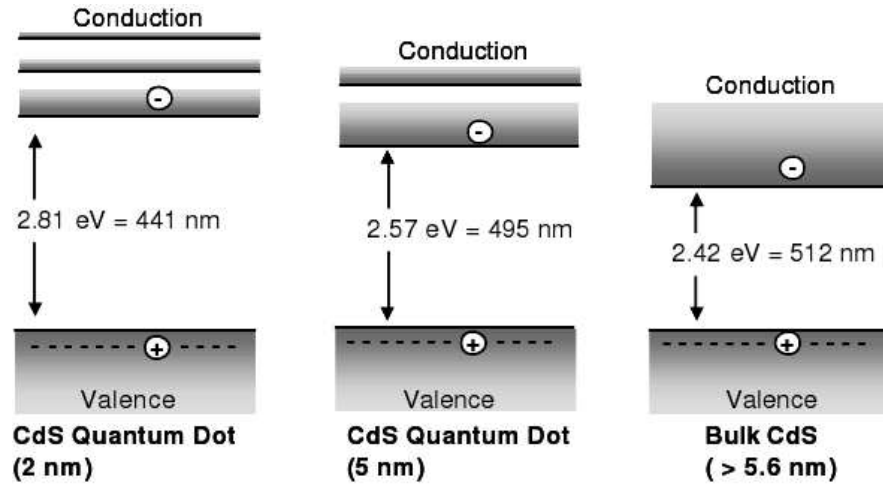
**Figure 3.4:** Band gap energy and optical absorption as a function of the crystal size. The band gap (eV) increases with decreasing nanoparticle size. Band gap is inversely related to the start in absorbance ($\lambda$) through the relationship $E = hc/\lambda$. Therefore smaller particles begin to absorb at shorter wavelengths [61] (Image courtesy of J. Winter [63]).

wavelength of emitted light will shift to the red (Figure 3.5b). Because the band gap is inversely proportional to nanocrystal size, larger nanocrystals display red-shifted emission. Additionally, the energy lost to heat decreases in a size-dependent manner. Figure 3.6 presents the emission spectra of quantum dots made from different materials and compare it to the visible wavelengths.

## 3.4  Electronic properties/Manipulation of quantum dots

*Electron-transfer between materials*   Quantum confinement also affects the electrical properties of nanocrystals. Since gap energies are size dependent, electrical properties that depend on this difference will display size dependence as well. One such property is electron transfer. Electrons with no additional energy added prefer to move to lower energy states within a given material. Because there are no energy states in the band gap, the electron will decay until it reaches the lowest state in the conduction band, and then return to the valence band through another mechanism (i.e. electron-hole recombination, non-radiative energy loss, etc). However, if the electron encounters a material with lower available energy states (i.e. lower conduction band), it can transfer its electron to that material (Figure 3.7). This process is dependent on the band gap. As the band gap increases, excited electrons occupy higher energy levels, and can decay to a greater number of lower state values. As a result of size-tunable band gaps within the quantum dot, electron transfer can be optimized to many materials.

*Single electron transport in quantum dots: Single-electron tunneling and Coulomb blockade*   Electron transport through a quantum dot is studied by connecting the
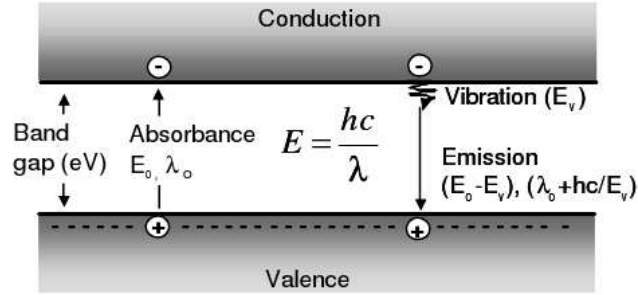
**(a)** Fluorescence and red-shift of $\lambda$ due to energy loss.
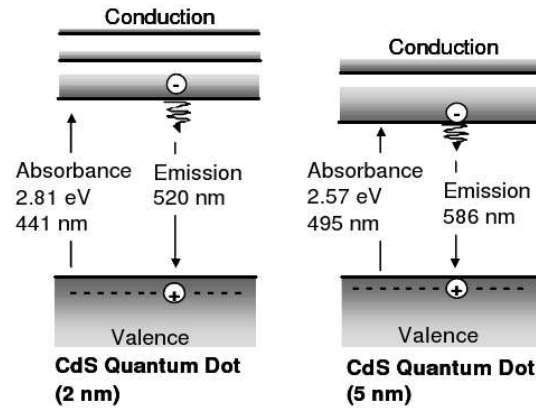


**(b)** Red-shifted emission due to crystal size.

**Figure 3.5:** Fluorescent emission and particle band gap, functions of the crystal size.
(a) Photon absorption creates an excited electron. This electron loses some energy to heat; then decays to ground, emitting a photon. The emitted photon has a longer wavelength than the absorbed photon because of the energy lost to heat.
(b) As the band gap decreases, the particle will absorb at longer wavelengths. This will produce a red-shift in particle fluorescent emission. (Image courtesy of J. Winter [63])
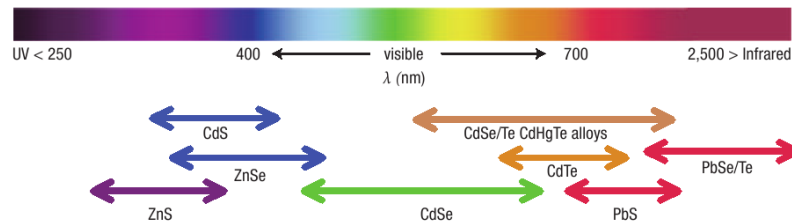


**Figure 3.6:** Emission spectra of quantum dots built from different materials.
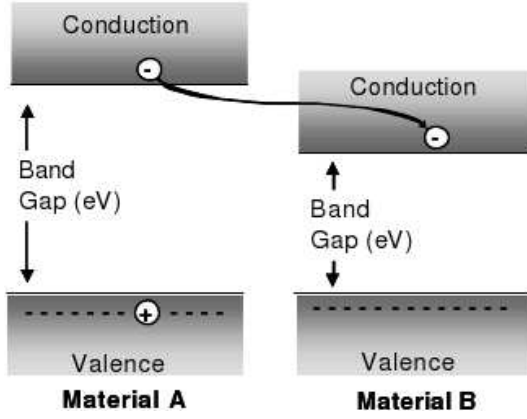
**Figure 3.7:** Electron transfer between materials with different band gaps.
If an excited electron in one material (A) encounters a second material (B) with a lower band gap energy, it can transfer its electron to that material. (Image courtesy of J. Winter [63])

quantum dot to surrounding reservoirs (Figure 3.8). The fact that the charge on the electron island is quantized in units of the elementary charge $e$ regulates transport through the quantum dot in the Coulomb blockade regime. Here the transport between the reservoirs and the dot occurs **via tunnel barriers**, which are thick enough so that the transport is dominated by resonances due to quantum confinement in the dot. This requires a small transmission coefficient through the barriers, and thus the tunnel resistance has to be larger than the quantum resistance $h/e^2$. If the dot is fully decoupled from its environment, it confines a well defined number $N$ of electrons. For weak coupling, deviations due to tunneling through the barriers are small, leading to discrete values in the total electrostatic energy of the dot. This energy can be estimated by $N(N-1)e^2/(2C)$, where $C$ is the capacitance of the dot. Thus the addition of a single electron requires energy $Ne^2/C$, which is discretely spaced by the charging energy $e^2/C$. If this charging energy exceeds the thermal energy $k_B T$, the electrons cannot tunnel on and off the dot by thermal excitations alone, and transport can be blocked, which is referred to as a **Coulomb blockade**.

The two barriers define the coupling of the channel to its surroundings. The conductance of the double-barrier channel is measured as a function of the gate voltage at different temperatures.

Following Kouwenhoven and McEuen (1999), figure 3.9a schematically illustrates an electron island connected to its environment by electrostatic barriers, the so-called source and drain contacts, and a gate to which one can apply a voltage $V_g$ as depicted in figure 3.8.

In this example, the level structure of the quantum dot connected to source and drain by tunneling barriers is sketched schematically in Figures. 3.9(a)-(c). The chemical potential inside the dot, where the discrete quantum states are filled with $N$ electrons [i.e. the highest solid line in Figures. 3.9(a)-(c)], equals $\mu_{dot}(N) = E(N) - E(N+1)$, where $E(N)$ is the total groundstate energy (here at zero temperature).

Figure 3.9d shows the results of the experiment. We can see how the Coulomb blockade affects transport: clear peaks, equidistantly spaced, are separated by regions of zero conductance.

When a bias voltage is applied to the source $s$ and the drain $d$, the electrochemical potentials $\mu_s$ and $\mu_d$ are different, and a transport window $\mu_s - \mu_d = -eV_{ds}$ opens up, where $e$ is the electron charge. In the linear regime the transport window $-eV_{ds}$
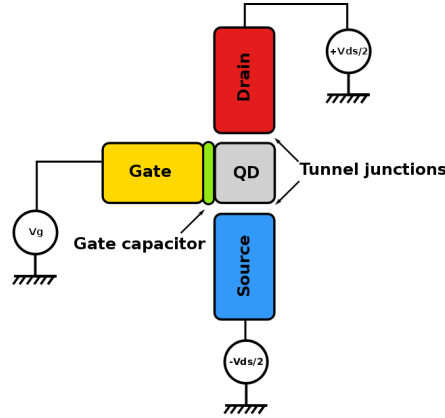
**Figure 3.8:** Schematic of a Single Electron Transistor (SET).
Setup for transport measurements on a lateral quantum dot. Because of the small size of the island or quantum dot (QD) in the middle of the two tunnel junctions the capacitance becomes very high and we see coulomb blockade effect.

is smaller than the spacing of the quantum states, and only the ground state of the dot can contribute to the conductance. By changing the voltage on the back gate, $\mu_{dot(N+1)}$ can be aligned with the transport window [Fig. 3.9b], and electrons can subsequently tunnel on and off the island at this particular gate voltage. This situation corresponds to a conductance maximum, as marked by the label (*b*) in Fig. 3.9d. Otherwise transport is blocked, as a finite energy is needed to overcome the charging energy. This scenario corresponds to zero conductance as marked by the labels (a) and (c) in Fig. 3.9. The mechanism of discrete charging and discharging of the dot leads to Coulomb blockade oscillations in the conductance as a function of gate voltage (as observed, for example, in Fig. 3.9d): at zero conductance, the number of electrons on the dot is fixed, whereas it is increased by one each time a conductance maximum is crossed. [48]

Spectroscopic information about the charge state and energy levels of the interacting quantum dot electrons can be obtained by analyzing the precise shape of the Coulomb oscillations and the Coulomb staircase. In this way, single electron transport can be used as a spectroscopic tool [42].

## 3.5   Quantum dot in a magnetic field

In many experimental situations with quantum dots, the electrons in quantum dots are manipulated using an external magnetic field. This field is usually created so that the magnetic field vector $\vec{B}$ is normal to the dot surface. For a typical quantum dot this results in a complicated spectrum of energy levels shown in figure 3.10.

The theoretical approach to the quantum dot given in the following chapter will serve as a basis to understand the spectrum of figure 3.10, even if the model used includes many approximations.
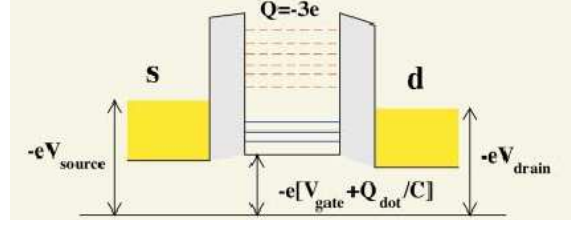
**(a)** Electron-transport blocked
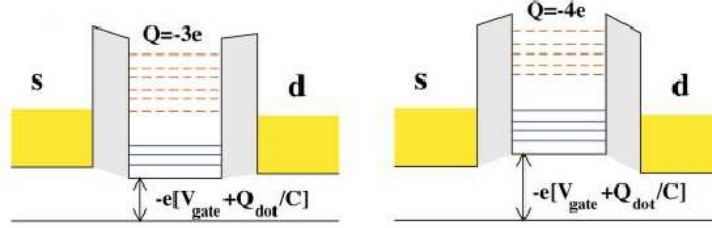


**(b)** Electron-transport allowed: maximum conductance
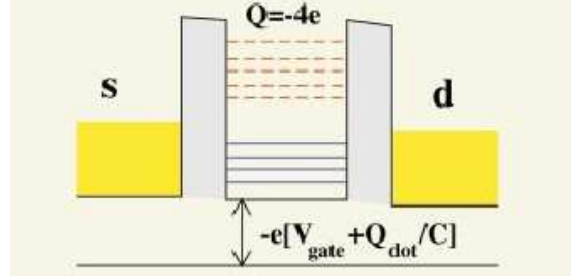


**(c)** Electron-transport blocked again
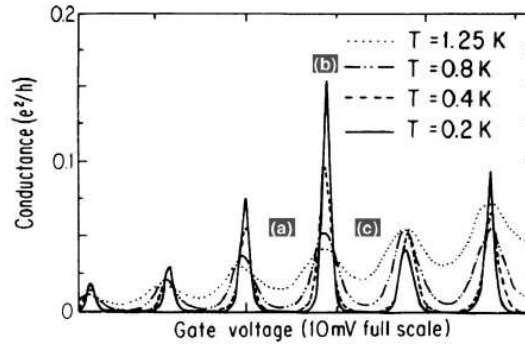


**(d)** Conductance of the double-barrier channel measured as a function of the gate voltage at different temperatures [40]

**Figure 3.9:** Single-electron transport in a quantum dot.
(a)-(c) Schematic picture of the level structures for single-electron transport (courtesy of A; Wacker). The solid lines represent the ionization potentials where the upper equals $\mu_{dot}(N)$, whereas the dashed lines refer to electron affinities, where the lowest one equals $\mu_{dot}(N+1)$. The gate bias increases from (a) to (c) [48].
(d) An example of the first measurements of Coulomb blockade as a function of the gate voltage.
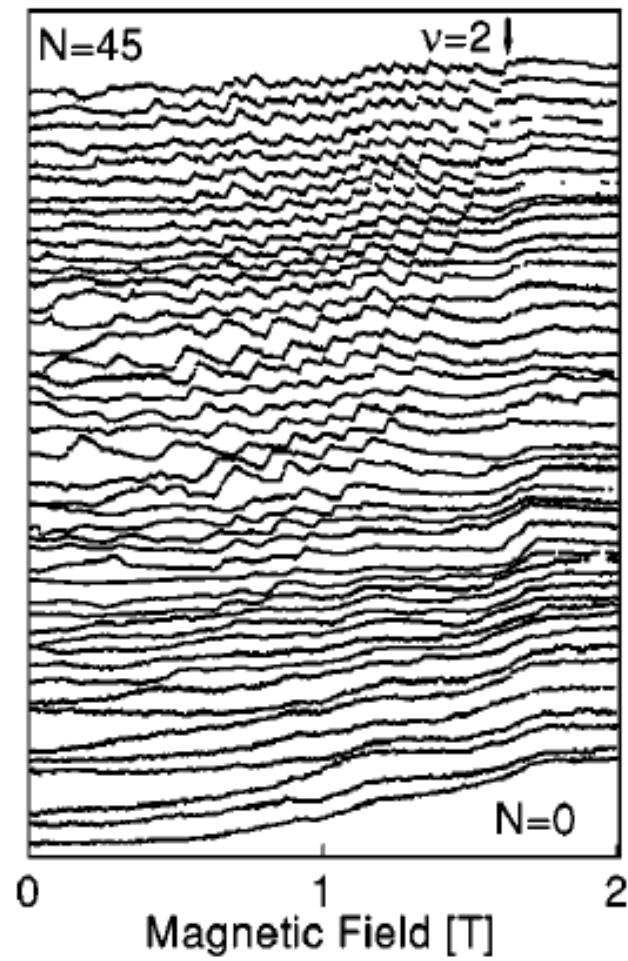
**Figure 3.10:** Additional energy spectrum as a function of a magnetic field. The magnetic field induces level crossings of single particle eigenstates which appear as cusps on the figure. (Image courtesy of M. Ciorga [10])

# Chapter 4

# Modelling of Quantum Dots

Quantum systems are governed by the Schrödinger equation (4$^{th}$ postulate of quantum mechanics):

$$H|\psi(t)\rangle = i\hbar \frac{d}{dt}|\psi(t)\rangle, \qquad (4.1)$$

where $H$ is the quantum Hamilton operator (or Hamiltonian) and $|\psi(t)\rangle$ the state vector of the system.

The solutions to the stationary form of this equation determine many physical properties of the system at hand, such as the ground state energy of the system which is the ultimate result of our simulations. Indeed as expressed in section 2.3 we need a way to validate our model and we choose the ground state energy as physical quantity that can be compared with experiments and other numerical simulations.

Solving the Schrödinger equation in the Hamiltonian formalism obviously requires a definition of this Hamiltonian which translates as well as possible our knowledge of the system into equations. We must identify the different forces/fields applied to the system in order to include their respective "potentials" into the Hamiltonian.

In the case of a quantum dot, the Hamiltonian is basically characterized by the different forces applied to its constituants. This could be done by summing over all the interactions between electrons and nuclei that constitute the quantum dot. However, if the final objective is to perform fast predictions about the system, the complexity of such a model may quickly reach the limits of the computational resources.

Therefore we prefer a simpler model in which the system is limited to the free charge-carriers by modelling a **confining potential** that traps them into the dot as well as an **interaction potential** that characterizes the repulsion between those electrons.

This chapter discusses possible models for those potentials. The derivation of a Hamiltonian is then given for electrons that repeal each other by a Coulomb interaction and that are trapped in a parabolic potential, and even more confined by applying or not an external magnetic field. We show finally that rescaling the problem with proper length and energy units leads to a simple form of the Hamiltonian even when applying an external magnetic field to the quantum dot.

## 4.1 Theoretical approximation of the quantum dot Hamiltonian

*Two-body interaction potential* The interaction potential between two electrons is usually approximated proportional to the Coulomb repulsion in free space $V(\vec{r_i}, \vec{r_j}) = 1/r_{ij}$. Other studies have investigated different forms of potential. For example Johnson and Payne [24] assumed the interaction potential $V(\vec{r_i}, \vec{r_j})$ between particles $i$ and $j$ moving in the confining potential to saturate at small particle separation and to decrease quadratically with increasing separation. More recently, in order to investigate spin relaxation in quantum dots, Chaney and Maksym in [9] built a model where the electron-electron interactions were designed to follow experimental data.

For sake of simplicity and since it is still in use in most studies of quantum dots, we will stick to the approximation of the interaction potential proportional to the Coulomb repulsion.

*The confining potential* Defining the second potential that confines these electrons is a more difficult issue when modelling a quantum dot. Some numerical [30,37,38,53] and experimental [27, 22, 21] studies have shown that for a small number of trapped electrons, the harmonic oscillator potential is a good approximation, at least to first approximation. In [24], the bare (i.e. unscreened) confining potential $V(\vec{r_i})$ for the $i^{th}$ particle is also modelled to be parabolic (i.e. the harmonic oscillator potential). It has been shown theoretically that for electrons contained in a parabolic potential there is a strong absorption of far-infrared light at the frequency corresponding to the bare parabola [6, 44, 64, 36]. This theoretical prediction is consistent with some experimental measurements on quantum dots [51]. Further evidence that the bare potential in many quantum-dot samples is close to parabolic is provided by simple electrostatic models [12].

*Relations between confining potential and electron interactions* Other studies tested different spherically symmetric confining potentials with different profiles ("soft" and "hard") on electrons in coupled QDs [34], and observed the resulting electron interactions. It shows very different behaviours of the electron interactions between the soft (Gaussian) and the hard (rectangular-like) confining potential. This means that the model of the confining potential has a strong influence on the electron-electron interactions, and that it depends itself on the type and shape of the QD under study.

*Motivation for the model chosen* Since we are focusing on the limits of the Hartree-Fock method with respect to other techniques rather than an exhaustive study of different types of quantum dots, we choose in the rest of the thesis to model the single quantum dot by a definite number of electron $N_e$, trapped by a pure isotropic harmonic oscillator potential and repealing each other with a two-body Coulomb interaction. Only closed shell systems are studied, meaning that the number of electrons present in the quantum dot are filling all single particle states until the Fermi level. This simplifies greatly the problem since all combinations of single

particle states are reduced to one Slater determinant as detailled in 5.2.2.

## *4.2 General form of $\hat{H}$ with explicit physical interactions*

In this section we derive the Hamiltonian of the quantum dot model with and without external magnetic field in order to show that the interaction with the external magnetic field will basically result in a modified harmonic oscillator frequency and a shift of the energy proportional to the strength of the field.

### *4.2.1 Electrons trapped in an harmonic oscillator potential*

We consider a system of electrons confined in a pure isotropic harmonic oscillator potential $V(\vec{r}) = m^*\omega_0^2 r^2/2$, where $m^*$ is the effective mass of the electrons in the host semiconductor (as defined in section 3.2), $\omega_0$ is the oscillator frequency of the confining potential, and $\vec{r} = (x, y, z)$ denotes the position of the particle.

The Hamiltonian of a single particle trapped in this harmonic oscillator potential simply reads

$$\hat{H} = \frac{\mathbf{p}^2}{2m^*} + \frac{1}{2}m^*\omega_0^2\|\mathbf{r}\|^2, \tag{4.2}$$

where $\mathbf{p}$ is the canonical momentum of the particle.

When considering several particles trapped in the same quantum dot, the Coulomb repulsion between those electrons has to be added to the single particle Hamiltonian which gives

$$\hat{H} = \sum_{i=1}^{N_e} \left( \frac{\mathbf{p_i}^2}{2m^*} + \frac{1}{2}m^*\omega_0^2\|\mathbf{r_i}\|^2 \right) + \frac{e^2}{4\pi\epsilon_0\epsilon_r} \sum_{i<j} \frac{1}{\|\mathbf{r_i} - \mathbf{r_j}\|}, \tag{4.3}$$

where $N_e$ is the number of electrons, $-e$ $(e > 0)$ is the charge of the electron, $\epsilon_0$ and $\epsilon_r$ are respectively the free space permitivity and the relative permitivity of the host material (also called dielectric constant), and the index $i$ labels the electrons.

### *4.2.2 Electrons trapped in an harmonic oscillator potential in the presence of an external magnetic field*

We assume that the magnetic field $\overrightarrow{B}$ is static and along the $z$ axis. At first we ignore the spin-dependent terms. The Hamiltonian of these electrons in a magnetic

field now reads [5]

$$\hat{H} = \sum_{i=1}^{N_e} \left( \frac{(\mathbf{p_i} + e\mathbf{A})^2}{2m^*} + \frac{1}{2}m^*\omega_0^2\|\mathbf{r_i}\|^2 \right) + \frac{e^2}{4\pi\epsilon_0\epsilon_r}\sum_{i<j}\frac{1}{\|\mathbf{r_i}-\mathbf{r_j}\|}, \tag{4.4}$$

$$= \sum_{i=1}^{N_e}\left( \frac{\mathbf{p_i}^2}{2m^*} + \frac{e}{2m^*}(\mathbf{A}\cdot\mathbf{p_i} + \mathbf{p_i}\cdot\mathbf{A}) + \frac{e^2}{2m^*}\mathbf{A}^2 + \frac{1}{2}m^*\omega_0^2\|\mathbf{r_i}\|^2 \right) \tag{4.5}$$

$$+ \frac{e^2}{4\pi\epsilon_0\epsilon_r}\sum_{i<j}\frac{1}{\|\mathbf{r_i}-\mathbf{r_j}\|}, \tag{4.6}$$

where $\mathbf{A}$ is the vector potential defined by $\mathbf{B} = \nabla \times \mathbf{A}$.

In coordinate space, $\mathbf{p_i}$ is the operator $-i\hbar\nabla_i$ and by applying the Hamiltonian on the total wave function $\Psi(\mathbf{r})$ in the Schrödinger equation, we obtain the following operator acting on $\Psi(\mathbf{r})$

$$\mathbf{A}\cdot\mathbf{p_i} + \mathbf{p_i}\cdot\mathbf{A} = -i\hbar\left(\mathbf{A}\cdot\nabla_i + \nabla_i\cdot\mathbf{A}\right)\Psi \tag{4.7}$$

$$= -i\hbar\left(\mathbf{A}\cdot(\nabla_i\Psi) + \nabla_i\cdot(\mathbf{A}\Psi)\right). \tag{4.8}$$

We note that if we use the product rule and the Coulomb gauge $\nabla\cdot\mathbf{A} = 0$ (by choosing the vector potential as $\mathbf{A} = \frac{1}{2}\mathbf{B}\times\mathbf{r}$), $\mathbf{p_i}$ and $\nabla_i$ commute and we obtain

$$\nabla_i\cdot(\mathbf{A}\Psi) = \mathbf{A}\cdot(\nabla_i\Psi) + \underbrace{(\nabla_i\cdot\mathbf{A})}_{0}\Psi = \mathbf{A}\cdot(\nabla_i\Psi). \tag{4.9}$$

This leads us to the following Hamiltonian:

$$\hat{H} = \sum_{i=1}^{N_e}\left( -\frac{\hbar^2}{2m^*}\nabla_i^2 - i\hbar\frac{e}{m^*}\mathbf{A}\cdot\nabla_i + \frac{e^2}{2m^*}\mathbf{A}^2 + \frac{1}{2}m^*\omega_0^2\|\mathbf{r_i}\|^2 \right) \tag{4.10}$$

$$+ \frac{e^2}{4\pi\epsilon_0\epsilon_r}\sum_{i<j}\frac{1}{\|\mathbf{r_i}-\mathbf{r_j}\|}, \tag{4.11}$$

The linear term in $\mathbf{A}$ becomes, in terms of $\mathbf{B}$:

$$\frac{-i\hbar e}{m^*}\mathbf{A}\cdot\nabla_i = -\frac{i\hbar e}{2m^*}(\mathbf{B}\times\mathbf{r_i})\cdot\nabla_i \tag{4.12}$$

$$= \frac{-i\hbar e}{2m^*}\mathbf{B}\cdot(\mathbf{r_i}\times\nabla_i) \tag{4.13}$$

$$= \frac{e}{2m^*}\mathbf{B}\cdot\mathbf{L}. \tag{4.14}$$

where $\mathbf{L} = -i\hbar(\mathbf{r_i}\times\nabla_i)$ is the orbital angular momentum operator of the electron $i$.

If we assume that the electrons are confined in the $xy$-plane, the quadratic term in $\mathbf{A}$ appearing in 4.10 can be written under the form

$$\frac{e^2}{2m^*}\mathbf{A}^2 = \frac{e^2}{8m^*}(\mathbf{B}\times\mathbf{r})^2 \tag{4.15}$$

$$= \frac{e^2}{8m^*}B^2r_i^2. \tag{4.16}$$

Until this point we have neglected the intrinsic magnetic moment of the electrons which is due to the electron spin in the host material. We will now add its effect to the Hamiltonian. This intrinsic magnetic moment is given by $\mathcal{M}_s = -g_s^*(e\mathbf{S})/(2m^*)$, where $\mathbf{S}$ is the spin operator of the electron and $g_s^*$ its effective spin gyromagnetic ratio (or effective *g-factor* in the host material).We see that the spin magnetic moment $\mathcal{M}_s$ gives rise to an additional interaction energy [5], linear in the magnetic field,

$$\hat{H}_s = -\mathcal{M}_s \cdot \mathbf{B} = g_s^* \frac{e}{2m^*} B \hat{S}_z = g_s^* \frac{\omega_c}{2} \hat{S}_z, \tag{4.17}$$

where $\omega_c = eB/m^*$ is known as the cyclotron frequency.

The final Hamiltonian reads

$$\hat{H} = \sum_{i=1}^{N_e} \left( \frac{-\hbar^2}{2m^*}\nabla_i^2 + \overbrace{\frac{1}{2}m^*\omega_0^2\|\mathbf{r_i}\|^2}^{\substack{\text{Harmonic ocscillator} \\ \text{potential}}} \right) + \overbrace{\frac{e^2}{4\pi\epsilon_0\epsilon_r}\sum_{i<j}\frac{1}{|\mathbf{r_i}-\mathbf{r_j}|}}^{\substack{\text{Coulomb} \\ \text{interactions}}}$$
$$+ \underbrace{\sum_{i=1}^{N_e} \left( \frac{1}{2}m^*\left(\frac{\omega_c}{2}\right)^2\|\mathbf{r_i}\|^2 + \frac{1}{2}\omega_c\hat{L}_z^{(i)} + \frac{1}{2}g_s^*\omega_c\hat{S}_z^{(i)} \right)}_{\substack{\text{single particle interactions} \\ \text{with the magnetic field}}}, \tag{4.18}$$

### 4.2.3 Scaling the problem: Dimensionless form of $\hat{H}$

In order to simplify the computation, the Hamiltonian can be rewritten on dimensionless form. For this purpose, we introduce the following constants:

- the oscillator frequency $\omega = \omega_0\sqrt{1 + \omega_c^2/(4\omega_0^2)}$,

- a new energy unit $\hbar\omega$,

- a new length unit, the oscillator length defined by $l = \sqrt{\hbar/(m^*\omega)}$, also called the characteristic length unit.

We rewrite the Hamiltonian in dimensionless units using:

$$\mathbf{r} \longrightarrow \frac{\mathbf{r}}{l}, \quad \nabla \longrightarrow l\,\nabla \quad \text{and} \quad \hat{L}_z \longrightarrow \hat{L}_z$$

It leads to the following Hamiltonian:

$$\hat{H} = \sum_{i=1}^{N_e} \left( -\frac{1}{2}\nabla_i^2 + \frac{1}{2}r_i^2 \right) + \overbrace{\frac{e^2}{4\pi\epsilon_0\epsilon_r}\frac{1}{\hbar\omega l}}^{\substack{\text{Dimensionless} \\ \text{confinement} \\ \text{strength } (\lambda)}}\sum_{i<j}\frac{1}{r_{ij}}$$
$$+ \sum_{i=1}^{N_e} \left( \frac{1}{2}\frac{\omega_c}{\hbar\omega}\hat{L}_z^{(i)} + \frac{1}{2}g_s^*\frac{\omega_c}{\hbar\omega}\hat{S}_z^{(i)} \right), \tag{4.19}$$

Lengths are now measured in units of $l = \sqrt{\hbar/(m^*\omega)}$, and energies in units of $\hbar\omega$.
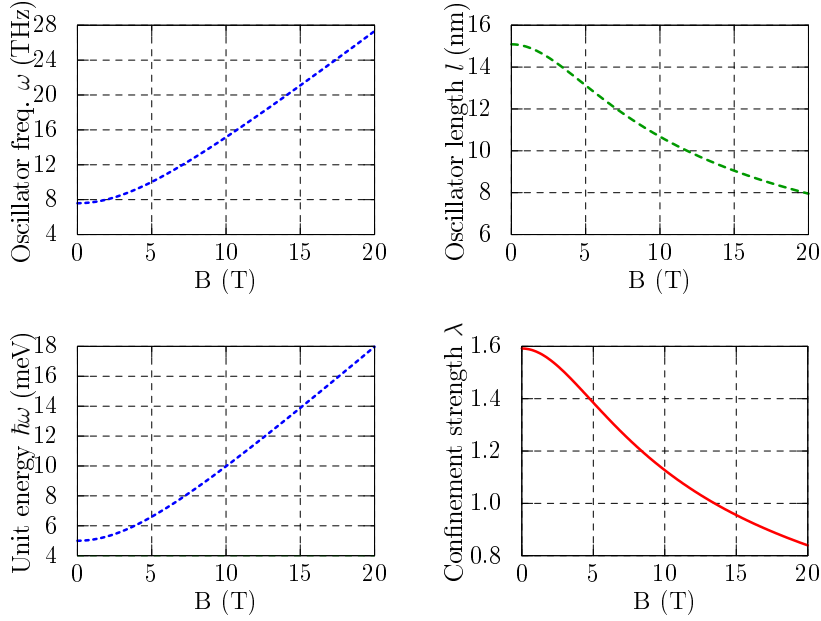
**Figure 4.1:** Typical values for the oscillator frequency $\omega$, the oscillator length $l$, the energy unit $\hbar\omega$ and the dimensionless confinement strength $\lambda$ as a function of the magnetic field strength in GaAs semiconductors assuming: $\hbar\omega_0 = 5 \times 10^{-3} eV$ [28], $\epsilon_r \simeq 12$ and $m^* = 0.067 \, m_e$

A new dimensionless parameter $\lambda = l/a_0^*$ (where $a_0^* = 4\pi\epsilon_0\epsilon_r\hbar^2/(e^2 m^*)$ is the effective Bohr radius) describes the strength of the electron-electron interaction. Large $\lambda$ implies strong interaction and/or large quantum dot [56]. Since both $\hat{L}_z$ and $\hat{S}_z$ commute with the Hamiltonian we can perform the calculations separately in subspaces of given quantum numbers $L_z$ and $S_z$. Figure 4.1 displays values of the different parameters as a function of the magnetic field strength for a particular type of semiconductor: Gallium arsenide (GaAs) with know characteristics given in table 3.1.

The simplified dimensionless Hamiltonian becomes

$$\hat{H} = \sum_{i=1}^{N_e} \left[ -\frac{1}{2}\nabla_i^2 + \frac{1}{2}r_i^2 \right] + \lambda \sum_{i<j} \frac{1}{r_{ij}} + \sum_{i=1}^{N_e} \left( \frac{1}{2}\frac{\omega_c}{\hbar\omega}L_z^{(i)} + \frac{1}{2}g_s^*\frac{\omega_c}{\hbar\omega}S_z^{(i)} \right). \qquad (4.20)$$

The last sum which is proportional to the magnetic field involves only the quantum numbers $L_z$ and $S_z$ and not the operators themselves [56]. Therefore these terms can be put aside during the resolution, the squizzing effect of the magnetic field being included simply in the parameter $\lambda$. The contribution of these terms will be added when the other part has been solved. This brings us to the simple and general form of the Hamiltonian:

$$\hat{H} = \sum_{i=1}^{N_e} \left( -\frac{1}{2}\nabla_i^2 + \frac{1}{2}r_i^2 \right) + \lambda \sum_{i<j} \frac{1}{r_{ij}}. \qquad (4.21)$$

In the next chapters, we will look for approximations of the ground state of the quantum dot by solving the Schrödinger equation using this definition $\hat{H}$.

# Chapter 5

# Many-body treatment: the Hartree-Fock method

A many-body system with interactions is generally very difficult to solve exactly, except for extremely simple cases [54, 55]. It is the same when it comes to quantum dots that can simply be seen as a many-electron problem.

In the first section of this chapter we will detail the derivation of exact solutions for the two-electrons quantum dot for some particular parameters. Then some numerical approximations techniques are used in order to get information about the properties of the system as close as possible from their real values. In this thesis we focus on the ground state energy of quantum dots (i.e. the energy of the system at rest without external time-dependent excitations). In order to calculate it, several many-body techniques with different accuray and efficiency can be used, some of them are presented here.

We will detail the Hartree-Fock method which is a major part of this thesis and introduce other *Ab initio* methods such as perturbation theory, variational Monte-Carlo or large scale diagonalisation.

## 5.1  Ab initio many-body techniques

The term *"ab initio"* indicates that the calculation is from first principles and that no empirical data is used.

The simplest type of *ab initio* electronic structure calculation is the Hartree-Fock (HF) scheme, in which the instantaneous Coulombic electron-electron repulsion is not specifically taken into account. Only its average effect (mean field) is included in the calculation. This is a variational procedure; therefore, the obtained approximate energies, expressed in terms of the system's wave function, are always equal to or greater than the exact energy, and tend to a limiting value called the Hartree-Fock limit as the size of the basis is increased [11].

Many types of calculations begin with a Hartree-Fock calculation and subsequently correct for electron-electron repulsion, referred to also as electronic correlation. Configuration Interaction (CI) and Coupled cluster theory (CC) may be some
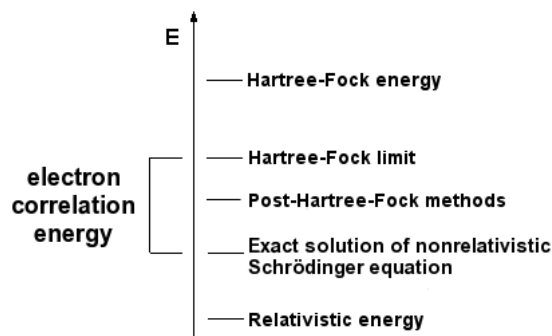
**Figure 5.1:** Electron correlation energy in terms of various levels of theory of solutions for the Schrödinger equation. (K. Langner, 2005)

examples of these post-Hartree-Fock methods.

Figure 5.1 presents a diagram illustrating electron correlation energy in terms of various levels of theory. As shown on the figure, HF may present the worse approximation to the exact energy of a many-body system, but its simplicity is on all fours with its computational efficiency (i.e. speed) compared to other methods.

In some cases, particularly for bond breaking processes, the Hartree-Fock method is inadequate and this single-determinant reference function is not a good basis for post-Hartree-Fock methods. It is then necessary to start with a wave function that includes more than one determinant.

A method that avoids making the variational overestimation of HF in the first place is Quantum Monte Carlo (QMC), in its variational, diffusion, and Green's function forms. These methods work with an explicitly correlated wave function and evaluate integrals numerically using a Monte Carlo integration. Such calculations can be very time-consuming, but they are probably the most accurate methods known today.

*Ab initio* electronic structure methods have the ability to converge toward the exact solution, when all approximations are sufficiently small in magnitude. In particular, configuration interaction, where all possible configurations are included (called "Full CI") tends to the exact non-relativistic solution of the Schrödinger equation, and therefore to the best possible solution in principle.

However Full CI is often impossible for anything but the smallest systems. More generally, the downside of ab initio methods is their computational cost. They often take enormous amounts of computer time, memory, and disk space.

## 5.2   Time-independent Hartree-Fock (HF) Theory

The Hartree-Fock method is a minimization method based on a mathematical technique known as the Lagrange multipliers, where the functional to minimize is the energy of the system. The energy, which is an expectation value of the Hamiltonian, can be written explicitly as an integral.

## 5.2.1 Variational Calculus and Lagrange Multipliers

As previously mentionned, we must resort to computers in most cases to determine the solutions of the Schrödinger equation. It is of course possible to integrate the equation using discretisation methods, but in most realistic electronic structure calculations we would need huge numbers of grid points, leading to high computer time and memory requirements. The variational method on the other hand enables us to solve the Schrödinger equation much more efficiently in many cases [57].

Based on the Lagrange multipliers for mathematical optimization (refer to appendix B for more details), the calculus of variations provides a strategy for finding the stationnary points of a function subject to some constraints. Maxima and minima can be found in this way when the function is differentiable.

More specifically the calculation of variations involves problems where the quantity to be minimized or maximized (the functional) is an integral.

In the general case we have an integral of the type

$$E[\Phi] = \int_a^b f(\Phi(x), \frac{\partial \Phi}{\partial x}, x)dx,$$

where $E$ is the quantity which is sought minimized or maximized.

The problem is that although $f$ is a function of the variables $\Phi$, $\partial\Phi/\partial x$ and $x$, the exact dependence of $\Phi$ on $x$ is not known. This means that even though the integral has fixed limits $a$ and $b$, the path of integration is not known. In our case the unknown quantities are the single-particle wave functions and we have to select an integration path which makes the functional $E[\Phi]$ stationary, ie we look for minima, or maxima or saddle points. In physics we search normally for minima.

Our task is therefore to find the minimum of $E[\Phi]$ so that its variation $\delta E$ is zero subject to specific constraints. In our case the constraints appear as the integral which expresses the orthogonality of the single-particle wave functions. The constraints can be treated via the technique of the Lagrange multipliers.

In the following, we will be more specific with the form of the functional which now reads

$$E[\Phi] = \frac{\langle\Phi|H|\Phi\rangle}{\langle\Phi|\Phi\rangle} = \frac{\int \Phi^* H \Phi d\tau}{\int \Phi^* \Phi d\tau}, \tag{5.1}$$

where the integration is extended over the full range of all the coordinates of the system.

We denote by $E_n$ the eigenvalues of the Hamiltonian and by $\Psi_n$ the corresponding orthonormal eigenfunctions, and assume that $\hat{H}$ has at least one discrete eigenvalue. It is clear that if the function $\Phi$ is identical to one of the exact eigenfunctions $\Psi_n$ of $\hat{H}$; then $E[\Phi]$ will be identical to the corresponding exact eigenvalue $E_n$.

In the following, we will show that:

1. any function $\Phi$ for which the functional $E[\Phi]$ is stationary is an eigenfunction of the discrete spectrum of $\hat{H}$.

2. using the method of the Lagrange multipliers and varying the functional $\langle\Phi|H|\Phi\rangle$ subject to the normalisation condition $\langle\Phi|\Phi\rangle = 1$, the Lagrange multiplier itself has the significance of an energy eigenvalue.

3. the functional $E[\Phi]$ gives an upper bound for the ground state energy, also known as the *variational principle.*

4. it is possible to solve the Schrödinger equation using the variational method.

*Any function $\Phi$ for which the functional $E[\Phi]$ is stationary is an eigenfunction of $\hat{H}$*
If $\Phi$ and an exact eigenfunction $\Psi_n$ differ by an arbitrary infinitesimal variation $\delta\Phi$,

$$\Phi = \Psi_n + \delta\Phi,$$

then the corresponding first-order variation of $E[\Phi]$ vanishes:

$$\delta E = 0, \tag{5.2}$$

and the eigenfunctions of $\hat{H}$ are solutions of the variational equation 5.2.

To prove this statement, we re-write the functional as

$$E[\Phi] \int \Phi^* \Phi d\tau = \int \Phi^* H \Phi d\tau.$$

When we vary it it gives:

$$\delta E \int \Phi^* \Phi d\tau + E \int \delta\Phi^* \Phi d\tau + E \int \Phi^* \delta\Phi d\tau = \int \delta\Phi^* H \Phi d\tau + \int \Phi^* H \delta\Phi d\tau.$$

Since $\Phi|\Phi$ is assumed to be finite and non-vanishing, we see that the variational equation 5.2 is equivalent to

$$\int \delta\Phi^*(H - E)\Phi d\tau + \int \Phi^*(H - E)\delta\Phi d\tau = 0. \tag{5.3}$$

Although the variations $\delta\Phi$ and $\delta\Phi^*$ are not independent, they may in fact be treated as such, so that the individual terms in 5.3 can be set equal to zero. To see how this comes about, we replace the arbitrary variation $\delta\Phi$ by $i\delta\Phi$ in 5.3 so that we obtain

$$-i \int \delta\Phi^*(H - E)\Phi d\tau + i \int \Phi^*(H - E)\delta\Phi d\tau = 0. \tag{5.4}$$

By combining 5.3 with 5.4 we then obtain the two equations

$$\begin{cases} \delta\Phi^*(H - E)\Phi d\tau = 0 \\ \Phi^*(H - E)\delta\Phi d\tau = 0, \end{cases} \tag{5.5}$$

which is the desired result. Using the fact that $\hat{H}$ is Hermitian, we see that the two equation 5.5 are equivalent to the Schödinger equation $(H - E[\Phi])\Phi = 0$.

Thus any function $\Phi = \Psi_n$ for which the functional 5.1 is stationary is an eigenvalue of $\hat{H}$ corresponding to the eigenvalue $E_n = E[\Psi_n]$. It is worth stressing that if $\Phi$ and $\Psi_n$ differ by $\delta\Phi$, the variational equation 5.2 implies that the leading term of the difference $E[\Phi] - E_n$ is quadratic in $\delta\Phi$. As a result, errors in the approximate energy are of second order in $\delta\Phi$ when the energy is calculated from the functional 5.1.

*The Lagrange multiplier has the significance of an energy eigenvalue*    We also remark that the functional 5.1 is independent of the normalisation and of the phase of $\Phi$. In particular, it is often convenient to impose the condition $\langle \Phi | \Phi \rangle = 1$. The above results may then be retrieved by varying the functional $\langle \Phi | H | \Phi \rangle = 1$ subject to the condition $\langle \Phi | \Phi \rangle = 1$, namely

$$\delta \int \Phi^* H \Phi d\tau = 0, \quad \int \Phi^* \Phi d\tau = 1.$$

The constraint $\langle \Phi | \Phi \rangle = 1$ may be taken care of by introducing a Lagrange multiplier (as described in appendix B) which we denote by $\Sigma$.

We define the Lagrangian $\Lambda$ as

$$\Lambda(\Phi, \Sigma) = \int \Phi^* H \Phi d\tau - \Sigma \left( \int \Phi^* \Phi d\tau - 1 \right),$$

so that the variational equation reads

$$\delta \Lambda(\Phi, \Sigma) = 0 \tag{5.6}$$

$$\delta \left[ \int \Phi^* H \Phi d\tau - \Sigma \int \Phi^* \Phi d\tau \right] = 0, \tag{5.7}$$

or

$$\int \delta \Phi^* (H - \Sigma) \Phi d\tau + \int \Phi^* (H - \Sigma) \delta \Phi d\tau = 0.$$

This equation is identical to 5.3, and we see that the Lagrange multiplier $\Sigma = E$ has the significance of an energy eigenvalue.

*The variational principle*    An important additional property of the functional 5.1 is that it provides an upper bound to the exact ground state $E_0$. To prove this result, we expand the arbitrary, normalisable function $\Phi$ in the complete set of orthonormal eigenfunctions $\Psi_n$ of $\hat{H}$. This reads

$$\Phi = \sum_n a_n \Psi_n. \tag{5.8}$$

Substituing the expansion 5.8 into the functional 5.1, we find that

$$E[\Phi] = \frac{\sum_n |a_n|^2 E_n}{\sum_n |a_n|^2}, \tag{5.9}$$

where we have used the fact that $H \Psi_n = E_n \Psi_n$ and $\langle \Phi | \Phi \rangle = \sum_n |a_n|^2$. If we now subtract $E_0$, the lowest energy eigenvalue, from both sides of the functional 5.9 we have

$$E[\Phi] - E_0 = \frac{\sum_n |a_n|^2 (E_n - E_0)}{\sum_n |a_n|^2}. \tag{5.10}$$

Since $E_n \geq E_0$, the right-hand side of 5.10 is non-negative, so that

$$E_0 \leq E[\Phi], \tag{5.11}$$

and the functional $E[\Phi]$ gives an upper-bound, or in order words a *minimum principle* for the ground state energy [5].

*Solving the Schrödinger equation using the variational method* In the variational method, the possible solutions (i.e. the stationary states of the energy functional) are restricted to a subspace of the Hilbert space, and in this subspace we seek the "best possible" solution. An important example is linear variational calculus, in which the subspace is spanned by a set of basis vectors $\chi_i$ for $i = 1, \ldots, P$ where $P$ is the size of the basis set. We take these to be orthonormal at first, that is,

$$\langle \chi_i | \chi_j \rangle = \delta_{ij}.$$

For an arbitrary state $|\Psi\rangle = \sum_i C_i |\chi_j\rangle$, the energy functional is given by

$$E = \frac{\langle \Psi | H | \Psi \rangle}{\langle \Psi | \Psi \rangle} = \frac{\sum_{i,j=1}^{R} C_i^* C_j H_{ij}}{\sum_{i,j=1}^{R} C_i^* C_j \delta_{ij}},$$

where $H_{ij} = \langle \chi_i | H | \chi_j \rangle$ is assumed to be known.

The stationary states follow from the condition that the derivative of this functional with respect to the $C_i$ vanishes, which leads to

$$\sum_{j=1}^{R} (H_{ij} - E\delta_{ij})C_j = 0, \qquad for \quad i = 1, \ldots, R. \tag{5.12}$$

Equation 5.12 is then an eigenvalue problem which can be written in matrix notation as

$$\mathbf{HC = EC}. \tag{5.13}$$

This is the Schrödinger equation, formulated for a finite, orthonormal basis.

The lowest eigenvalue of eq. 5.13 is always higher than or equal to the ground state energy, as we proved that the ground state is the minimal value assumed by the energy-functional in the full Hilbert space. If we restrict ourselves to a part of this space, then the minimum value of the energy functional must always be higher than or equal to the ground state of the full Hilbert space. Including more basis functions into our basis set will increase the size of the subspace and consequently the minimum of the energy functional will decrease (or stay the same). The behaviour of the spectrum found by solving 5.13 when increasing size of the basis set $R$ is depicted in figure 5.2.

The variational approach discussed here provides a powerful method for obtaining approximate solutions of the wave function. However this might not be sufficient when dealing with a system made of many interacting particles, where more approximations have to be done about the wave function of the system in order to lead again to a simple eigenvalue problem.

## 5.2.2 The many-body system with interacting particles

The Schrodinger equation for a system of $N$ electron reads:

$$\hat{H}(\mathbf{r_1, r_2, \ldots, r_N})\Psi_\eta(\mathbf{r_1, r_2, \ldots, r_N}) = E_\eta \Psi_\eta(\mathbf{r_1, r_2, \ldots, r_N}), \tag{5.14}$$
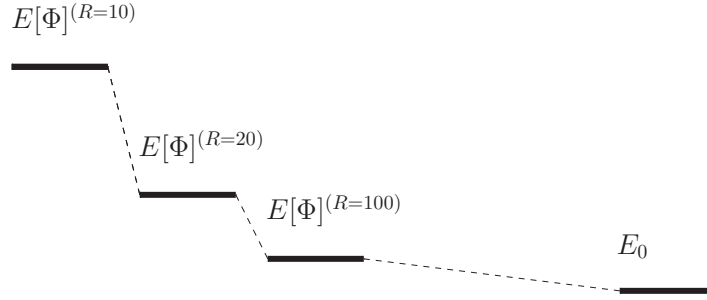
**Figure 5.2:** The behaviour of the ground state energy of eq. 5.12 when increasing basis set size $R$ in linear variational calculus. The upper index is the number of states in the basis set.

where the vector $\mathbf{r}_i$ represents the coordinates (spatial and spin) of a particle $i$, $\eta$ stands for all the quantum numbers needed to classify a given $N$-particle state and $\Psi_\eta$ is the corresponding eigenfunction.

The Hamiltonian can be written under the form

$$\hat{H} = \hat{T} + \hat{V},$$

where $\hat{T}$ represents the kinetic energy of the system

$$\hat{T} = \sum_{i=1}^{N} \frac{\mathbf{p_i^2}}{2m_i} = \sum_{i=1}^{N} \left( -\frac{\hbar^2}{2m_i} \nabla_i^2 \right) = \sum_{i=1}^{N} t(\mathbf{r_i}),$$

and $\hat{V}$ represents the potential energy (e.g. the harmonic oscillator potential in our case),

$$\hat{V} = \underbrace{\sum_{i=1}^{N} u(\mathbf{r_i})}_{\substack{\text{one-particle} \\ \text{interaction}}} + \underbrace{\sum_{i<j}^{N} v(\mathbf{r_i}, \mathbf{r_j})}_{\substack{\text{two-particles} \\ \text{interaction}}}. \tag{5.15}$$

Hereafter we use atomic units, viz. $\hbar=c=e=1$ with $e$ the elementary charge and $c$ the speed of light. This means that momenta and masses have dimension energy. In the last equation we have singled out an external one-body potential term $u$ which is meant to represent an effective one-body field in which our particles move (i.e. the harmonic oscillator potential in our first approximation for the confining potential of the QD model) .

We have therefore assumed that a picture consisting of individual electrons is a viable starting point for wave function approximations. We can rewrite the Hamiltonian for $N$ electrons as

$$\hat{H} = \hat{H}_0 + \hat{H}_1 = \sum_{i=1}^{N} \hat{h}_i + \sum_{i<j}^{N} v(\mathbf{r_i}, \mathbf{r_j}), \tag{5.16}$$

where we have defined $r_{ij} = \parallel \vec{r_i} - \vec{r_j} \parallel$ and $\hat{h}_i = t(\mathbf{r_i}) + u(\mathbf{r_i})$.

The first term of the eq.(5.16), $\hat{H}_0$, is the sum of the $N$ one-body Hamiltonians $\hat{h}_i$. Each individual Hamiltonian $\hat{h}_i$ contains the kinetic energy operator of an electron and its potential energy due to the confining potential. The potential energy term due to the harmonic oscillator potential defines the one-body field $u_i = u(\mathbf{r_i})$ of eq.( 5.15). We have moved this term into the $\hat{H}_0$ part of the Hamiltonian, instead of keeping it in $\hat{V}$ as in eq.( 5.15). The reason is that we will hereafter treat $\hat{H}_0$ as our non-interacting Hamiltonian. For a many-body wavefunction $\Psi_\eta$ defined by an appropriate single-particle basis, we can solve exactly the non-interacting eigenvalue problem

$$\hat{H}_0 \Psi_\eta = E_\eta \Psi_\eta,$$

with $E_\eta$ being the non-interacting energy. This energy is defined by the sum over single-particle energies. In our model of the quantum dot, the single-particle energies are the harmonic oscillator single-particle energies in 2D or 3D respectively.

The second term of the eq.(5.16), $\hat{H}_1$, is the sum of the $N(N-1)/2$ two-body interactions between each pair of electrons. Note that the double sum carries a restriction $i < j$.

Irrespective of these approximations, there is a wealth of experimental evidence that these interactions have to obey specific symmetries. The total Hamiltonian should be translationally invariant. If angular momentum is conserved, the Hamiltonian is invariant under rotations. Furthermore, it is invariant under the permutation (interchange) of two particles. Since we deal with fermions, the total wave function is antisymmetric.

Let $\hat{P}$ be an operator which interchanges two particles. Due to the symmetries we have assigned to our Hamiltonian, this operator commutes with the total Hamiltonian,

$$[\hat{H}, \hat{P}] = 0,$$

meaning that $\Psi_\eta(\mathbf{r_1}, \mathbf{r_2}, \ldots, \mathbf{r_N})$ is an eigenfunction of $\hat{P}$ as well, that is

$$\hat{P}_{ij} \Psi_\eta(\mathbf{r_1}, \mathbf{r_2}, \ldots, \mathbf{r_i}, \ldots, \mathbf{r_j}, \ldots, \mathbf{r_N}) = \beta \Psi_\eta(\mathbf{r_1}, \mathbf{r_2}, \ldots, \mathbf{r_j}, \ldots, \mathbf{r_i}, \ldots, \mathbf{r_N}),$$

where $\beta$ is the eigenvalue of $\hat{P}$. We have introduce the suffix $ij$ in order to indicate that we permute particles $i$ and $j$. The Pauli principle tell us that the total wave function for a system of fermions has to be antisymmetric, resulting in the eigenvalue $\beta = -1$.

We approximate our many-body wave function with the product of single-particle wave functions. Since we assume that our Hamiltonian is time-independent, these single-particle wave functions are normally the eigenfunctions of a selected one-body Hamiltonian $\hat{h}_i$ acting on particle $i$.

In Hartree-Fock we approximate the exact eigenfunction[1] $\Psi_\lambda$ by a trial wave

---

[1]We reserve $\Psi$ as labelling for our exact wave function (eigen function, since there is no time-dependence). The Slater determinant is only an approximation of the exact solution.

function $\Phi$ built as a Slater determinant

$$\Phi(\mathbf{r_1}, \mathbf{r_2}, \ldots, \mathbf{r_N}, \alpha, \beta, \ldots, \sigma) = \frac{1}{\sqrt{N!}} \begin{vmatrix} \psi_\alpha(\mathbf{r}_1) & \psi_\beta(\mathbf{r}_2) & \ldots & \psi_\sigma(\mathbf{r}_N) \\ \psi_\alpha(\mathbf{r}_1) & \psi_\beta(\mathbf{r}_2) & \ldots & \psi_\sigma(\mathbf{r}_N) \\ \vdots & \vdots & \ddots & \vdots \\ \psi_\alpha(\mathbf{r}_1) & \psi_\beta(\mathbf{r}_2) & \ldots & \psi_\sigma(\mathbf{r}_N) \end{vmatrix}, \quad (5.17)$$

where the variables $\mathbf{r_i}$ include the coordinates of spin and space of particle $i$, and $\alpha, \beta, \ldots, \sigma$ encompass all possible quantum numbers needed to specify a particular system.

The single-particle function $\psi_\alpha(\mathbf{r_i})$ are eigenfunctions of the onebody Hamiltonian $\hat{h}_i$, that is

$$\hat{h}_i = h(\mathbf{r_i}) = t(\mathbf{r_i}) + u(\mathbf{r_i}),$$

with eigenvalues

$$\hat{h}_i \psi_\alpha(\mathbf{r_i}) = [t(\mathbf{r_i}) + u(\mathbf{r_i})] \psi_\alpha(\mathbf{r_i}) = \epsilon_\alpha \psi_\alpha(\mathbf{r_i}).$$

For modelling a quantum dot we will equate $\hat{h}_i$ with the single-particle Hamiltonian of the harmonic oscillator. Then the energies $\epsilon_\alpha$ are the so-called non-interacting single-particle energies, or unperturbed energies. The total energy is in this case the sum over all single-particle energies, if no two-body or more complicated many-body interactions are present.

We note again that the wave-function is antisymmetric with respect to an interchange of any two particles, as required by the Pauli principle. For an $N$-body Slater determinant we have thus (omitting the quantum numbers $\alpha, \ldots, \sigma$)

$$\Phi(\mathbf{r_1}, \mathbf{r_2}, \ldots, \mathbf{r_i}, \ldots, \mathbf{r_j}, \ldots, \mathbf{r_N}) = -\Phi(\mathbf{r_1}, \mathbf{r_2}, \ldots, \mathbf{r_j}, \ldots, \mathbf{r_i}, \ldots, \mathbf{r_N}).$$

### 5.2.3 *The approximated energy of the system*

We note $E_0$ the ground state energy. According to the variational principle (given in eq. 5.11) we have

$$E_0 \leq E[\Phi_T] = \int \Phi_T^* \hat{H} \Phi_T d\tau,$$

where we have used the shorthand $d\tau = d\mathbf{r_1}, d\mathbf{r_2}, \ldots, d\mathbf{r_N}$, and where $\Phi_T$ is a trial function which we assume to be normalized

$$\int \Phi_T^* \Phi_T d\tau = 1.$$

In the Hartree-Fock method, correlations between electrons are not taken into account and the trial function is just the Slater determinant of eq. (5.17) which can be rewritten as

$$\Phi_T(\mathbf{r_1}, \mathbf{r_2}, \ldots, \mathbf{r_N}, \alpha, \beta, \ldots, \sigma) = \frac{1}{\sqrt{N!}} \sum_p (-)^p P \Psi_\alpha(\mathbf{r_1}) \Psi_\beta(\mathbf{r_2}) \ldots \Psi_\sigma(\mathbf{r_N}) \quad (5.18)$$

$$= \sqrt{N!} \mathcal{A} \Phi_H, \quad (5.19)$$

where we have introduced the antisymmetrization operator $\mathcal{A}$ defined by the summation over all possible permutations of 2 nucleons. It is defined as

$$\mathcal{A} = \frac{1}{N!} \sum_P (-)^p \hat{P}, \tag{5.20}$$

with $p$ standing for the number of permutations. We have introduced here the so-called Hartree function, defined by the simple product of all possible single-particle functions

$$\Phi_H(\mathbf{r_1}, \mathbf{r_2}, \ldots, \mathbf{r_N}, \alpha, \beta, \ldots, \sigma) = \Psi_\alpha(\mathbf{r_1})\Psi_\beta(\mathbf{r_2}) \ldots \Psi_\sigma(\mathbf{r_N}). \tag{5.21}$$

Both $\hat{H}_0$ and $\hat{H}_1$ are invariant under all possible permutations of any two electrons and hence commute with $\mathcal{A}$

$$[\hat{H}_0, \hat{\mathcal{A}}] = [\hat{H}_1, \hat{\mathcal{A}}] = 0. \tag{5.22}$$

Furthermore, $\mathcal{A}$ satisfies

$$\mathcal{A}^2 = \mathcal{A}, \tag{5.23}$$

since every permutation of the Slater determinant reproduces it.
The expectation value of $\hat{H}_0$

$$\begin{aligned}
\langle \Phi_T | \hat{H}_0 | \Phi_T \rangle = \int \Phi_T^* \hat{H}_0 \Phi_T d\tau &= N! \int \mathcal{A}\Phi_H^* \hat{H}_0 \mathcal{A}\Phi_H d\tau \\
&= N! \int \Phi_H^* \hat{H}_0 \mathcal{A}^2 \Phi_H d\tau \\
&= N! \int \Phi_H^* \hat{H}_0 \mathcal{A}\Phi_H d\tau,
\end{aligned}$$

where we have used eq. (5.22) and ( 5.23). The next step is to replace the antisymmetrization operator by its definition in eq.(5.20) and to replace $\hat{H}_0$ with the sum of one-body operators as in eq.(5.16)

$$\int \Phi_T^* \hat{H}_0 \Phi_T d\tau = \sum_{i=1}^N \sum_P (-)^p \int \Phi_H^* \hat{h}_i \hat{P} \Phi_H d\tau.$$

The integral vanishes if two or more electrons are permuted in only one of the Hartree functions $\Phi_H$ because the individual single-particle wave functions are assumed orthogonal ($\langle \Psi_\alpha | \Psi_\beta \rangle = \delta_{\alpha\beta}$).
We obtain then

$$\int \Phi_T^* \hat{H}_0 \Phi_T d\tau = \sum_{i=1}^N \int \Phi_H^* \hat{h}_i \Phi_H d\tau.$$

The orthogonality of the single-particle functions allows us to further simplify the integral, and we arrive at the following expression for the expectation values of

the sum of one-body Hamiltonians (i.e. the expectation value of the non-interacting single particle energies)

$$\int \Phi_T^* \hat{H}_0 \Phi_T d\tau = \sum_{\mu=1}^{N} \int \Psi_\mu^*(\mathbf{r}) \hat{h} \Psi_\mu(\mathbf{r}) d\mathbf{r} = \sum_{\mu=1}^{N} \langle \mu | h | \mu \rangle. \qquad (5.24)$$

Regarding the interaction part, the expectation value of the two-body Hamiltonian is obtained in a similar manner. We have

$$\langle \Phi_T | \hat{H}_1 | \Phi_T \rangle = \int \Phi_T^* \hat{H}_1 \Phi_T d\tau = N! \int \mathcal{A} \Phi_H^* \hat{H}_1 \mathcal{A} \Phi_H d\tau,$$

which reduces to

$$\int \Phi_T^* \hat{H}_1 \Phi_T d\tau = \sum_{i<j=2}^{N} \sum_{P} (-)^p \int \Phi_H^* V(r_{ij}) \hat{P} \Phi_H d\tau,$$

by following the same arguments as for the one-body Hamiltonian. Because of the dependence on the inter-electron distance $r_{ij}$, permutations of any two electrons no longer vanish.

$$\int \Phi_T^* \hat{H}_1 \Phi_T d\tau = \sum_{i<j=2}^{N} \int \Phi_H^* V(r_{ij}) \Phi_H d\tau - \int \Phi_H^* V(r_{ij}) P_{ij} \Phi_H d\tau$$

$$= \sum_{i<j=2}^{N} \int \Phi_H^* V(r_{ij})(1 - P_{ij}) \Phi_H d\tau,$$

where $P_{ij}$ is the permutation operator that interchanges electron $i$ and electron $j$. Again we use the assumption that the single-particle wave functions are orthogonal (as eigenvectors of an hermitian operator, the Hamiltonian), and we get

$$\int \Phi^* \hat{H}_1 \Phi d\tau \quad = \tfrac{1}{2} \sum_{\mu=1}^{N} \sum_{\nu=1}^{N} \left[ \int \Psi_\mu^*(\mathbf{r_i}) \Psi_\nu^*(\mathbf{r_j}) V(r_{ij}) \Psi_\mu(\mathbf{r_i}) \Psi_\nu(\mathbf{r_j}) d\mathbf{r_i} d\mathbf{r_j} \right] \quad (5.25)$$

$$-\tfrac{1}{2} \sum_{\mu=1}^{N} \sum_{\nu=1}^{N} \left[ \int \Psi_\mu^*(\mathbf{r_i}) \Psi_\nu^*(\mathbf{r_j}) V(r_{ij}) \Psi_\mu(\mathbf{r_j}) \Psi_\nu(\mathbf{r_i}) d\mathbf{r_i} d\mathbf{r_j} \right]. \quad (5.26)$$

The first term is the so-called direct term. It is frequently also called the Hartree term, while the second is due to the Pauli exclusion principle and is called the exchange term or just the Fock term. The factor 1/2 is introduced because we now run over all pairs twice.

The last equation allows us to introduce some additional definitions. The single-particle wave functions $\Psi_\mu(\mathbf{r})$, defined by the quantum number $\mu$ and $\mathbf{r}$ (recall that $\mathbf{r}$ also includes spin degree) are defined as

$$\Psi_\alpha(\mathbf{r}) = \langle \mathbf{r} | \alpha \rangle.$$

We introduce the following shorthands for the above two integrals

$$\langle \mu\nu | V | \mu\nu \rangle = \int \Psi_\mu^*(\mathbf{r_i}) \Psi_\nu^*(\mathbf{r_j}) V(r_{ij}) \Psi_\mu(\mathbf{r_i}) \Psi_\nu(\mathbf{r_j}) d\mathbf{r_i} d\mathbf{r_j},$$

and

$$\langle \mu\nu | V | \nu\mu \rangle = \int \Psi_\mu^*(\mathbf{r_i}) \Psi_\nu^*(\mathbf{r_j}) V(r_{ij}) \Psi_\nu(\mathbf{r_i}) \Psi_\mu(\mathbf{r_j}) d\mathbf{r_i} d\mathbf{r_j}.$$

Since the interaction is invariant under the interchange of two particles it means for example that we have

$$\langle \mu\nu | V | \mu\nu \rangle = \langle \nu\mu | V | \nu\mu \rangle,$$

or in the more general case

$$\langle \mu\nu | V | \sigma\tau \rangle = \langle \nu\mu | V | \tau\sigma \rangle.$$

The direct and exchange matrix elements can be brought together if we define the antisymmetrized matrix element

$$\langle \mu\nu | V | \mu\nu \rangle_{AS} = \langle \mu\nu | V | \mu\nu \rangle - \langle \mu\nu | V | \nu\mu \rangle,$$

or for a general matrix element

$$\langle \mu\nu | V | \sigma\tau \rangle_{AS} = \langle \mu\nu | V | \sigma\tau \rangle - \langle \mu\nu | V | \tau\sigma \rangle.$$

It has the symmetry property

$$\langle \mu\nu | V | \sigma\tau \rangle_{AS} = -\langle \mu\nu | V | \tau\sigma \rangle_{AS} = \langle \nu\mu | V | \sigma\tau \rangle_{AS}.$$

The antisymmetric matrix element is also hermitian, implying

$$\langle \mu\nu | V | \sigma\tau \rangle_{AS} = \langle \sigma\tau | V | \mu\nu \rangle_{AS}.$$

With these notations we can rewrite eq.(5.25) as

$$\langle \Phi_T | \hat{H}_1 | \Phi_T \rangle = \int \Phi_T^* \hat{H}_1 \Phi_T d\tau = \frac{1}{2} \sum_{\mu=1}^{N} \sum_{\nu=1}^{N} \langle \mu\nu | V | \mu\nu \rangle_{AS}. \tag{5.27}$$

Combining eqs.(5.24) and (5.27) we obtain the energy functional

$$E[\Phi_T] = \sum_{\mu=1}^{N} \langle \mu | h | \mu \rangle + \frac{1}{2} \sum_{\mu=1}^{N} \sum_{\nu=1}^{N} \langle \mu\nu | V | \mu\nu \rangle_{AS}. \tag{5.28}$$

which we will use as our starting point for the Hartree-Fock calculations.

## 5.2.4   *The restricted Hartree-Fock equations and their self-consistent solutions*

Based on the variational method discussed in section 5.2.1, the Hartree-Fock technique aims at minimizing the energy functional given in eq. 5.28. Nevertheless obtaining an eigenvalue problem to solve is not straight forward when dealing with

many interacting particles (as shown in 5.2.1) until we do a second approximation on the interacting potential.

The Coulomb repulsion induces a two-body interaction. As we show in the following, this leads to a system of coupled single-particle equations. A way to decouple those equations is to define an *effective potential*, which is an average of the Coulomb repulsion over all the electrons of the system. That is why the Hartree-Fock method is categorized as a *mean-field approximation*.

One technique for solving this problem starts by expanding each single-particle eigenvector $\Psi_i$ in terms of any convenient complete set of single-particle states $|\alpha\rangle$:

$$\Psi_i = |i\rangle = \sum_\alpha c_i^\alpha |\alpha\rangle. \tag{5.29}$$

In our case, the complete set of single-particle states $|\alpha\rangle$ corresponds to the harmonic oscillator states. While the expansion (5.29) in general involves an infinite number of terms, we always truncate it in approximation procedures, so that we shall assume here that (5.29) is a finite sum [43].

$$\Psi_i = |i\rangle = \sum_\alpha c_i^\alpha |\alpha\rangle. \tag{5.30}$$

Introducing the expansion (5.30) in the expectation value of $\hat{H}$ (eq. 5.28), we can write

$$E[\Phi] = \langle\Phi|\hat{H}_0|\Phi\rangle + \langle\Phi|\hat{H}_1|\Phi\rangle \tag{5.31}$$

$$= \sum_{i=1}^N \langle i|h|i\rangle + \frac{1}{2}\sum_{i=1}^N\sum_{j=1}^N \langle ij|V|ij\rangle_{AS} \tag{5.32}$$

$$= \sum_{i=1}^N \sum_{\alpha\gamma} C_i^{\alpha*} C_i^\gamma \langle\alpha|h|\gamma\rangle + \frac{1}{2}\sum_{i,j=1}^N \sum_{\alpha\beta\gamma\delta} C_i^{\alpha*} C_j^{\beta*} C_i^\gamma C_j^\delta \langle\alpha\beta|V|\gamma\delta\rangle_{AS}. \tag{5.33}$$

The objective is of course to minimize the energy functional in eq. 5.31 with respect to some constraints that ensure the orthonormality of the single-particle eigenvectors. For that purpose we introduce the $\epsilon_i$ as Lagrange multipliers to ensure the constraints of orthonormality, meaning for any particle $i$ and $j$

$$\langle i|j\rangle = \delta_{ij}$$

$$\sum_{\alpha\beta} C_i^{\alpha*} C_j^\beta \underbrace{\langle\alpha|\beta\rangle}_{\delta_{\alpha\beta}} = \delta_{ij} \tag{5.34}$$

$$\sum_\alpha C_i^{\alpha*} C_j^\alpha = \delta_{ij}. \tag{5.35}$$

Then a variatonal analysis implies minimizing the Lagrangian $\Lambda$

$$\Lambda = \Lambda(C_1^\alpha, C_2^\alpha, \ldots, C_N^\alpha, \epsilon_1, \epsilon_2, \ldots, \epsilon_N) \tag{5.36}$$

$$= E[\Phi] - \sum_{i=1}^N \epsilon_i \left(\sum_\alpha C_i^{\alpha*} C_i^\alpha\right), \tag{5.37}$$

with respect to the coefficient $C_i^{\alpha *}$ (or $C_i^\alpha$).

The variational equation as defined in 5.6 leads to take the derivative of (5.36) with respect to $C_i^{\alpha *}$ and to set it to zero

$$\frac{d}{dC_i^{\alpha *}}\left[\Lambda(C_1^\alpha, C_2^\alpha, \ldots, C_N^\alpha, \epsilon_1, \epsilon_2, \ldots, \epsilon_N)\right] = 0, \quad \forall\, i \in \mathbb{N}^*$$

$$\frac{d}{dC_i^{\alpha *}}\left[E[\Phi] - \sum_{i=1}^N \epsilon_i \sum_\alpha C_i^{\alpha *} C_i^\alpha\right] = 0, \quad \forall\, i \in \mathbb{N}^*.$$

Remembering that $C_i^\alpha$ and $C_i^{\alpha *}$ can be treated as independent, we arrive at the Hartree-Fock equations (one equation for each particle $i$ in its state $|\alpha\rangle$)

$$\sum_\gamma \langle\alpha|h|\gamma\rangle\, C_i^\gamma + \sum_{j=1}^N \sum_{\beta\gamma\delta} C_j^{\beta *} \langle\alpha\beta|V|\gamma\delta\rangle_{AS}\, C_i^\gamma\, C_j^\delta = \epsilon_i\, C_i^\alpha \quad, \forall\, i \in \mathbb{N}^* \qquad (5.38)$$

The Hartree-Fock equations in (5.38) may be rewritten as

$$\sum_\gamma \langle\alpha|h|\gamma\rangle\, C_i^\gamma + \sum_\gamma \left[\sum_{j=1}^N \sum_{\beta\delta} C_j^{\beta *} \langle\alpha\beta|V|\gamma\delta\rangle_{AS}\, C_j^\delta\right] C_i^\gamma = \epsilon_i\, C_i^\alpha, \quad \forall\, i \in \mathbb{N}^*$$

$$\sum_\gamma \mathcal{O}_{\alpha\gamma}\, C_i^\gamma = \epsilon_i\, C_i^\alpha, \quad \forall\, i \in \mathbb{N}^*. \quad (5.39)$$

which shows that eq.(5.38) is a system of non-linear equations in the $C_i^\alpha$, $C_i^{\alpha *}$, since $\mathcal{O}_{\alpha\gamma}$ depends itself on the unknowns, which may be solved by an iterative procedure.

The iterative (self-consistant) procedure may be derived as follows. We define an *effective Coulomb interaction potential U* as

$$\langle\alpha|U|\gamma\rangle \equiv \sum_{j=1}^N \sum_{\beta\delta} C_j^{\beta *} \langle\alpha\beta|V|\gamma\delta\rangle_{AS}\, C_j^\delta, \qquad (5.40)$$

and calculate these matrix elements with initial values for $C_i^\alpha$, say $\delta_i^\alpha$. When we substitute the result in eq.(5.38), we get a system of linear equations in the $C_i^\alpha$; this we can now solve in the standard way. If we started with a set of $K$ states $|\alpha\rangle$, the vectors $C_i^\alpha$ are $K$-dimensional and orthogonal, and so obey

$$\sum_\alpha C_i^{\alpha *} C_j^\alpha = \delta_{ij}.$$

There are thus $K$ independent vector solutions of the linearised version of eq.(5.38),

$$\sum_\gamma \left[\langle\alpha|h|\gamma\rangle + \langle\alpha|U|\gamma\rangle\right] C_i^\gamma = \epsilon_i\, C_i^\alpha.$$

Among those solutions we select those for the $n$ lowest eigenvalues $\epsilon_i$ and substitute them back into (5.40); this provides the starting point for the next iteration.

The process is continued until self-consistency is reached, or in other words until the $C_i^\alpha$ converge within a certain approximation [43].

The Hartree-Fock equations in (5.38) may again be rewritten as

$$\sum_\gamma \langle\alpha|h|\gamma\rangle \, C_i^\gamma + \sum_\gamma \left[\sum_{j=1}^N \sum_{\beta\delta} C_j^{\beta*} \langle\alpha\beta|V|\gamma\delta\rangle_{AS} \, C_j^\gamma \, C_j^\delta\right] C_i^\gamma = \epsilon_i \, C_i^\alpha, \quad \forall \, i \in \mathbb{N}^*$$

$$\sum_\gamma \left[t_{\alpha\gamma} + \sum_{j=1}^N \sum_{\gamma,\delta=1} V_{\alpha\beta\gamma\delta} \, C_j^{\beta*} \, C_j^\delta\right] C_i^\gamma = \epsilon_i \, C_i^\alpha, \quad \forall \, i \in \mathbb{N}^*$$

$$(5.41)$$

where the two-body interaction matrix element $V_{\alpha\beta\gamma\delta}$ can be computed in advance

$$V_{\alpha\beta\gamma\delta}(ij) = \langle\alpha\beta|V(ij)|\gamma\delta\rangle_{AS}, \tag{5.42}$$

as well as the one-body part $t_{\alpha\gamma}(i)$

$$\sum_\gamma t_{\alpha\gamma}(i) = \sum_\gamma \langle\alpha|h(i)|\gamma\rangle = \epsilon_\alpha^{HO},$$

where $\epsilon_\alpha^{HO}$ are the energy eigenvalues of the one-body harmonic oscillator in state $|\alpha\rangle$ (then solution of the eigenproblem: $h_{HO}|\alpha\rangle = \epsilon_\alpha^{HO}|\alpha\rangle$).

## 5.3 Many-body perturbation corrections (MBPT)

When we start developing the expression of an excited state of the unperturbed Hamiltonian as given from the perturbation theory, it becomes complicated to write the combinations of Slater determinants in terms of permutations of occupied and unoccupied single particle orbitals. Refer to [19, 47] for an introduction to the occupation number formalism, also known as second quantization.

In this section we describe the Rayleigh-Schrödinger perturbation theory, which is the elementary time-independent perturbation theory described in most text-books [47].

Let us take the Hamiltonian to be

$$\hat{H} = \hat{H}_0 + \hat{H}',$$

but now we shall treat $\hat{H}'$ as any perturbation, such as the Coulomb interaction. We suppose that $\Phi_n$ is an eigenfunction of $\hat{H}_0$ corresponding to the eigenvalue $E_n$, that is,

$$\hat{H}_0\Phi_n = E_n\Phi_n,$$

and wish to consider the effect of the perturbation on a particular state $\Phi_0$, where

$$\hat{H}_0\Phi_0 = E_0\Phi_0.$$

We denote by $\Psi_0$ the state into which $\Phi_0$ changes under the action of the perturbation, so that $\Psi_0$ is an eigenfunction of $\hat{H}$, corresponding to the eigenvalue $E$, say

$$\hat{H}\Psi_0 = E\Psi_0.$$

Therefore $\Phi_0$ and $\Psi_0$ denote the ground states of the unperturbed and perturbed systems respectively. We thus have

$$\hat{H}'\Psi_0 = (\hat{H} - \hat{H}_0)\Psi_0 = (E - \hat{H}_0)\Psi_0, \tag{5.43}$$

so that

$$\langle\Phi_0|\hat{H}'|\Psi_0\rangle = E\langle\Phi_0|\Psi_0\rangle - \langle\Phi_0|\hat{H}_0|\Psi_0\rangle. \tag{5.44}$$

Now, since $\hat{H}_0$ is Hermitian, $\langle\Phi_0|\hat{H}_0|\Psi_0\rangle = E_0\langle\Phi_0|\Psi_0\rangle$, and substitution in (5.44) gives:

$$E - E_0 = \frac{\langle\Phi_0|\hat{H}'|\Psi_0\rangle}{\langle\Phi_0|\Psi_0\rangle}.$$

This expression is, of course, exact and independent of any particular perturbation method. However, it cannot be used immediately, because the right-hand side contains the perturbed wave function, which is unknown.

We now define a so-called *projection operator* $\mathbf{R}$ for the state $\Phi_0$ by the equation

$$\mathbf{R}\Psi = \Psi - \Phi_0\langle\Phi_0|\Psi\rangle, \tag{5.45}$$

where $\Psi$ is any function of the same variables as $\Phi_0$. This operator removes the $\Phi_0$ component of the function $\Psi$. Thus, if

$$\Psi = \sum_{n=0}^{\infty} B_n\Phi_n$$

is the expansion of $\Psi$ in terms of the functions $\Phi_n$, assumed orthonormal, we find

$$\mathbf{R}\Psi = \Psi - \Phi_0\sum_{n=0}^{\infty} B_n\langle\Phi_0|\Phi_n\rangle \tag{5.46}$$

$$= \Psi - B_0\Phi_0.$$

In particular,

$$\mathbf{R}\Phi_0 = 0. \tag{5.47}$$

If we subsitute $\mathbf{R}\Psi$ for $\Psi$ in eq.(5.45), we obtain

$$\begin{aligned}\mathbf{R}^2\Psi &= \mathbf{R}\Psi - \Phi_0\langle\Phi_0|\mathbf{R}\Phi\rangle \\ &= \mathbf{R}\Psi - \Phi_0\left(\langle\Phi_0|\Psi\rangle - \langle\Phi_0|\Phi_0\rangle\langle\Phi_0|\Psi\rangle\right) \\ &= \mathbf{R}\Psi.\end{aligned} \tag{5.48}$$

This also follows immediately from eq.(5.46) and (5.47).

We shall in future write

$$\langle\Phi_0|\Psi_0\rangle = C,$$

a constant depending upon the normalization of $\Psi_0$. Eq.(5.45) gives

$$
\begin{aligned}
\mathbf{R}(E - \hat{H}_0)\Phi_0 &= (E_0 - \hat{H}_0)\Psi_0 - \Phi_0\langle\Phi_0|E_0 - \hat{H}_0|\Psi_0\rangle \\
&= (E_0 - \hat{H}_0)\Psi_0 - CE_0\Phi_0 + \Phi_0\langle\Phi_0|\hat{H}_0|\Psi_0\rangle \qquad (5.49) \\
&= (E_0 - \hat{H}_0)\Psi_0.
\end{aligned}
$$

In other words, $\mathbf{R}$ commutes with $E_0 - \hat{H}_0$.

Now,

$$
(E_0 - \hat{H}_0)\Psi_0 = (E_0 - \hat{H} + \hat{H}')\Psi_0 = (E_0 - E + \hat{H}')\Psi_0,
$$

so that

$$
(E_0 - \hat{H}_0)\mathbf{R}\Psi_0 = \mathbf{R}(E_0 - \hat{H}_0)\Psi_0 = \mathbf{R}(E_0 - E + \hat{H}')\Psi_0,
$$

and therefore, it is possible to write [47]

$$
\mathbf{R}\Psi_0 = \frac{\mathbf{R}}{E_0 - \hat{H}_0}(E_0 - E + \hat{H}')\Psi_0 = \Psi_0 - \Phi_0\langle\Phi_0|\Psi_0\rangle,
$$

again using eq.(5.45). The perturbed wave function $\Psi_0$ thus satisfies the equation

$$
\Psi_0 = C\Phi_0 + \frac{\mathbf{R}}{E_0 - \hat{H}_0}(E_0 - E + \hat{H}')\Psi_0,
$$

which may be iterated to give

$$
\begin{aligned}
\Psi_0 &= C\Phi_0 + \frac{\mathbf{R}}{E_0 - \hat{H}_0}(E_0 - E + \hat{H}')\left(C\Phi_0 + \frac{\mathbf{R}}{E_0 - \hat{H}_0}(E_0 - E + \hat{H}')\Psi_0\right) \\
&= C\Phi_0 + \frac{C\mathbf{R}}{E_0 - \hat{H}_0}(E_0 - E + \hat{H}')\Phi_0 + \left(\frac{\mathbf{R}}{E_0 - \hat{H}_0}(E_0 - E + \hat{H}')\Psi_0\right)^2(C\Phi_0 + \dots)
\end{aligned}
$$

$$
(5.50)
$$

$$
= C\sum_{n=0}^{\infty}\left(\frac{\mathbf{R}}{E_0 - \hat{H}_0}(E_0 - E + \hat{H}')\right)^n\Phi_0.
$$

The perturbed energy can be obtained by substituting this expression in eq.(5.45), thus:

$$
E - E_0 = \sum_{n=0}^{\infty}\left\langle\Phi_0|\hat{H}'\left(\frac{\mathbf{R}}{E_0 - \hat{H}_0}(E_0 - E + \hat{H}')\right)^n|\Phi_0\right\rangle. \qquad (5.51)
$$

It will be observed that the right-hand side of this equation also contains $E$, but this is eliminated when the terms are expanded. We shall write

$$
\Delta E = E - E_0 = \Delta E^{(1)} + \Delta E^{(2)} + \Delta E^{(3)} + \dots
$$

where $\Delta E^{(m)}$, the $m^{th}$-order energy correction, contains the $m^{th}$-order power of the perturbation $\hat{H}'$. The first-order correction is the term of (5.51) with $n = 0$, that is

$$
\Delta E^{(1)} = \langle\Phi_0|\hat{H}'|\Phi_0\rangle.
$$

The second-order correction is

$$\Delta E^{(2)} = \langle \Phi_0 | \hat{H}' \frac{\mathbf{R}}{E_0 - \hat{H}_0} (E_0 - E + \hat{H}') | \Phi_0 \rangle. \tag{5.52}$$

From eq.(5.47)

$$\mathbf{R}(E_0 - E + \hat{H}') \Phi_0 = \mathbf{R}\hat{H}'\Phi_0,$$

so that (5.52) can also be written

$$\Delta E^{(2)} = \langle \Phi_0 | \hat{H}' \frac{\mathbf{R}}{E_0 - \hat{H}_0} \hat{H}' | \Phi_0 \rangle. \tag{5.53}$$

We may expand $\hat{H}'\Phi_0$ in terms of the $\Phi_n$, thus:

$$\hat{H}'\Phi_0 = \sum_{n=0}^{\infty} B_n \Phi_n.$$

The coefficient $B_n$ are obtained by multiplying both sides of this equation by $\Phi_m^*$ and integrating over the configuraiton space of the system. This gives

$$\langle \Phi_m | \hat{H}' | \Phi_0 \rangle = \sum_{n=0}^{\infty} B_n \langle \Phi_m | \Phi_n \rangle = B_m,$$

and

$$\hat{H}'\Phi_0 = \sum_{n=0}^{\infty} \langle \Phi_n | \hat{H}' | \Phi_0 \rangle \Phi_n, \tag{5.54}$$

so that

$$\mathbf{R}\hat{H}'\Phi_0 = \sum_{n=0}^{\infty} \langle \Phi_n | \hat{H}' | \Phi_0 \rangle \Phi_n,$$

which simply removes the $\Phi_0$ term from eq.(5.54). It then follows from eq.(5.53) that

$$\Delta E^{(2)} = \langle \Phi_0 | \hat{H}' \frac{1}{E_0 - \hat{H}_0} \sum_{n=0}^{\infty} \langle \Phi_n | \hat{H}' | \Phi_0 \rangle | \Phi_n \rangle$$

$$= \sum_{n=0}^{\infty} \frac{\langle \Phi_0 | \hat{H}' | \Phi_n \rangle \langle \Phi_n | \hat{H}' | \Phi_0 \rangle}{E_0 - E_n},$$

or, on the assumption that $\hat{H}'$ is Hermitian,

$$\Delta E^{(2)} = \sum_{n=0}^{\infty} \frac{|\langle \Phi_n | \hat{H}' | \Phi_0 \rangle|^2}{E_0 - E_n}. \tag{5.55}$$

This depends only upon $\hat{H}'$ and the unperturbed energy levels and wave functions.

The higher-order energy corrections may be found in the same way. For example the third-order energy correction reads
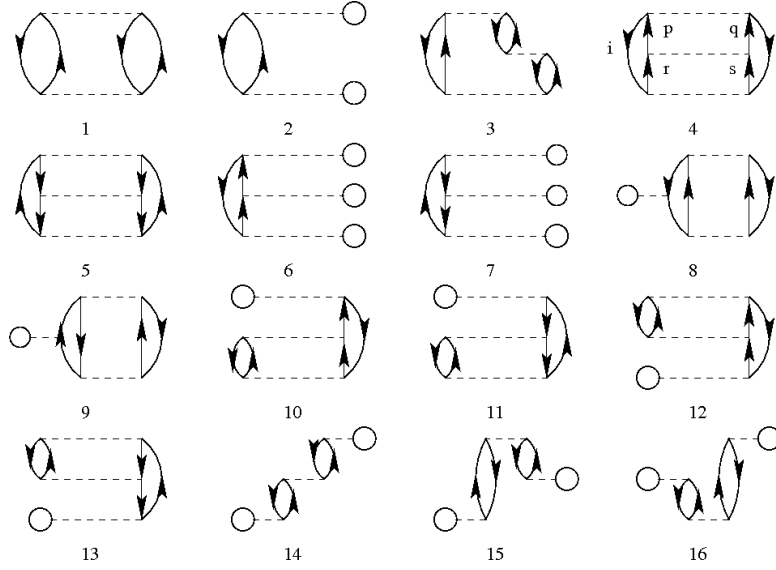
**Figure 5.3:** Antisymmetrized Goldstone diagrams through third order in perturbation theory. The dashed lines represents the interaction. Particle and hole states are represented by upward and downward arrows, respectively. The first-order diagram is omitted. All closed circles stand for a summation over hole states.(Image courtesy of M. Hjorth-Jensen)

$$\Delta E^{(3)} = \sum_{n=0}^{\infty} \sum_{n=0}^{\infty} \frac{\langle \Phi_0 | \hat{H}' | \Phi_m \rangle \langle \Phi_m | \hat{H}' | \Phi_n \rangle \langle \Phi_n | \hat{H}' | \Phi_0 \rangle}{(E_0 - E_m)(E_0 - E_n)} \qquad (5.56)$$

$$- \langle \Phi_0 | \hat{H}' | \Phi_0 \rangle \sum_{n=0}^{\infty} \frac{\langle \Phi_0 | \hat{H}' | \Phi_n \rangle \langle \Phi_n | \hat{H}' | \Phi_0 \rangle}{(E_0 - E_n)^2}.$$

When re-writing the many-body energy corrections in particle and hole state formalism, we may benefit from using the Goldstone diagrams [13]. Figure 5.3 shows all antisymmetrized Goldstone diagrams through third order in perturbation theory (we omit the first-order diagram). All closed circles stand for a summation over hole states.

In the occupation number representation, $\hat{H}'$ can be expressed in terms of anihilation $(c_i = k)$ and creation operators $(c_k^\dagger)$ as

$$\hat{H}' = \frac{1}{2} \sum_{ijkl} \langle ij|v|kl \rangle c_i^\dagger c_j^\dagger c_l c_k,$$

where

$$\langle ij|v|kl \rangle = \int \int \phi_i^*(\mathbf{x_1}) \phi_j^*(\mathbf{x_2}) v(\mathbf{x_1}, \mathbf{x_2}) \phi_k^*(\mathbf{x_1}) \phi_l^*(\mathbf{x_2}) d\mathbf{x_1} d\mathbf{x_2},$$

and the sum is over all values of $i$, $j$, $k$ and $l$.

This notation leads us to the following expression for the many-body energy

corrections

$$\Delta E^{(1)} = \langle \Phi_0 | \hat{H}' | \Phi_0 \rangle. \tag{5.57}$$

$$= \frac{1}{2} \sum_{h_1 h_2} (\langle h_1 h_2 | v | h_1 h_2 \rangle - \langle h_1 h_2 | v | h_2 h_1 \rangle)$$

$$= \frac{1}{2} \sum_{h_1 h_2} \langle h_1 h_2 | v | h_1 h_2 \rangle_{as},$$

where $h_1$ and $h_2$ are hole states.

$$\Delta E^{(2)} = \sum_{n=0}^{\infty} \frac{\langle \Phi_0 | \hat{H}' | \Phi_n \rangle \langle \Phi_n | \hat{H}' | \Phi_0 \rangle}{E_0 - E_n} \tag{5.58}$$

$$= \frac{1}{4} \sum_{h_1 h_2 p_1 p_2} \frac{|\langle h_1 h_2 | v | p_1 p_2 \rangle|^2_{as}}{\epsilon_{h_1} + \epsilon_{h_2} - \epsilon_{p_1} - \epsilon_{p_2}},$$

where $p_1$ and $p_2$ are particle states, and $\epsilon_{h_1}, \epsilon_{h_2}, \epsilon_{p_1}$ and $\epsilon_{p_2}$ are the single particle energies of the basis set.

$$\Delta E^{(3)} = \sum_{n=0}^{\infty} \sum_{n=0}^{\infty} \frac{\langle \Phi_0 | \hat{H}' | \Phi_m \rangle \langle \Phi_m | \hat{H}' | \Phi_n \rangle \langle \Phi_n | \hat{H}' | \Phi_0 \rangle}{(E_0 - E_m)(E_0 - E_n)}$$

$$- \langle \Phi_0 | \hat{H}' | \Phi_0 \rangle \sum_{n=0}^{\infty} \frac{\langle \Phi_0 | \hat{H}' | \Phi_n \rangle \langle \Phi_n | \hat{H}' | \Phi_0 \rangle}{(E_0 - E_n)^2}$$

$$= \Delta E^{(3)}_{4p-2h} + \Delta E^{(3)}_{2p-4h} + \Delta E^{(3)}_{3p-3h}, \tag{5.59}$$

where $\Delta E^{(3)}_{4p-2h}$ is the contribution to the third-order energy correction due to the 4-particle/2-hole excitations, $\Delta E^{(3)}_{2p-4h}$ is the contribution to the third-order energy correction due to the 2-particle/4-hole excitations and $\Delta E^{(3)}_{3p-3h}$ is the contribution to the third-order energy correction due to the 3-particle/3-hole excitations.

The contributions can be written as

$$\Delta E^{(3)}_{4p-2h} = \frac{1}{8} \sum_{h_1 h_2 p_1 p_2} \left( \frac{\langle h_1 h_2 | v | p_1 p_2 \rangle_{as}}{\epsilon_{h_1} + \epsilon_{h_2} - \epsilon_{p_1} - \epsilon_{p_2}} \sum_{p_3 p_4} \frac{\langle p_1 p_2 | v | p_3 p_4 \rangle_{as} \langle p_3 p_4 | v | h_1 h_2 \rangle_{as}}{\epsilon_{h_1} + \epsilon_{h_2} - \epsilon_{p_3} - \epsilon_{p_4}} \right), \tag{5.60}$$

$$\Delta E^{(3)}_{2p-4h} = \frac{1}{8} \sum_{h_1 h_2 p_1 p_2} \left( \frac{\langle h_1 h_2 | v | p_1 p_2 \rangle_{as}}{\epsilon_{h_1} + \epsilon_{h_2} - \epsilon_{p_1} - \epsilon_{p_2}} \sum_{h_3 h_4} \frac{\langle h_1 h_2 | v | h_3 h_4 \rangle_{as} \langle h_3 h_4 | v | h_1 h_2 \rangle_{as}}{\epsilon_{h_3} + \epsilon_{h_4} - \epsilon_{p_1} - \epsilon_{p_2}} \right), \tag{5.61}$$

$$\Delta E^{(3)}_{3p-3h} = \sum_{h_1 h_2 p_1 p_2} \left( \frac{\langle h_1 h_2 | v | p_1 p_2 \rangle_{as}}{\epsilon_{h_1} + \epsilon_{h_2} - \epsilon_{p_1} - \epsilon_{p_2}} \left( \sum_{h_3} \sum_{p_3} \frac{\langle h_1 h_3 | v | p_1 p_3 \rangle_{as} \langle p_3 h_2 | v | h_3 h_2 \rangle_{as}}{\epsilon_{h_1} + \epsilon_{h_3} - \epsilon_{p_1} - \epsilon_{p_3}} \right) \right), \tag{5.62}$$

where the $p_i$ denote the particle states, $h_i$ the hole states, and $\epsilon_i$ the single particle energies of the corresponfing state.

## 5.4 Variational Monte-Carlo (VMC) method

Variational Monte Carlo (VMC) is based on Quantum Monte Carlo method where the wave function is written as a function of the distance between each pair of quantum particles to explicitly include correlation between the electrons. This increases the accuracy, however the many-body integral becomes unseparable, so Monte Carlo is the only way to evaluate it efficiently.

The basic Monte Carlo strategy consists in analysing hundreds to millions of possible configurations (here: positions of the electrons) instead of few discrete scenarios. The results provide the probabilities of the different outcomes to occur. The points can be sampled with an homogeneous random distribution, or preference can be given to points located in areas where the distribution is large to obtain more accurate results and avoid wasting time in regions of low interest. This is called importance sampling. A flowchart of a typical variatonal Monte Carlo method is given in figure 5.4.

First an initial point $R$ is chosen and $\psi(R)$ is computed. Then at each step a new position $R'$ is generated by adding a random vector to $R$ (this random vector having a "drift" component towards the region of large distribution in the case of importance sampling). The Metropolis algorithm is used to check whether the move is accepted by calculating the ratio $\omega = P(R)/P(R')$. If $\omega \geq s$, where $s$ is a random number between 0 and 1, the new position is accepted, otherwise the electron stays in the same place. At the end of Monte Carlo sampling the mean energy and the standard deviation are calculated.

In VMC the variational method is used to approximate the ground state of the system. It consists in choosing a "trial wavefunction" depending on one or more parameters, and finding the values of these parameters for which the expectation value of the energy is the lowest possible. The difficulty in the VMC method is the construction of a trial wave function: it is essential to have an optimized wave function as close as possible to the exact wave function, ie it must satisfy as many known properties of the exact wave function as possible: for example it should be well defined at the origin and the derivative should be well defined too; the "cusps" of the wave function (discontinuities in the first derivative of the wave function when two charged particles come close together) can be used as constraints that the trial wave function has to respect. It is also important that the value, gradient and laplacian of the trial wave function can be efficiently computed. Different strategies are used to adjust the trial wave function: optimization of energy, variance, or a combination of both.

*Advantages of VMC* This method is relatively simple to understand and then to program. Once the trial wave function is built no further approximation is needed. With VMC you can tell how important a given correlation is by systematically adding terms to the trial wave function. In addition, you end up with an explicit form of the trial wave function which helps understanding the system.

*Disadvantages of VMC*   In order to get reliable results the trial wave function has to be optimized. However, there is nothing internal to the method that tells us when we should stop to introduce additional corrections. The optimization of the trial wave function is very time consuming, and usually it is stopped when the expected result is obtained. This brings an element of human bias, which inevitably introduces systematic errors. Therefore the VMC method may become less reliable as the physics of system gets more complex.

## 5.5   Full Configuration Interaction (FCI) method

The Hamiltonian of a N-electron system can usually be writen under the form

$$\hat{H} = \hat{H}_0 + \hat{H}', \tag{5.63}$$

where $\hat{H}_0$ is the single-particle part of the Hamiltonian and $\hat{H}'$ the two-particle part. Let $\{|\phi_i\rangle\}_{i=1}^{N_B}$ be an arbitrary complete orthonormal basis of the given truncated Hilbert space with dimension $N_B$. Then the eigenvalue equation of the Hamiltonian $\hat{H}$ can be written in the matrix representation as

$$\mathbf{Hc} = E\mathbf{c}, \tag{5.64}$$

where $\mathbf{H}$ is a matrix with the matrix elements $H_{nm} = \langle \Phi_n | \hat{H} | \Phi_m \rangle$, $\mathbf{c}$ is a vector with elements $(c_n)_{n=1}^{N_B}$, and $E$ is the energy of the system. By solving this matrix eigenvalue equation the exact solution of the Hamiltonian equation can ideally be calculated and the eigenstate $|\psi\rangle$ is the linear combination of the basis states $|\phi_i\rangle$:

$$|\psi\rangle = \sum_{i=1}^{N_B} c_i |\phi_i\rangle. \tag{5.65}$$

In real computations only a finite number of basis functions can be included. This is the most basic idea of the full configuration interaction (FCI) (*Exact or Large Scale Diagonalization*) method.

In the FCI method the basis states $|\phi_i\rangle$ are chosen to be N-electron eigenstates of the single-particle Hamiltonian $\hat{H}_0$. The basis states are Slater determinants

$$|\phi_i\rangle = Slater(\{|\varphi_j\rangle, j \in \mathcal{S}\}), \tag{5.66}$$

where the $N$ different single-particle wave functions $|\varphi_j\rangle$ are eigenstates of $\hat{H}_0$, and $\mathcal{S}$ is a set of $N$ indices chosen among totally $M$ possible states. The total number of basis states $|\phi_i\rangle$ is thus the number of possible combinations $N_B = \binom{M}{N}$. A basis function $|\phi_\alpha\rangle$ can be written in the occupation number representation as

$$|\phi_\alpha\rangle = |n_{\alpha 1}, n_{\alpha 2}, ..., n_{\alpha M}\rangle, \tag{5.67}$$

where $n_{\alpha j}$ is the number of particles in the state $j$. Pauli exclusion principle sets the restriction $n_{\alpha j} \in \{0, 1\}$ for fermions. $N$ states have to be occupied and the rest unoccupied.
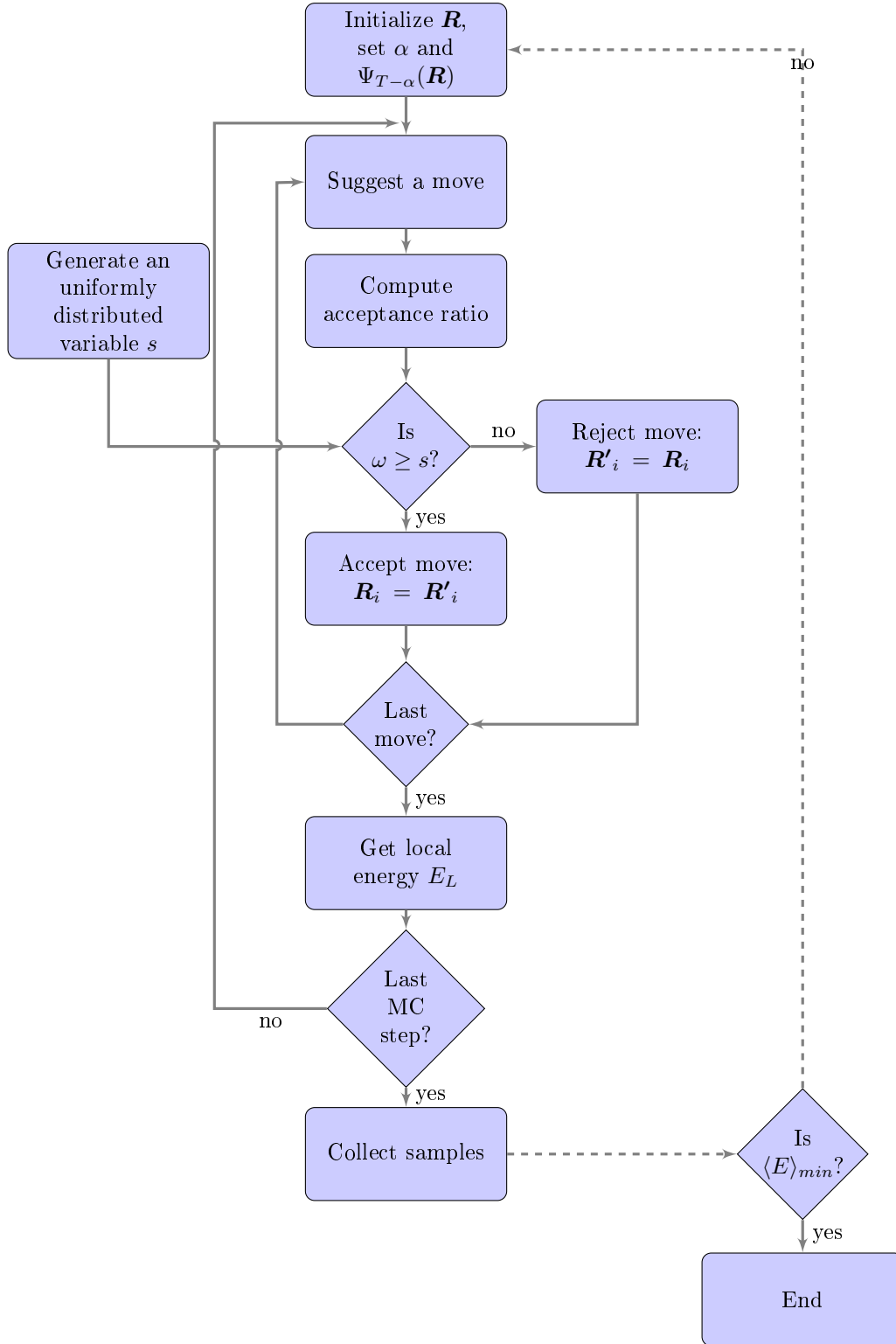
**Figure 5.4:** Flowchart of our implementation of the Hartree-Fock algorithm.
(Image courtesy of I. Vallejo Henao)

To solve the eigenvalue equation 5.64 the matrix elements $H_{nm}$ must be calculated first. In second quantization the single-particle operator can be written as [47]

$$\hat{H}_0 = \sum_{i,j} h_{ij} c_i^\dagger c_j, \tag{5.68}$$

where

$$h_{ij} = \langle i|\hat{h}|j\rangle = \int d\mathbf{r}\varphi_i^*(\mathbf{r})h(\mathbf{r})\varphi_j(\mathbf{r}). \tag{5.69}$$

The states $|i\rangle = \varphi_i(\mathbf{r})$ are single-particle basis functions and $\hat{h} = h(\mathbf{r})$ is the single-particle operator. The creation operator $c_i^\dagger$ increases the number of particles in state $i$ by 1 and the annihilation operator decreases the same by 1.

The two-particle part of the Hamiltonian can be written in the same way as the single-particle part:

$$H' = \frac{1}{2}\sum_{i,j,k,l} \langle ij|\hat{v}|kl\rangle c_i^\dagger c_j^\dagger c_k c_l, \tag{5.70}$$

where

$$\langle ij|\hat{v}|kl\rangle = v_{ijkl} = \delta_{\sigma_i,\sigma_k}\delta_{\sigma_j,\sigma_l} \int d\mathbf{r} \int d\mathbf{r}'\varphi_i^*(\mathbf{r})\varphi_j^*(\mathbf{r}')v(\mathbf{r},\mathbf{r}')\varphi_k(\mathbf{r})\varphi_l(\mathbf{r}'). \tag{5.71}$$

The states $|i\rangle$ are single-particle basis functions and $v(\mathbf{r},\mathbf{r}')$ is the two-particle operator in the coordinate representation.

As the single-particle basis functions $|i\rangle$ in this case are eigenstates of $\hat{h}$, the single-particle parts of the matrix elements are

$$H_{0\alpha\beta} = \langle\Phi_\alpha|\hat{H}_0|\Phi_\beta\rangle = \delta_{\alpha\beta}\sum_i n_{\alpha i}\epsilon_i, \tag{5.72}$$

where $\epsilon_i$ are single-particle energy eigenvalues.

The two-particle parts of the matrix elements

$$\hat{H}'_{\alpha\beta} = \langle\Phi_\alpha|\hat{H}'|\Phi_\beta\rangle, \tag{5.73}$$

can be derived using the properties of creation and annihilation operators. These elements are different sums of $v_{ijkl}$ terms multiplied by $n_{\alpha i}$ terms. More details can be found in [4].

The total number of basis functions $N_B$ can be reduced by using the symmetries of the Hamiltonian, for example fixing the z-component of the total spin and/or angular momentum. Finally the Hamiltonian matrix is diagonalized.

The most serious disadvantage of the FCI method is that the basis size grows exponentially with the number of electrons $N$ and the number of Slater determinants $M$ as $N_B = \binom{M}{N}$.

# Chapter 6

# Implementation

This chapter presents the simulator, its structure and a description of its implementation. First we give a description of the project to clarify the structure of the code implementation. Then we focus on important parts of the simulator and we finally explain how to run it in order to obtain the approximated ground state of a quantum dot.

The $C++$ language has been chosen in this project for its efficiency as a low-level language which becomes important when running expensive simulations, and for its flexibility as an object oriented language. Classes have been developed in order to reflect the independent parts of the simulator or to define global functions. We also make important use of the BLITZ++ and LPP / LAPACK libraries which provide performances on par with $Fortran$ 77/90, respectively managing dense arrays and vectors, and providing routines for linear algebra.

## 6.1 Overview

Our *simulator* [41] computes approximations to the ground state energy of quantum dots in two-dimensions using two many-body techniques: the *Hartree-Fock* method and the *many-body perturbation theory*. Both calculations are implemented in an harmonic oscillator basis, but our simulator allows also to combine the methods in order to compute the second and third order many-body perturbation corrections to the HF energy. Making use of the nice properties of the harmonic oscillator eigenstates, we developed a simple and efficient code in the *energy basis*. This means that we actually avoid to compute the matrix elements by numerical integration, but we use analytical expressions to compute them.

The current version only considers closed-shell systems where particles are trapped within an isotropic harmonic oscillator potential in two-dimensions. However the code is organized in a way to allow generalization of the problem, and more particularly the possibilities to compute the Hartree-Fock approximation of the total energy in three-dimensions, to use numerical integration for computing the matrix elements, to include different types of basis and the possibility to include different forms of the confining potential.

This short description allows us to identify the main elements of the implementation for which we built the corresponding classes: `simulator`, `HartreeFock`, `PerturbationTheory`, `singleOrbitalEnergies`. Other classes can be derived on the need for flexibility and will be detailed in the following.

The accuracy and the stability of the simulator will depend on the arbitrary set of input parameters associated to the Hartree-Fock technique (size of the basis set, precision required in the self-consistent process), and also the parameters used to model the quantum dot (the number of electrons trapped into the dot, the strength of its parabolic potential), leading to the following set of simulation parameters:

*The Fermi level $R^f$* $(R^f \in \mathbb{N} \; R^f \geq 0)$ which characterizes the number of charge-carriers trapped into the dot, since our closed-shell system "fills" the shells with electrons up to the Fermi level (i.e. in the harmonic oscillator basis: $R^f = 0 \Rightarrow 2$ electrons in the dot, $R^f = 1 \Rightarrow 6$ electrons in the dot, $R^f = 2 \Rightarrow 12$ electrons, $\cdots$).

*The size of the basis set characterized by $R^b$* $(R^b \in \mathbb{N} \; R^b \geq R^f)$ which defines the maximum shell number in the model space (i.e. the shell-truncated Hilbert space) for our Hartree-Fock computation. It implies the number of orbitals in which each single particle wavefunction will be expanded. So the bigger the basis set, the more accurate the single particle wavefunction is expected. In mathematical notation, $R^b$ and the size of the basis set $\mathcal{B}$ are defined by

$$\mathcal{B} = \mathcal{B}(R^b) = \left\{ |\phi_{nm_l}(\mathbf{r})\rangle \quad : 2n + |m_l| \leq R^b \right\}, \tag{6.1}$$

where $|\phi_{nm_l}(\mathbf{r})\rangle$ are the single orbital in the Harmonic oscillator basis with quantum numbers $n$, $m_l$ such that the single orbital energy reads: $\epsilon_{nm_l} = 2n + |m_l| + 1$ in two-dimensions.

*The confinement strength $\lambda$* $(\lambda \in \mathbb{R}^+)$ defines the strength of the Coulomb interaction. It is a dimensionless parameter which depends on the type and size of the material, and also incorporate the change in confinement strength due to an external magnetic field as described in section 4.2.3.

*The precision of the self-consistent Hartree-Fock process $\epsilon^{HF}$* $(\epsilon^{HF} \in \mathbb{R}^+)$ has default value set to $10^{-12}$ which is a good approximation with respect to the accuracy of other constants of the system (i.e. $e$, $m_e$, $a_0^*$, $\hbar$, ... whose accuracy does not undergo $10^{-12}$). This arbitrary parameter may have important consequences for the convergence of Hartree-Fock when the electron interaction becomes too high if a maximum number of iterations was not set.

## 6.2   Class implementation

This section presents a short description of the important classes implemented in our simulator.

## 6.2.1 The `simulator` *class*

Figure 6.1 is a flowchart of the overall simulator where each block corresponds to a specific function and most of the time associated to one or several classes. The `simulator` class is the main class which links all the building blocks of the simulator. It starts by initializing the parameters with the input file written in the configuration file `parameters.inp` and eventual overwrite them using arguments given in the command line. The simulator checks if the combination of parameters is correct in order to avoid any memory conflict. For example one cannot compute a 20-electron quantum dot within a model space containing only the first two shells. The model space is built by allocating memory for all the particle states and the hole states. This is done by creating an `orbitalsQuantumNumbers` object. Once the tables of states are built and containes their associated quantum numbers $n$, $m_l$ and $m_s$, the simulator is almost ready to start the Hartree-Fock algorithm.

A way to improve greatly the performance is done by computing the matrix of the two-body interactions in the harmonic oscillator basis (also called the *Coulomb matrix*) apart from the HF algorithm and to store it for all future simulation using the same model space. This is done in a specific class called `CoulombMatrix` which reads the matrix from file when it exists. Otherwise it builds it and store it to file for other simulations. The `HartreeFock` is then used to compute the Hartree-Fock approximation to the ground state energy of the quantum dot. Other outputs of the Hartree-Fock algorithm includes the HF eigenenergies, the HF eigenstates and eventually the HF matrix of the two-body interaction which can be reused as input for other *ab initio* techniques to improve their performance. Once HF has converged, the functions of the class `PerturbationTheory` can be used to compute the second and third-order many-body perturbation corrections using the new HF interaction matrix and the HF eigenenergies. Independently of the Hartree-Fock algorithm, the simulator can reuse the table of particle and hole states, as well as the Coulomb matrix in order to compute all many-body perturbation corrections up to third order directly in the harmonic oscillator basis set Therefore our simulator permits an easy comparison of the performance of both many-body techniques (HF, MBPT) and also permits to investigate the performance of HF imporved by MBPT corrections.

The overall simulation can be optimized using parallelization of the code on a cluster of nodes and using the Message-Passing Interface (MPI) to manage the communication between the nodes. This gretaly improves some bottlenecks of the simulator which are: the construction of the two-body interaction matrices and the high order terms in the many-body perturbation theory. This is implemented in our simulator using the `mpi_parameters` class. The performance of the parallelization is discussed in section 7.4.

## 6.2.2 The `orbitalsQuantumNumbers` *class*

The `orbitalsQuantumNumbers` class mainly generates the list of all possible states ($|\alpha\rangle \rightarrow |n, m_l, m_s\rangle$) in the model space up to a maximum number of shell defined by the parameter $R^b$. It also generates a list of couple of states that will be used in the computation of the two-body interactions. In order to reduce the complexity of the
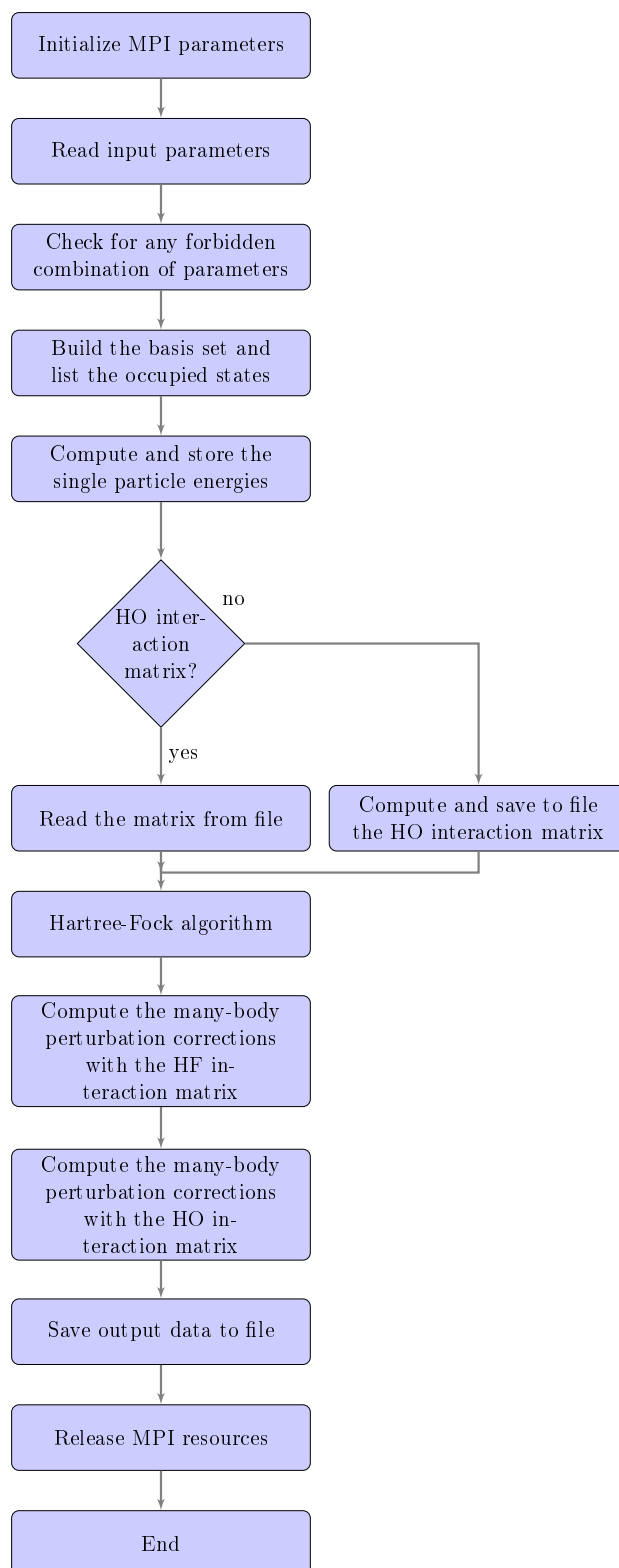
**Figure 6.1:** Flowchart of the complete simulator.

computations, we exploit invariance of the Hamiltonian with respect to angular momentum and spin. Indeed, since $[\hat{H}, \hat{L}^2] = [\hat{H}, \hat{L}_z] = 0$ and $[\hat{H}, \hat{S}^2] = [\hat{H}, \hat{S}_z] = 0$, the Hamiltonian matrix can be written as a block diagonal matrix where each block can be trated independently thus improving drastically the computation of the eigenvalue problem. This requires a function `orbitalsQuantumNumbers::sort_TableOfStates()` to organize the harmonic oscillator states with respect to their angular momentum and spin quantum numbers.

### 6.2.3 The `CoulombMatrix` class

The Coulomb matrix in our simulator corresponds to the two-body Coulomb interaction computed in the harmonic oscillator basis set:

$$V_{\alpha\beta\gamma\delta} = \langle \alpha\beta | V_{ij} | \gamma\delta \rangle_{as}.$$

This matrix will increase exponentially with respect to the size of the basis. As for the Hamiltonian, we should note that the Coulomb interaction conserves the total spin and the total angular momentum of the two-body interaction. This also requires some sorting of the table of couple of state. This is also done in the `orbitalsQuantumNumbers` class. Instead of computing the matrix element (5.42), using numerical integration, we implemented the analytical expression derived by Anisimovas and Matulis [3] (The analytical expression and its implementation is given in appendix A). The implementation requires many loops over the quantum numbers of the four states involved in the two-body interaction, and the computation of each element can really slow down the complete simulation. Therefore we implemented a way to read the direct terms from files generated from OPENFCI, an open source simulator computing the full configuration interaction ground state of quantum dots. An exhausive list of direct terms is generated with a simple modification of the `tabulate()` function provided by OPENFCI. The results are stored in an textual output file (e.g. `R06.txt` for direct terms in a model space with $R^b = 6$), which is then used by our simulator to compute the matrix elements of the Coulomb interaction. A comparison of the results obtained using the anaytical expression and using the numerical integration of OPENFCI is given in section 7.1.2.

### 6.2.4 The `HartreeFock` class

An important part of our simulator is included in the `HartreeFock` class. A flowchart of the Hartree-Fock algorithm is given in figure 6.2 which resumes the initialization of HF and iterative procedure already discussed in section 5.2.4.

While the eigenvalue problem may lead to an impracticable matrix diagonalization in a big model space, the use of symmetry and invariance greatly simplifies the problem. As we mentionned it, the construction of the Fock matrix to diagonalize and its splitting into smaller matrices depends on the block diagonal form of the Coulomb matrix, since the one-body part of the Hamiltonian is simply a diagonal matrix in the harmonic oscillator basis set.

Therefore the construction of the eigenvalue problem is really quick and easy in the energy basis once the Coulomb matrix is known. We initialize the coefficients
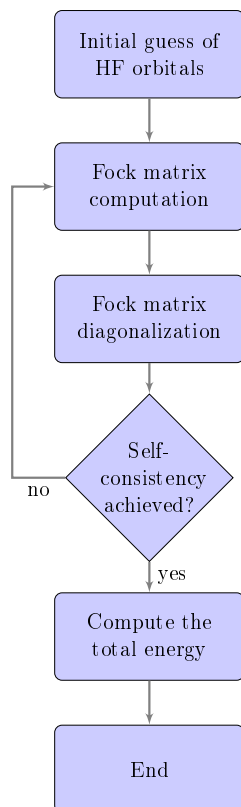
**Figure 6.2:** Flowchart of our implementation of the Hartree-Fock algorithm computing the Hartree-Fock energy, the $2^{nd}$ and $3^{rd}$-order many-body perturbation corrections to the HF energy, and the many-body perturbation corrections in the harmonic oscillator basis set from $1^{st}$ to $3^{rd}$-order.

$C_i^\alpha$ for particle $i$ such that each state below the Fermi level is occupied by one and only one particle. This corresponds to the implementation of the closed-shell model.

With this first set of coefficients, we can now compute the initial effective Coulomb potential $U$ defined in equation (5.40). The HF algorithm simply reads the harmonic oscillator energies ($|\alpha\rangle \to \epsilon_\alpha = \langle\alpha|\hat{h}|\alpha\rangle$) from the `singleOrbitalEnergies` class in order to complete the Fock matrix with elements $\mathcal{O}_{\alpha\gamma}$ defined in (5.39). In order to solve the eigenvalue problem, we implemented the class `algebra` which interfaces BLITZ++ and LAPACK and computes the Hartree-Fock eigenenergies and eigenvectors.

The function `HartreeFock::compute_Sigma()` computes the average difference between eigenvalues of two successive iterations. This provides a criteria for stopping the iterative process when compared to the precision parameter arbitrary set in the configuration file. If the eigenvalues differ from the ones of the previous iteration, the HF algorithm will use the HF eigenvectors to compute a new effective Coulomb potential $U^{(k+1)}$, which then leads to a new eigenvalue problem and so on until self-consistency is reached.

The total energy is then computed with the optimized coefficients $C_i^\alpha$ as detailed in eq.(5.31).

### 6.2.5   The `PerturbationTheory` *class*

The computation of the many-body perturbation corrections is developed in a general form, to be computed either with the eigenenergies/eigenvectors of the either the harmonic oscillator basis, or with those computed from the Hartree-Fock algorithm. We simply implemented the different many-body perturbation corrections, from $0^{th}$-order, to $3^{rd}$-order. Each correction term can be computed in any basis set, which makes it general for computing the pure many-body perturbation energy in the harmonic oscillator basis from $0^{th}$-order, to $3^{rd}$-order, or to compute only $2^{nd}$-order and $3^{rd}$-order corrections to the Hartree-Fock energy using the HF eigenstates and eigenvalues as single particle states and single particles energies. Since the second- and third-order correction terms are require many summation over the two-body interaction matrix elements, we optimized their calculation with MPI parallelization, where each node of the supercluster compute parts of the sums detailed in 5.58 and 5.60.

## 6.3   Running a simulation

Running the simulator [41] for different set of parameters is rather easy. The main program PROJECT reads the input parameters from file (`parameters.inp`) and eventually overwrite them with command line arguments before proceeding with the Hartree-Fock algorithm and the calculations of the many-body corrections. While running the executable, the Hartree-Fock approximation of the total energy is computed in a self-consistent way, followed by the many-body perturbation corrections first wihtin the Hartree-Fock basis, then in the harmonic oscillator basis. The results

are finally printed out to screen and to file.

You can either launch the simulator with default parameters included in the configuration file with:

> ./project

or overwrite some of the parameters with a set of command line arguments, like in the following example:

> ./project dim 2 Rf 1 Rb 5 lambda 1.4

which runs a simulation in two-dimensions, with particles filling the harmonic oscillator states $|n, m_l, m_s\rangle$ up to the maximum shell number $R^f = 2n + |m_l| = 1$ (including spin degeneracy), in a model space containing all harmonic oscillator states up to the maximum shell number $R^b = 5$, and finally with a confinement strength set to $\lambda = 1$.

A list of command line parameters is given in table 6.1 and an example of configuration file is given in table 6.2.

The command lines are particularly useful for production runs where the scripts can simply change the arguments in the command line in order to run a different set simulation.

| PARAMETERS | COMMAND LINE SHORTCUTS [OPTIONS] | [VALUES] |
|---|---|---|
| Dimension of the dot | `d` OR `dim` | $\{2,3\}$ |
| Size of the closed-shell model ($R^f$) | `f` OR `Rf` OR `Rfermi` | $\in \mathbb{N}$ |
| Size of the model space ($R^b$) | `b` OR `Rb` OR `R_basis` | $\in \mathbb{N}$ with $R^b \geq R^f$ |
| Dimensionless confinement strength ($\lambda$) | `lambda` OR `l` | $\in \mathbb{R}^+$ |
| SCF precision | `epsilon` OR `e` | $\in \mathbb{R}^{+*}$ |
| boolean for including the Coulomb interactions | `coulomb` OR `cp` | $\{0,1\}$ |
| boolean for computing MBPT in the harmonic oscillator basis | `perturbationTheory` OR `pt` | $\{0,1\}$ |
| boolean for computing MBPT corrections in HF basis | `HF_PT_correction` OR `HF_PT` | $\{0,1\}$ |
| boolean for reading the direct terms from OPENFCI output files | `openFCI` OR `readCI` OR `r` | $\{0,1\}$ |
| boolean for writing input/output data to file | `logInfos` OR `log` | $\{0,1\}$ |

**Table 6.1:** List of possible command line arguments for running the HF/MBPT simulator. ex.: > ./project [option1] [value1] [option2] [value2]...

```
###################################################################
# *** parameters.inp contains input parameters for the simulation of #
#     a quantum dot using closed-shell Hartree-Fock  ***               #
###################################################################

###############################
# --- model space parameters ---

dimension = 2    # [dim or d] 2D or 3D
R_basis = 3      # [Rb or b] maximum shell number for the HO basis
        set (ex. R=2n+|m| in 2D)
R_fermi = 1      # [Rf or f] Fermi level defining #electrons in the
        closed shell system
includeCoulombInteractions = yes # [coulomb or c] Switch ON/OFF the
          Coulomb piece

###############################
# --- interaction parameters ---
lambda = 1.0     # [lambda or l] strength of the interaction

###############################
# --- Hartree-Fock parameters ---
epsilon = 1e-12; # [epsilon or e] precision used for self-consistency
                  of the total energy

###############################
# --- computational parameters ---
readFromOpenFCI = yes # [openFCI or r] read single element for Coulomb
        piece from OpenFCI instead of analytical
                        expression of Rontani
perturbationTheory  = yes # compute the Perturbation theory up to 3rd order
          with the interaction expressed in the HO basis
HF_PT_correction    = yes # compute the Perturbation theory up to 3rd order
          with the interaction expressed in the HF basis

save_states         = no # write table of quantum states

save_EigValPb       = no # write the Blocks to diagonalize and the
              eigenvalues to file
```

**Table 6.2:** Example of input file configuration.

# Chapter 7

# Computational Results and Analysis

## 7.1 Validation of the simulator

The aim of this chapter is to give a critical survey of the applicability of the Hartree-Fock method and many-body perturbation theory. We apply the theory to studies of quantum dots with several electrons. We present several results for these systems and compare our calculations with exact diagonalization results where possible. We present also several validations and benchmarks of the developed codes.

### 7.1.1 Reproducing the non-interacting ground state energy

A first simple test consists in checking if the simulator reproduces the exact ground state energy for a QD with non-interacting particles. It is done by switching off the interaction (possible by setting `includeCoulombInteractions = false` in the input parameter file), or by zeroing the confinement strength $\lambda$ (also accessible from the `parameters.inp`). The expected energy is the sum over each occupied single harmonic oscillator orbital with the definite energy $\epsilon_{nm_l} = 2n + |m_l| + 1$. The results of this test are summarized in table 7.1 and correspond exactly to the ground state energy of particles trapped in a harmonic oscillator when neglecting the electron interaction.

| Basis Size $R^b$ | Particles in the Quantum dot | | | |
|---|---|---|---|---|
| | 2 $(R^f = 0)$ | 6 $(R^f = 1)$ | 12 $(R^f = 2)$ | 20 $(R^f = 3)$ |
| 0 | 2 $\hbar\omega$ | 10 $\hbar\omega$ | 28 $\hbar\omega$ | 60 $\hbar\omega$ |
| 1 | 2 $\hbar\omega$ | 10 $\hbar\omega$ | 28 $\hbar\omega$ | 60 $\hbar\omega$ |
| 2 | 2 $\hbar\omega$ | 10 $\hbar\omega$ | 28 $\hbar\omega$ | 60 $\hbar\omega$ |
| ⋮ | ⋮ | ⋮ | ⋮ | ⋮ |
| 12 | 2 $\hbar\omega$ | 10 $\hbar\omega$ | 28 $\hbar\omega$ | 60 $\hbar\omega$ |

**Table 7.1:** Ground state energy of quantum dots with non-interacting particles.

## *7.1.2 Checking the two-body interaction matrix with* OPENFCI *results*

Another test consists in comparing the Coulomb interaction matrix computed analytically in our simulator (the analytical expression is detailled in appendix A) to the numerical computation developed by S. Kvaal in his Configuration interaction simulator called "OPENFCI" [32].

The two-body interaction $V_{\alpha\beta\gamma\delta}$ is stored as a matrix and acts on two couples of single orbitals ($|\alpha\rangle$, $|\beta\rangle$), ($|\gamma\rangle$, $|\delta\rangle$):

$$
\begin{aligned}
V_{\alpha\beta\gamma\delta} &= \langle\alpha(r_i)\beta(r_j)|V(r_{ij})|\gamma(r_i)\delta(r_j)\rangle_{as} \\
&= \underbrace{\langle\alpha(r_i)\beta(r_j)|V(r_{ij})|\gamma(r_i)\delta(r_j)\rangle}_{\text{Direct term}} - \underbrace{\langle\alpha(r_i)\beta(r_j)|V(r_{ij})|\gamma(r_j)\delta(r_i)\rangle}_{\text{Exchange term}},
\end{aligned}
$$

where $V(r_{ij}) = 1/r_{ij}$ is the Coulomb interaction operator acting on particles $i$ and $j$.

It is actually possible to compare the direct term of each simulator by comparing the results of the functions that generate them: `anisimovas()` in our simulator and `singleElement()` in OPENFCI.

```
double anisimovas (const int n1, const int m1, const int n2, const int m2,
                   const int n3, const int m3, const int n4, const int m4);

double QdotInteraction::singleElement(int N1, int m1, int N2, int m2,
                                      int N1pr, int m1pr, int N2pr, int m2pr);
```

It should be noted that the quantum numbers called in both functions do not exactly correspond. Indeed if the state $|\alpha\rangle$ corresponds to both states $|n_1\,m_1\rangle$ from `anisimovas()` and $|N_1\,m_1\rangle$ from `singleElement()`, the quantum number $N$ is here defined by $N = 2n + |m|$. Therefore it is possible to call the function in OPENFCI using the quantum numbers as defined in our simulator as follow

```
singleElement(2*n1+abs(m1), m1, 2*n2+abs(m2), m2,
              2*n3+abs(m3), m3, 2*n4+abs(m4), m4);
```

Several outputs of the functions have been computed and compared (see table 7.2). The difference between the results of the functions is of the order of $10^{-15}$ or lower, showing an excellent agreement to numerical precision. The computation of these direct terms based on numerical integrations in OPENFCI is much faster than using our analytical expression, so a modification of the code has been made in order to build the Coulomb matrix of interactions by reading the values from a file previously obtained by running the `tabulate()` function of OPENFCI (see [33] for more information).

## *7.1.3 Comparison of MBPT results with a similar numerical experiment*

In a similar study of quantum dots by Waltersson [59], many-body perturbation theory (MBPT) and many-body perturbation correction to the Hartree-Fock energy are performed on an open-shell system. Whereas closed-shell and open-shell systems may not yield the same results, we try here to compare and observe our results with

| Quantum numbers | | | | | | | | Direct terms | | Difference |
|---|---|---|---|---|---|---|---|---|---|---|
| n1 | m1 | n2 | m2 | n3 | m3 | n4 | m4 | singleElement() | anisimovas() | |
| 0 | -2 | 0 | -2 | 0 | -2 | 0 | -2 | +0.71600465852496875 | +0.716004658524967640 | 1.11e-15 |
| 0 | -2 | 0 | -1 | 0 | -2 | 0 | -1 | +0.75394678572885431 | +0.753946785728855317 | 9.99e-16 |
| 0 | -2 | 0 | -1 | 0 | -1 | 0 | -2 | +0.30353701763109730 | +0.303537017631097860 | 5.55e-16 |
| 0 | -2 | 0 | 0 | 0 | -2 | 0 | 0 | +0.74415526903108020 | +0.744155269031077759 | 2.44e-15 |
| 0 | -2 | 0 | 0 | 0 | -1 | 0 | -1 | +0.27694591420398728 | +0.276945914203986898 | 3.89e-16 |
| 0 | -2 | 0 | 0 | 0 | 0 | 0 | -2 | +0.11749820037332800 | +0.117498200373328198 | 1.94e-16 |
| 0 | -2 | 0 | 1 | 0 | -2 | 0 | 1 | +0.75394678572885809 | +0.753946785728855317 | 2.78e-15 |
| 0 | -2 | 0 | 1 | 0 | -1 | 0 | 0 | +0.27694591420398728 | +0.276945914203986898 | 3.89e-16 |
| 0 | -2 | 0 | 1 | 0 | 0 | 0 | -1 | +0.16616754852239221 | +0.166167548522392211 | 0.00e+00 |
| 0 | -2 | 0 | 1 | 0 | 1 | 0 | -2 | +0.14687275046666059 | +0.146872750466660123 | 4.72e-16 |
| 0 | -2 | 0 | 2 | 0 | -2 | 0 | 2 | +0.71600465852497219 | +0.716004658524967640 | 4.55e-15 |
| 0 | -2 | 0 | 2 | 0 | -1 | 0 | 1 | +0.30353701763109858 | +0.303537017631097860 | 7.22e-16 |
| 0 | -2 | 0 | 2 | 0 | 0 | 0 | 0 | +0.11749820037332819 | +0.117498200373328198 | 0.00e+00 |
| 0 | -2 | 0 | 2 | 0 | 1 | 0 | -1 | +0.14687275046666051 | +0.146872750466660123 | 3.89e-16 |
| 0 | -2 | 0 | 2 | 0 | 2 | 0 | -2 | +0.12851365665832831 | +0.128513656658326258 | 2.05e-15 |
| 0 | -1 | 0 | -2 | 0 | -2 | 0 | -1 | +0.30353701763109730 | +0.303537017631097749 | 4.44e-16 |
| 0 | -1 | 0 | -2 | 0 | -1 | 0 | -2 | +0.75394678572885442 | +0.753946785728855317 | 8.88e-16 |
| 0 | -1 | 0 | -1 | 0 | -2 | 0 | 0 | +0.27694591420398728 | +0.276945914203986842 | 4.44e-16 |
| 0 | -1 | 0 | -1 | 0 | -1 | 0 | -1 | +0.86165346940440823 | +0.861653469404406013 | 2.22e-15 |
| 0 | -1 | 0 | -1 | 0 | 0 | 0 | -2 | +0.27694591420398728 | +0.276945914203986898 | 3.89e-16 |
| 0 | -1 | 0 | 0 | 0 | -2 | 0 | 1 | +0.27694591420398728 | +0.276945914203986842 | 4.44e-16 |
| 0 | -1 | 0 | 0 | 0 | -1 | 0 | 0 | +0.93998560298662536 | +0.939985602986624479 | 8.88e-16 |
| 0 | -1 | 0 | 0 | 0 | 0 | 0 | -1 | +0.31332853432887497 | +0.313328534328874808 | 1.67e-16 |
| 0 | -1 | 0 | 0 | 0 | 1 | 0 | -2 | +0.16616754852239229 | +0.166167548522392211 | 8.33e-17 |
| 0 | -1 | 0 | 1 | 0 | -2 | 0 | 2 | +0.30353701763109858 | +0.303537017631097749 | 8.33e-16 |
| 0 | -1 | 0 | 1 | 0 | -1 | 0 | 1 | +0.86165346940440690 | +0.861653469404406013 | 8.88e-16 |
| 0 | -1 | 0 | 1 | 0 | 0 | 0 | 0 | +0.31332853432887491 | +0.313328534328874808 | 1.11e-16 |
| 0 | -1 | 0 | 1 | 0 | 1 | 0 | -1 | +0.23499640074665628 | +0.234996400746656397 | 1.11e-16 |
| 0 | -1 | 0 | 1 | 0 | 2 | 0 | -2 | +0.14687275046666051 | +0.146872750466660123 | 3.89e-16 |
| 0 | -1 | 0 | 2 | 0 | -1 | 0 | 2 | +0.75394678572885776 | +0.753946785728855317 | 2.44e-15 |
| 0 | -1 | 0 | 2 | 0 | 0 | 0 | 1 | +0.27694591420398717 | +0.276945914203986898 | 2.78e-16 |
| 0 | -1 | 0 | 2 | 0 | 1 | 0 | 0 | +0.16616754852239229 | +0.166167548522392211 | 8.33e-17 |
| 0 | -1 | 0 | 2 | 0 | 2 | 0 | -1 | +0.14687275046666059 | +0.146872750466660123 | 4.72e-16 |

**Table 7.2:** Comparison of a few Direct terms $\langle n_1\, m_1, n_2\, m_2 | V(r_{ij}) | n_3\, m_3, n_4\, m_4 \rangle$ computed using numerical integration within OPENFCI, or computed from an analytical expression within our simulator

these calculations. Therefore we aim at reproducing a study of the convergence of the second order perturbation correction to the Hartree-Fock energy as a function of the basis size. In his open-shell model, Waltersson represents the basis size either by $max(n)$ or $max(|m_l|)$, whereas in our closed-shell model both $max(n)$ and $max(|m_l|)$ depend on the value of the maximum shell number $R^b$ which are here

$$max(n) = floor(R^b/2), \tag{7.1}$$

$$max(|m_l|) = R^b. \tag{7.2}$$

The convergence of the second order many-body perturbation correction as a function of the basis size by Waltersson is given in figure 7.1 while our reproduction is given in figure 7.2.

The two figures look similar in shape and values. However, the results from Waltersson are slightly shifted to lower values when the size of the basis increases which could represent a better correction to the positive Hartree-Fock energy. This shift probably results from the different shell models.
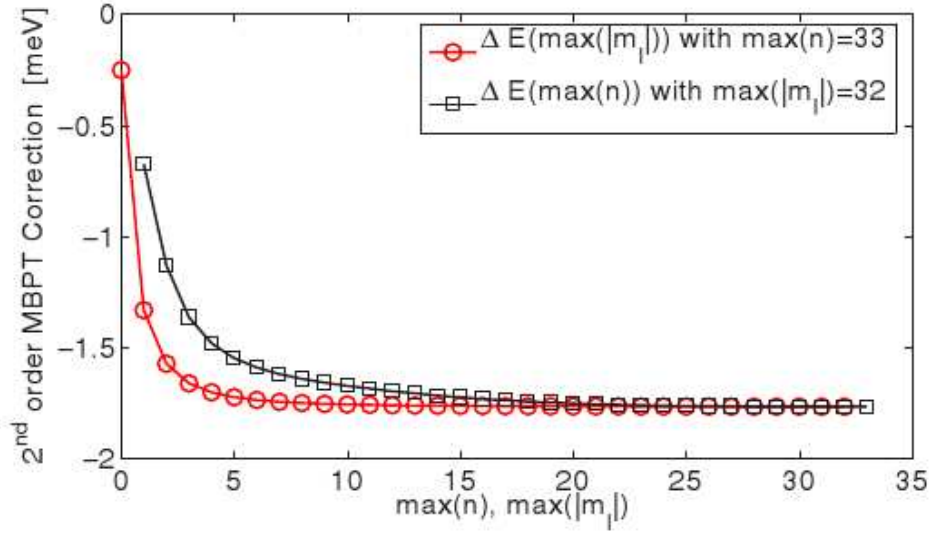
**Figure 7.1:** Second-order perturbation theory correction to the energy as a function of $max(n)$ (squares) and $max(|m_l|)$ (circles) for the two electron dot with the confinement strength $\hbar\omega = 6\,meV$. [59]
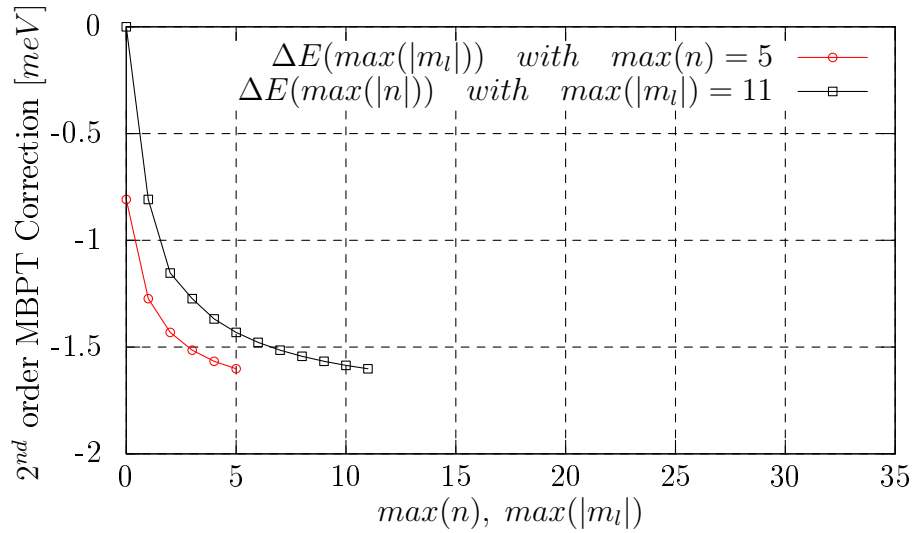


**Figure 7.2:** Second-order perturbation theory correction to the energy as a function of $max(n)$ (squares) and $max(|m_l|)$ (circles) for the two electron dot with the confinement strength $\hbar\omega = 6\,meV$ which translates into a dimensionless confinement strength of $\lambda = 1.406$ using the same material characteristics of GaAs than Waltersson in [59].

## 7.2 Restrictions to the closed-shell model

### 7.2.1 Limits of the model through a theoretical approximation

In this section we will show the theoretical limit of our closed-shell model as function of the strength of the external magnetic field. This is supposed to provide a theoretical upper bound to the external magnetic field, above which the electronic structure is not anymore correctly represented by the particles filling all the shells up to the Fermi level, but possibly by a new structure where the total spin or total angular momentum might differ from zero.

When neglecting the repulsions between the particles, the eigenenergies $\epsilon_{n\,m_l}$ as a function of the magnetic field $B$ can be solved analytically for a parabolic confining potential $V(r) = 1/(2m^*\omega_0^2 r^2)$ leading to a spectrum known as the Fock-Darwin states [14, 31]

$$\epsilon_{n\,m_l} = (2n + |m_l| + 1)\,\hbar\omega - \frac{1}{2}\hbar\omega_c\,m_l \tag{7.3}$$

$$= (2n + |m_l| + 1)\,\hbar\omega_0\sqrt{1 + \frac{\omega_c^2}{4\omega_0^2}} - \frac{1}{2}\hbar\omega_c\,m_l, \tag{7.4}$$

where $\hbar\omega_0$ is the electrostatic confinement strength, and $\omega_c = e\,B/m^*$ is the cyclotron frequency. Each state $|n, m_l\rangle$ is spin-degenerate.

Rewriting the eigenenergies in units of $\hbar\omega_0$, $\epsilon_{n\,m_l}$ becomes dimensionless and we obtain

$$\epsilon_{n\,m_l} = (2n + |m_l| + 1)\sqrt{1 + \frac{(\omega_c/\omega_0)^2}{4}} - \frac{1}{2}(\omega_c/\omega_0)\,m_l \tag{7.5}$$

$$= (2n + |m_l| + 1)\sqrt{1 + (\frac{eB}{2m^*\omega_0})^2} - \frac{eB}{2m^*\omega_0}\,m_l. \tag{7.6}$$

These eigenenergies are plotted in figure 7.3 as function of the magnetic field. The orbital degeneracies at $B = 0$ are lifted in a magnetic field. As $B$ increases, a single-particle state with a positive or negative angular momentum ($m_l$) shifts to lower or higher energy, respectively. The lowest energy state $|n, m_l\rangle = |0, 0\rangle$ is a two-fold spin degenerate (The Zeeman spin-splitting in a magnetic field is neglected). The next state has a double orbital degeneracy, $\epsilon_{0,1} = \epsilon_{0,-1}$. This degeneracy forms the second shell, which can contain up to four electrons when we include the two-fold spin degeneracy. It will be filled for $N = 6$. The third shell has a triple-orbital degeneracy formed by $|1, 0\rangle$, $|0, 2\rangle$ and $|0, -2\rangle$ so that it can hold up to six electrons. This shell leads to the magic number $N = 12$.

When the magnetic field is increased, the electron occupying the highest energy state is forced into different orbitals states. As an example, consider a seven non-interacting electrons system. The transitions for the state of the $7^{th}$ electron is indicated in figure 7.3 by a thicker line. At low $B$, the highest occupied state is $|0, 2\rangle$, which decreases in energy with $B$. At some point it crosses the increasing energy state $|0, -1\rangle$. With a slightly higher magnetic field, $|0, 2\rangle$ has now a lower
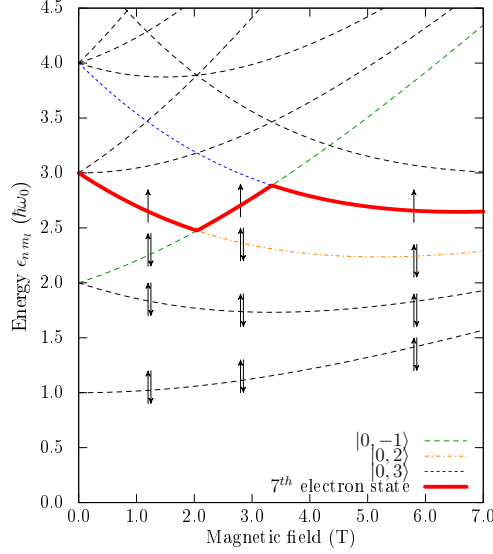
**Figure 7.3:** Spectrum of Fock-Darwin orbitals for a system of seven non-interacting particles with typical values for GaAs: confinement energy $\hbar\omega_0 = 5meV$, relative permittivity $\epsilon_r = 12$, effective mass $m^* = 0.067m_e$.

energy than $|0, -1\rangle$. This forces the electrons to switch states and it ends up with two electrons in state $|0, 2\rangle$ and only one in state $|0, -1\rangle$. For $\hbar\omega_0 = 3meV$ this occurs at $B \simeq 2.1\,T$. The seventh electron makes a second transition into the state $|0, 3\rangle$ at $2\,T$. Similar transitions are also seen for different numbers of particles and with an increasing number of crossings for larger systems. After the last crossing the electrons occupy states forming the so-called, lowest orbital Landau level. These states are characterized by the quantum numbers $(0, m_l)$ with $m_l \geq 0$.

Considering such transitions, we see that increasing the magnetic field will change the shell structure of our system and we may wonder what happens to the closed-shell model. The closed-shell system is described by a single Slater determinant. Therefore any new configuration implying the occupation of a state with an energy higher than the Fermi level would break it. Since our simulator is based on a single Slater determinant, our shell structure is initialized and kept with particles occupying the lowest states identical to those with a zero magnetic field. Therefore any transition from an occupied state to an "excited" state (non-occupied state when $B$ was low or null) will mark the end of the model. In this case the total angular momentum $M$ or total spin $S$ may change from zero to a positive value, the single particle energies associated with the new occupied states will switch to a higher value, and our complete computation of the ground state with constant non-interacting eigenenergies, zero total angular momentum and zero total spin fails.

Figures 7.4 and 7.5 display with thick lines the different transitions of states when the magnetic field is increased respectively for a six- and twelve-particle quantum dot. For the six-particle dot we see for example that the two electrons in the $3^{rd}$ shell (figure (7.4)) are in the state $|0, -1\rangle$ without magnetic field, but switch to the state $|0, 3\rangle$ when the magnetic field exceeds 2.1 $T$, whereas electrons in the first and second shell stay respectively in the states $|0, 0\rangle$ and$|0, 1\rangle$, even under a high magnetic field.
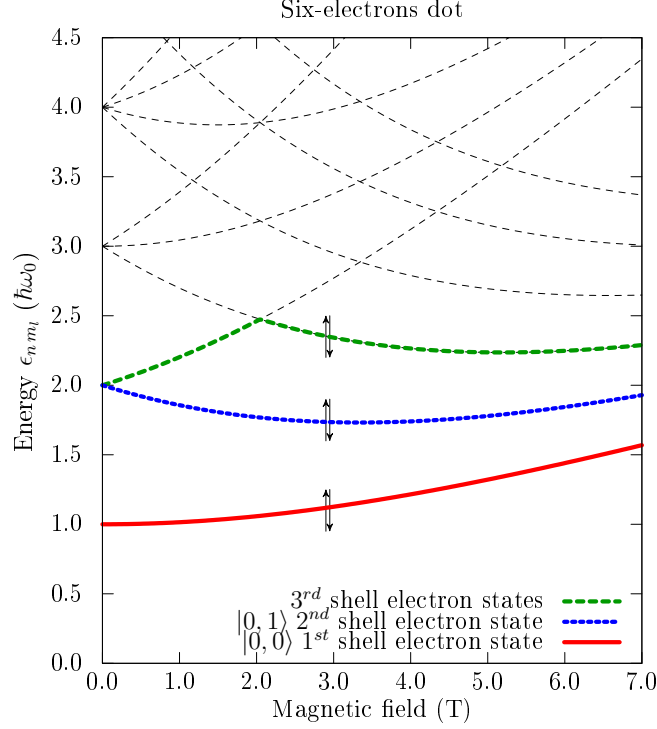
**Figure 7.4:** Spectrum of Fock-Darwin orbitals for a system with six non-interacting particles and using typical values for GaAs: confinement energy $\hbar\omega_0 = 5meV$, relative permittivity $\epsilon_r = 12$.

Therefore a theoretical study of the Fock-Darwin orbitals predicts that our model should be restricted to a maximum $B$ field of $2.1\,T$ for a six-particle dot, and $1.2\,T$ for a twelve-particle dot. In the quantum dot model the parameter is not $B$ but the dimensionless confinement strength parameter $\lambda$, which is related to $B$ by the following expression (see section 4.2.3)

$$\lambda(B) = \frac{1}{a_0^*} \left( \frac{4\hbar^2}{4\omega_0^2 m^* + e^2 B} \right)^{1/4} . \tag{7.7}$$

Considering a material like GaAs (with typical values $\hbar\omega_0 = 5meV$, $m^* = 0.067m_e$ and $\epsilon_r = 12 \Rightarrow a_0^* = 9.47 \times 10^{-9}m$), this gives $\lambda \geq 1.543$ for a six-particle dot, and $\lambda \geq 1.575$ for a twelve-particle dot, and no lower bound for $\lambda$ (i.e. no upper bound for $B$) in the case of a two-particle dot as summarized in table 7.3. Note that a refrigerator magnet has a magnetic field of about $5\ mT$, magnetic resonance imaging (MRI) field strengths range from $1.5\ T$ to $3\ T$, while an NMR spectrometer works with a field strength of $11.7\ T$. Higher strengths can be achieved: for example $16\ T$ are necessary to levitate a frog and the strongest continuous magnetic field yet produced in a laboratory is about $45\ T$. This gives a rough idea of the domain of application of the closed shell model for the simulation in laboratory experiments.

However, the above analysis does not take into account the repulsion between the electrons. This repulsion will change the shell structure and obviously the limitations on $B$ and $\lambda$ mentioned previously. As seen in section 4.2.3 the characteristic length $l$
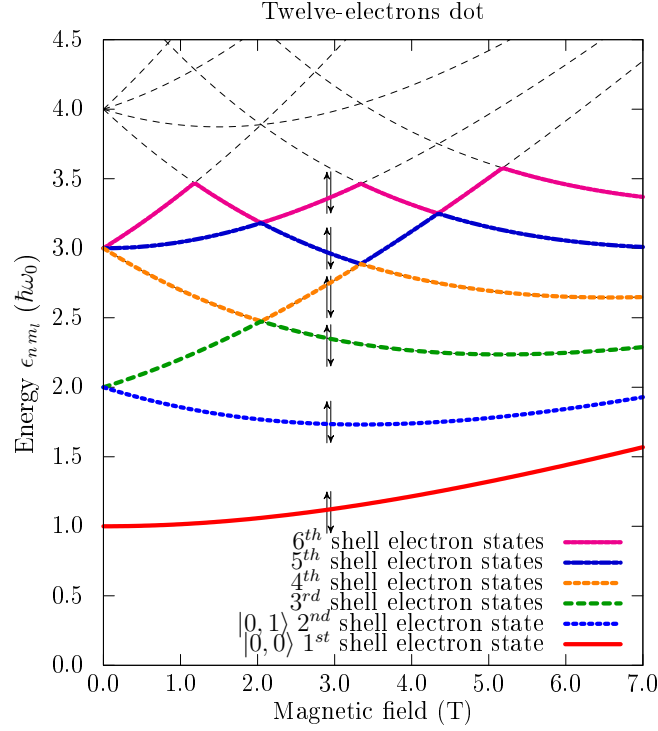
**Figure 7.5:** Spectrum of Fock-Darwin orbitals for a system with twelve non-interacting particles and using typical values for GaAs: confinement energy $\hbar\omega_0 = 5meV$, relative permittivity $\epsilon_r = 12$.

| Nb. of electrons | Maximum $B$ field | Minimum confinement strenght $\lambda$ |
|---|---|---|
| 2 | $\infty$ | 0 |
| 6 | 2.1 T | 1.543 |
| 12 | 1.2 T | 1.575 |
| 20 | 0.85 T | 1.583 |

**Table 7.3:** Restriction on $\lambda$ and $B$ for a valid closed-shell model

decreases with an increasing magnetic field, indicating that the confinement becomes stronger for larger $B$. This is also observed as a shrinking of the wavefunctions [28]. The effect is that when $B$ is increased, two electrons occupying the same state will be pushed closer together. The decreasing distance between the electrons will increase the Coulomb interactions which may change the electron configuration. This would cause a breakdown of the closed-shell model and eventually may result in wrong predictions by our Hartree-Fock technique. Numerical calculations which include the electron interactions are then necessary to build an accurate shell structure as a function of the magnetic field. This is done in the next section using full configuration interaction.

### 7.2.2 Limits of the closed-shell model better approximated with full configuration interaction

It was a rough approximation to neglect the Coulomb interaction as we did in the previous study of the Fock-Darwin orbitals. A more realistic study of the reliability of the closed-shell model requires to take these interactions into account. However, as discussed in chapter 5, only numerical methods are able to provide approximations to the ground state energy of a general quantum dot. Among *ab initio* methods, full configuration interaction provides normally the best approximation to the ground state because it considers almost all possible excitations within a given space.

In this section results of full configuration interaction are produced and discussed in order to find the real limits of the closed shell model when including the electron-electron interactions.

With a two-electron quantum dot, it is likely that the ground state remains characterized by the two electrons lying in the first shell $(n, m_l) = (0, 0)$ when increasing the magnetic field up to the maximum values achievable in laboratory.

For 6 electrons, the closed-shell model with the six electrons occupying the first levels $(n, m_l) = \{(0, 0), (0, 1), (0, -1)\}$ might not always be the optimal electron configuration as the magnetic field increases. This is what we tried to show by using the OPENFCI (full configuration interaction) simulator and running it for different electron configurations. Taking as minimum input parameters the number of particles $N$, the total angular momentum $M$, the total spin $S$ and the confinement strength $\lambda$, this simulator computes the first minimum eigenenergies (the lowest one being the ground state energy of the system) using large scale diagonalisation.

Figures 7.6, 7.7 and 7.8 show the ground state energies of a **six-particle** quantum dot for various combinations of $M$ and $S$, each plot corresponding to different confinement strength $\lambda = \{0.1, 0.5, 1, 2\}$ in figure 7.6 and $\lambda = \{5, 10, 20, 50\}$ in figure 7.7 respectively from top to bottom. By finding the exact minimum through all possible combinations of $(M, S)$ 7.6 and 7.7, we discovered that $(M, S) = (0, 0)$ is the lowest ground state energy for a six-particle dot up to a confinement strength $\lambda = 10$, whereas with $\lambda = 15$, the prefered electron configuration exhibits $(M, S) = (1, 2)$.

In spite of the trend of the ground state energy in the 3D plots as a function of $M$ and $S$, it might not be easy to distinguish which combination $(M, S)$ gives the lowest energy. Tables 7.4 and 7.5 list the energies corresponding to each combination and the lowest energy for each value of the confinement strength $\lambda$ is highlighted in bold face.
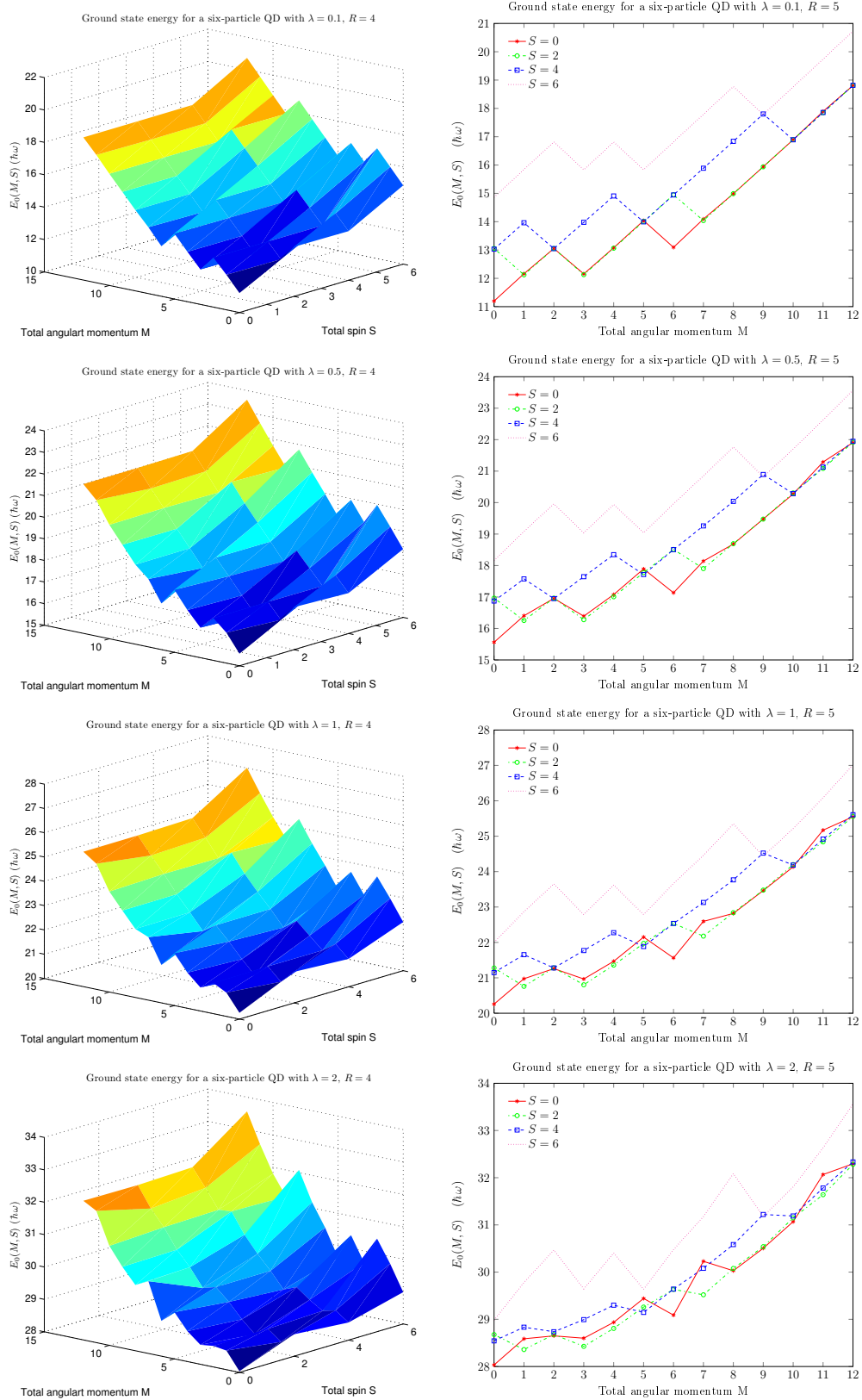
**Figure 7.6:** Ground state energies for a six-particle QD computed using OPENFCI as a function of the total spin $S$ and total angular momentum $M$. Each plot corresponds to a given value of the confinement strength $\lambda = 0.1$, $0.5$, $1$ and $2$. Up to the dimensionless confinement strength $\lambda = 2$, the lowest energy state is obtained for the configuration $(M, S) = (0, 0)$, validating thereby the closed-shell model up to $\lambda = 2$.
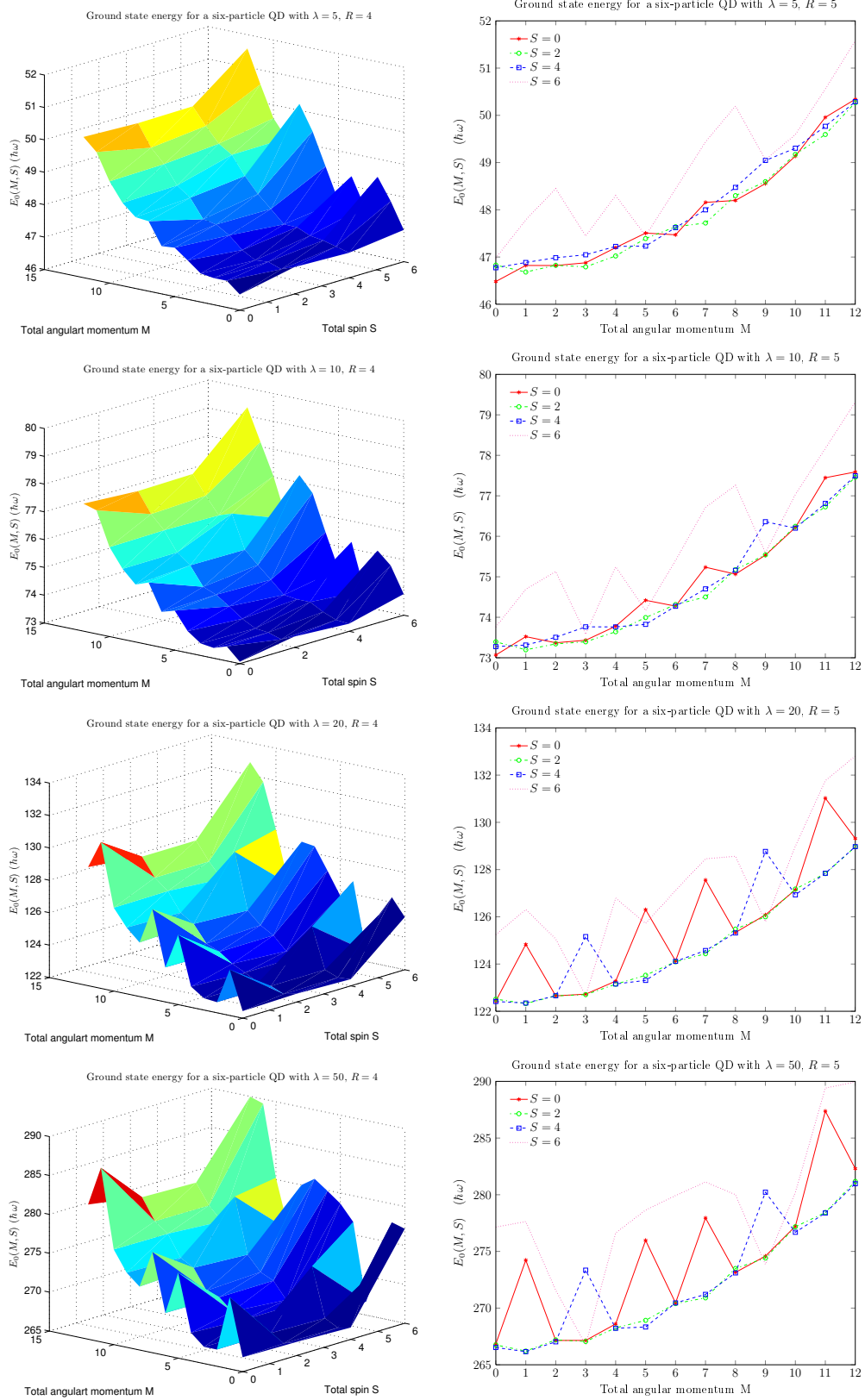
**Figure 7.7:** Ground state energies for a six-particle QD computed using OPENFCI as a function of the total spin $S$ and total angular momentum $M$. Each plot corresponds to a given value of the confinement strength $\lambda = 5$, $10$, $20$ and $50$. One can observe that the lowest energy is not anymore obtained for $(M, S) = (0, 0)$ as the confinement strength increases. This is a demonstration that the closed-shell model breaks at least from $\lambda = 20$ and that we cannot trust it anymore for confinement strength higher than $\lambda = 10$.
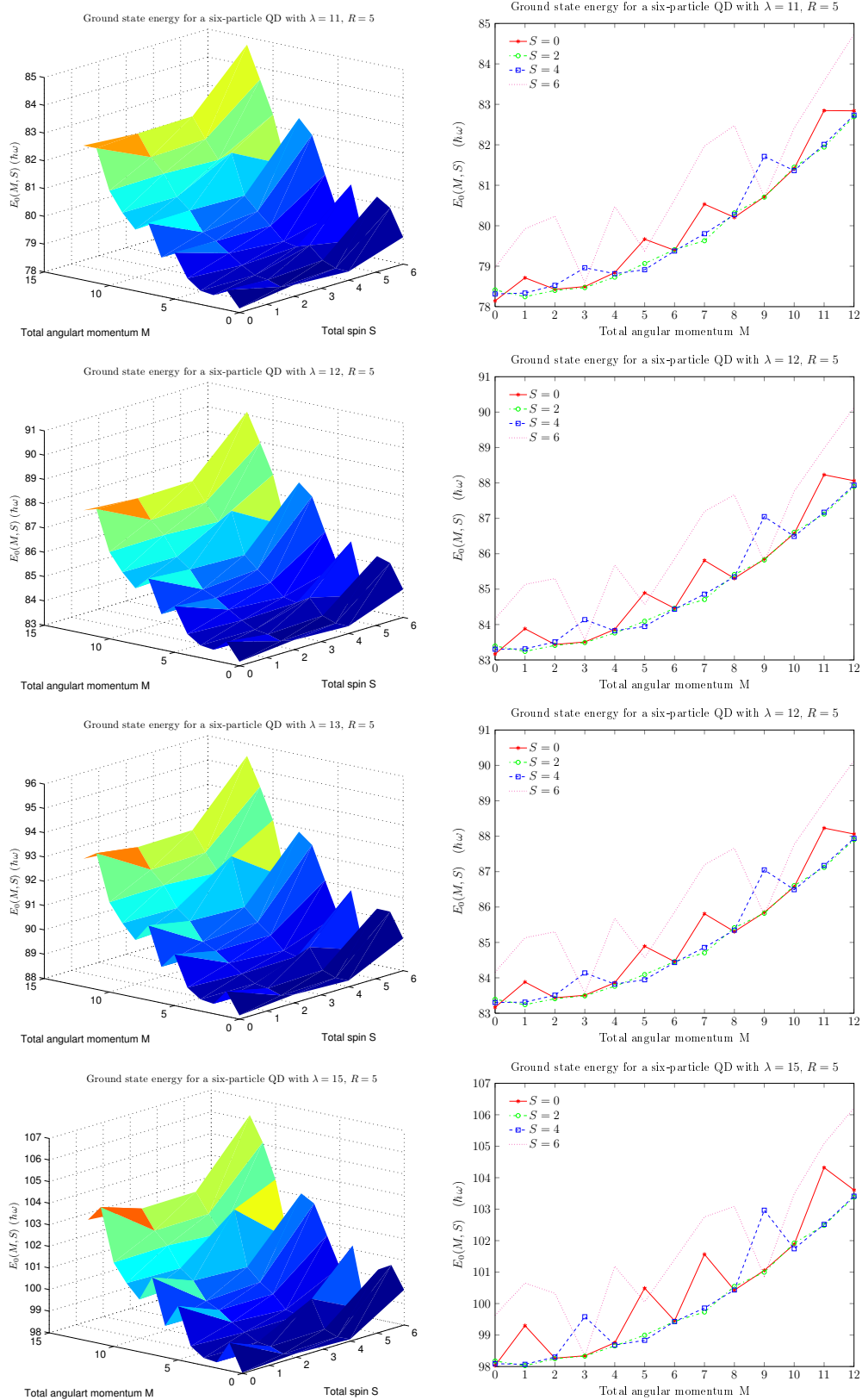
**Figure 7.8:** Ground state energies for a six-particle QD computed using OPENFCI as a function of the total spin $S$ and total angular momentum $M$. Each plot corresponds to a given value of the confinement strength $\lambda = 11, 12, 13$ and $15$. This figure shows that the first change in the electronic configuration from $(M, S) = (0, 0)$ occurs for $13 < \lambda \leq 15$. We can conclude that the closed-shell model cannot be trusted for $\lambda \geq 13$.

| | | Energy in unit of $\hbar\omega$ of a **six-particle** dot obtained for each combination of ($M$,$S$ and $\lambda$) | | | | | | |
|---|---|---|---|---|---|---|---|---|
| $\lambda$ | $M$ | $S=0$ | $S=1$ | $S=2$ | $S=3$ | $S=4$ | $S=5$ | $S=6$ |
| | 0 | **11.1978891344** | − | 13.0565458509 | − | 13.0306198232 | − | 14.8617426362 |
| | 1 | 12.161788636 | − | 12.1228998086 | − | 13.9619523669 | − | 15.8438291847 |
| | 2 | 13.0541409412 | − | 13.0543696462 | − | 13.0479092548 | − | 16.8150801525 |
| | 3 | 12.1565732709 | − | 12.1286041835 | − | 13.9783634734 | − | 15.8336957766 |
| | 4 | 13.0808492317 | − | 13.0642360558 | − | 14.9084543531 | − | 16.8102750026 |
| | 5 | 14.0377732477 | − | 14.0097760564 | − | 13.9937294856 | − | 15.8342807494 |
| 0.1 | 6 | 13.0936355988 | − | 14.9480199174 | − | 14.944795351 | − | 16.8159076585 |
| | 7 | 14.0939135823 | − | 14.0386678117 | − | 15.8883056992 | − | 17.7896003155 |
| | 8 | 14.9868752972 | − | 14.9897402773 | − | 16.8362996072 | − | 18.7685556996 |
| | 9 | 15.941652286 | − | 15.9381674099 | − | 17.8024364205 | − | 17.7820000116 |
| | 10 | 16.8929103322 | − | 16.8993329996 | − | 16.8911751901 | − | 18.7560481367 |
| | 11 | 17.8934864395 | − | 17.8470437348 | − | 18.8557578353 | − | 19.7384254286 |
| | 12 | 18.8059869671 | − | 18.8084023637 | − | 18.8153875945 | − | 20.7254199174 |
| | 0 | **15.5617751019** | − | 16.966166432 | − | 16.871772355 | − | 18.1622424979 |
| | 1 | 16.4044292865 | − | 16.2537138896 | − | 17.5752283136 | − | 19.0834975974 |
| | 2 | 16.9555562338 | − | 16.9636785505 | − | 16.9488349783 | − | 19.9589980355 |
| | 3 | 16.3909605917 | − | 16.279069572 | − | 17.6459810924 | − | 19.0380846039 |
| | 4 | 17.077692629 | − | 17.0081494281 | − | 18.345626646 | − | 19.9390056216 |
| | 5 | 17.8923198765 | − | 17.7746900892 | − | 17.7147205056 | − | 19.0403232195 |
| 0.5 | 6 | 17.1345648299 | − | 18.5115121013 | − | 18.5052825396 | − | 19.9636653826 |
| | 7 | 18.1412125077 | − | 17.9027034622 | − | 19.2596187485 | − | 20.8466577601 |
| | 8 | 18.6823740646 | − | 18.6940902667 | − | 20.0384606413 | − | 21.765094962 |
| | 9 | 19.4781018652 | − | 19.4754973684 | − | 20.8935077402 | − | 20.8207439572 |
| | 10 | 20.272873974 | − | 20.3068987984 | − | 20.2841911217 | − | 21.6997487647 |
| | 11 | 21.2895239718 | − | 21.0858286183 | − | 21.1290221438 | − | 22.623042277 |
| | 12 | 21.9075379553 | − | 21.9160281905 | − | 21.9475742808 | − | 23.5741455919 |
| | 0 | **20.2571791113** | − | 21.2789981289 | − | 21.1483419586 | − | 22.0022205941 |
| | 1 | 20.9749296631 | − | 20.7598331889 | − | 21.6538800561 | − | 22.8661695662 |
| | 2 | 21.2599579854 | − | 21.2821095699 | − | 21.2792687299 | − | 23.6550135103 |
| | 3 | 20.9671026881 | − | 20.8035334518 | − | 21.7707471281 | − | 22.7866733195 |
| | 4 | 21.4667705078 | − | 21.359594087 | − | 22.2749375665 | − | 23.6214565309 |
| | 5 | 22.150155073 | − | 21.9721573278 | − | 21.884399932 | − | 22.7881516577 |
| 1 | 6 | 21.5630576706 | − | 22.5351676942 | − | 22.5364737402 | − | 23.663506028 |
| | 7 | 22.5942511253 | − | 22.1780128424 | − | 23.1282803854 | − | 24.4604431194 |
| | 8 | 22.8188269396 | − | 22.8406352537 | − | 23.7672441229 | − | 25.3487993204 |
| | 9 | 23.4647807574 | − | 23.4774102878 | − | 24.5237438226 | − | 24.437111507 |
| | 10 | 24.1348663101 | − | 24.1974193667 | − | 24.1850198476 | − | 25.2140293553 |
| | 11 | 25.1712359394 | − | 24.8418490148 | − | 24.9187878288 | − | 26.0851798722 |
| | 12 | 25.5513885819 | − | 25.5581213564 | − | 25.6071999655 | − | 27.0164861198 |
| | 0 | **28.0329550231** | − | 28.6765243777 | − | 28.5433569395 | − | 28.9829490384 |
| | 1 | 28.5875104818 | − | 28.3590590553 | − | 28.8329004272 | − | 29.7800781342 |
| | 2 | 28.6493239207 | − | 28.6775309794 | − | 28.7364010594 | − | 30.4662810353 |
| | 3 | 28.5996827157 | − | 28.4274289424 | − | 28.9932495629 | − | 29.644371783 |
| | 4 | 28.9358749584 | − | 28.8071713271 | − | 29.2994140078 | − | 30.4045371792 |
| | 5 | 29.4418369302 | − | 29.2587757025 | − | 29.1463913256 | − | 29.6368235281 |
| 2 | 6 | 29.0891272881 | − | 29.6336201736 | − | 29.6403711077 | − | 30.4767147494 |
| | 7 | 30.2288380451 | − | 29.5200135448 | − | 30.0805742171 | − | 31.1766133172 |
| | 8 | 30.0290919414 | − | 30.0780756092 | − | 30.5833574696 | − | 32.0854456593 |
| | 9 | 30.5051303098 | − | 30.5382881767 | − | 31.2206550065 | − | 31.1827194217 |
| | 10 | 31.0686354739 | − | 31.149558625 | − | 31.1891682104 | − | 31.804014365 |
| | 11 | 32.0668783868 | − | 31.6399906569 | − | 31.7814747312 | − | 32.6329816775 |
| | 12 | 32.2950020122 | − | 32.2812570977 | − | 32.3335540202 | − | 33.5602013595 |

**Table 7.4:** Ground state energies in units of $\hbar\omega$ obtained with OPENFCI which implements the full configuration interaction method (with the maximum shell number $R = 5$). The ground state energy for each value of the confinement strength $\lambda = \{0.1, 0.5, 1, 2\}$ is boldfaced, showing the lowest energy configuration with respect to the total angular momentum $M$ and total spin $S$.

| λ | M | Energy in unit of $\hbar\omega$ of a six-particle dot obtained for each combination of ($M$,$S$ and $\lambda$) | | | | | | |
|---|---|---|---|---|---|---|---|---|
| | | $S = 0$ | $S = 1$ | $S = 2$ | $S = 3$ | $S = 4$ | $S = 5$ | $S = 6$ |
| 5 | 0 | **46.4816466894** | — | 46.8289419415 | — | 46.7729495876 | — | 46.9796295496 |
| | 1 | 46.821461584 | — | 46.6822362309 | — | 46.8843337823 | — | 47.7848726408 |
| | 2 | 46.8201453068 | — | 46.8249059264 | — | 46.9848775309 | — | 48.4486722898 |
| | 3 | 46.8779563634 | — | 46.7912636224 | — | 47.0478259205 | — | 47.4454818065 |
| | 4 | 47.1987202116 | — | 47.0226098251 | — | 47.2249177042 | — | 48.3011580081 |
| | 5 | 47.5068819564 | — | 47.3915579062 | — | 47.2320124154 | — | 47.4490465265 |
| | 6 | 47.4707134722 | — | 47.6406084941 | — | 47.6225860534 | — | 48.4409476451 |
| | 7 | 48.1568096159 | — | 47.7204807904 | — | 47.9994772522 | — | 49.4379811615 |
| | 8 | 48.1984357789 | — | 48.2999644817 | — | 48.4746160616 | — | 50.1957421823 |
| | 9 | 48.5541561686 | — | 48.59619815 | — | 49.0445852679 | — | 49.0600386679 |
| | 10 | 49.1359494783 | — | 49.1738310071 | — | 49.3040250889 | — | 49.5922406417 |
| | 11 | 49.9574758125 | — | 49.5945573352 | — | 49.7675922721 | — | 50.5562628698 |
| | 12 | 50.3406681585 | — | 50.2685117969 | — | 50.2883288438 | — | 51.5769349731 |
| 10 | 0 | **73.0673544574** | — | 73.3937354921 | — | 73.2756230049 | — | 73.7604409912 |
| | 1 | 73.5223189729 | — | 73.1969130995 | — | 73.314432723 | — | 74.6926730698 |
| | 2 | 73.369959718 | — | 73.3430190975 | — | 73.505676967 | — | 75.1294284718 |
| | 3 | 73.4328685759 | — | 73.3935786445 | — | 73.7640234958 | — | 73.5827509737 |
| | 4 | 73.7779468448 | — | 73.6422706745 | — | 73.7622908159 | — | 75.2480804704 |
| | 5 | 74.4201391726 | — | 73.9923135684 | — | 73.8249480462 | — | 74.1676534336 |
| | 6 | 74.275657278 | — | 74.3145190656 | — | 74.2719444082 | — | 75.4031376911 |
| | 7 | 75.2365149728 | — | 74.5014772184 | — | 74.7022012351 | — | 76.7150715151 |
| | 8 | 75.065712931 | — | 75.1754875658 | — | 75.1587445552 | — | 77.2589383227 |
| | 9 | 75.5338734086 | — | 75.5425839372 | — | 76.3604025086 | — | 75.5927771225 |
| | 10 | 76.2182975427 | — | 76.2458499788 | — | 76.2016020677 | — | 77.0332670376 |
| | 11 | 77.446936995 | — | 76.7277275927 | — | 76.8120478435 | — | 78.1695584306 |
| | 12 | 77.5889257943 | — | 77.4613580659 | — | 77.4947139477 | — | 79.31688644 |
| 20 | 0 | 122.433260001 | — | 122.513927462 | — | 122.412603516 | — | 125.245351666 |
| | 1 | 124.83102857 | — | **122.325695478** | — | 122.349574793 | — | 126.305882321 |
| | 2 | 122.651699164 | — | 122.652094474 | — | 122.656796984 | — | 125.06124293 |
| | 3 | 122.724689893 | — | 122.704445685 | — | 125.162233987 | — | 122.655970732 |
| | 4 | 123.274569702 | — | 123.144311312 | — | 123.155865954 | — | 126.791966535 |
| | 5 | 126.304835917 | — | 123.524537031 | — | 123.307211571 | — | 125.717615043 |
| | 6 | 124.131186017 | — | 124.096504504 | — | 124.112622923 | — | 127.11380913 |
| | 7 | 127.556372534 | — | 124.437366492 | — | 124.571606214 | — | 128.454779116 |
| | 8 | 125.334635172 | — | 125.480351924 | — | 125.316900883 | — | 128.563403526 |
| | 9 | 126.083358337 | — | 126.001938857 | — | 128.767780557 | — | 125.791509155 |
| | 10 | 127.141726105 | — | 127.175867638 | — | 126.930157706 | — | 128.98634957 |
| | 11 | 131.023783431 | — | 127.831188112 | — | 127.842559193 | — | 131.765377421 |
| | 12 | 129.313935266 | — | 128.962957408 | — | 128.970840663 | — | 132.806412758 |
| 50 | 0 | 266.841126092 | — | 266.750910329 | — | 266.526734173 | — | 277.147035697 |
| | 1 | 274.228755187 | — | 266.208423455 | — | **266.157018073** | — | 277.62841964 |
| | 2 | 267.147031866 | — | 267.194265882 | — | 267.023748867 | — | 271.5724201 |
| | 3 | 267.147365528 | — | 267.057824922 | — | 273.347485885 | — | 266.753856556 |
| | 4 | 268.599530467 | — | 268.252383419 | — | 268.218253995 | — | 276.629703425 |
| | 5 | 275.976226157 | — | 268.916913575 | — | 268.334355515 | — | 278.64440077 |
| | 6 | 270.45288965 | — | 270.396270638 | — | 270.458488948 | — | 279.926665828 |
| | 7 | 277.94909902 | — | 270.902043113 | — | 271.210761746 | — | 281.122638855 |
| | 8 | 273.150436294 | — | 273.492671773 | — | 273.101699304 | — | 280.003137843 |
| | 9 | 274.583720663 | — | 274.417711384 | — | 280.223263543 | — | 273.854144798 |
| | 10 | 277.220770836 | — | 277.175271179 | — | 276.687664537 | — | 280.205053778 |
| | 11 | 287.375386311 | — | 278.435414894 | — | 278.391012402 | — | 289.407892825 |
| | 12 | 282.30352042 | — | 281.17733536 | — | 280.970785713 | — | 289.947408632 |

**Table 7.5:** Ground state energies in units of $\hbar\omega$ obtained with OPENFCI which implements the full configuration interaction method (with the maximum shell number $R = 5$). The ground state energy for each value of the confinement strength $\lambda = \{5, 10, 20, 50\}$ is boldfaced, showing the lowest energy configuration with respect to the total angular momentum $M$ and total spin $S$.

| λ | M | Energy in unit of $\hbar\omega$ of a six-particle dot obtained for each combination of ($M$,$S$ and $\lambda$) | | | | | | |
|---|---|---|---|---|---|---|---|---|
| | | $S=0$ | $S=1$ | $S=2$ | $S=3$ | $S=4$ | $S=5$ | $S=6$ |
| 11 | 0 | **78.143195073** | — | 78.413381482 | — | 78.313931985 | — | 78.969623622 |
| | 1 | 78.712832202 | — | 78.244926651 | — | 78.336027604 | — | 79.924885843 |
| | 2 | 78.429726984 | — | 78.401027036 | — | 78.526842185 | — | 80.233679779 |
| | 3 | 78.495978621 | — | 78.470202649 | — | 78.961969108 | — | 78.595911825 |
| | 4 | 78.842138362 | — | 78.729075331 | — | 78.814661711 | — | 80.477073212 |
| | 5 | 79.667256553 | — | 79.066249937 | — | 78.912363711 | — | 79.377156886 |
| | 6 | 79.392872079 | — | 79.409142326 | — | 79.375032229 | — | 80.641855045 |
| | 7 | 80.532580259 | — | 79.629358838 | — | 79.802617965 | — | 81.968771076 |
| | 8 | 80.207571918 | — | 80.316653671 | — | 80.271088646 | — | 82.477310161 |
| | 9 | 80.715571857 | — | 80.706306048 | — | 81.713423473 | — | 80.701437675 |
| | 10 | 81.414817055 | — | 81.446423472 | — | 81.362609720 | — | 82.412650789 |
| | 11 | 82.845941833 | — | 81.944130787 | — | 82.010984011 | — | 83.581918646 |
| | 12 | 82.840631132 | — | 82.697400291 | — | 82.734429127 | — | 84.733613844 |
| 12 | 0 | **83.167708584** | — | 83.394193093 | — | 83.303740571 | — | 84.156600106 |
| | 1 | 83.881409398 | — | 83.240872661 | — | 83.313514747 | — | 85.132918037 |
| | 2 | 83.437378073 | — | 83.410427035 | — | 83.509490136 | — | 85.297706724 |
| | 3 | 83.507358020 | — | 83.490277525 | — | 84.138461310 | — | 83.571238814 |
| | 4 | 83.863297552 | — | 83.762128115 | — | 83.823591310 | — | 85.679797042 |
| | 5 | 84.893845201 | — | 84.093502988 | — | 83.944788679 | — | 84.566628964 |
| | 6 | 84.457542775 | — | 84.457589780 | — | 84.432637253 | — | 85.856187641 |
| | 7 | 85.810237363 | — | 84.705736390 | — | 84.857914806 | — | 87.194074485 |
| | 8 | 85.304914828 | — | 85.414959288 | — | 85.347083513 | — | 87.663225340 |
| | 9 | 85.848424314 | — | 85.822908124 | — | 87.048635983 | — | 85.777393353 |
| | 10 | 86.570487591 | — | 86.605228217 | — | 86.490101785 | — | 87.765581961 |
| | 11 | 88.229997119 | — | 87.118791595 | — | 87.173065337 | — | 88.976696821 |
| | 12 | 88.061974379 | — | 87.900242635 | — | 87.938543965 | — | 90.128654898 |
| 13 | 0 | **88.151505022** | — | 88.344328182 | — | 88.257577395 | — | 89.326338416 |
| | 1 | 89.033058061 | — | 88.197386078 | — | 88.257291889 | — | 90.321520824 |
| | 2 | 88.406631105 | — | 88.383064086 | — | 88.462011769 | — | 90.330196713 |
| | 3 | 88.479619296 | — | 88.466751712 | — | 89.298397953 | — | 88.516500173 |
| | 4 | 88.851639268 | — | 88.754730627 | — | 88.800436095 | — | 90.862030864 |
| | 5 | 90.104399883 | — | 89.085726594 | — | 88.935726594 | — | 89.740601801 |
| | 6 | 89.483225708 | — | 89.472470474 | — | 89.455809279 | — | 91.051419446 |
| | 7 | 91.073352679 | — | 89.742146874 | — | 89.880653364 | — | 92.396900798 |
| | 8 | 90.368739460 | — | 90.481168561 | — | 90.395396440 | — | 92.823919873 |
| | 9 | 90.943614219 | — | 90.905029823 | — | 92.369007344 | — | 90.827942565 |
| | 10 | 91.695847699 | — | 91.732671823 | — | 91.592274306 | — | 93.077104797 |
| | 11 | 93.602413719 | — | 92.262446130 | — | 92.307361308 | — | 94.357271821 |
| | 12 | 93.260556659 | — | 93.078253978 | — | 93.115930138 | — | 95.505968804 |
| 15 | 0 | 98.030368353 | — | 98.175943830 | — | 98.089020148 | — | 99.627578422 |
| | 1 | 99.298992309 | — | **98.026884251** | — | 98.070911523 | — | 100.653451690 |
| | 2 | 98.265358634 | — | 98.249612566 | — | 98.299715129 | — | 100.324678925 |
| | 3 | 98.341455866 | — | 98.329682836 | — | 99.581785412 | — | 98.339262951 |
| | 4 | 98.756777622 | — | 98.656448463 | — | 98.684658346 | — | 101.180676624 |
| | 5 | 100.489379141 | — | 98.996614532 | — | 98.832723557 | — | 100.054283015 |
| | 6 | 99.455054715 | — | 99.431922968 | — | 99.428397280 | — | 101.399088100 |
| | 7 | 101.565816782 | — | 99.731093247 | — | 99.857712159 | — | 102.751758487 |
| | 8 | 100.425553944 | — | 100.545499985 | — | 100.431859839 | — | 103.089812111 |
| | 9 | 101.055134783 | — | 100.998311122 | — | 102.966578977 | — | 100.873025038 |
| | 10 | 101.882958568 | — | 101.921395902 | — | 101.741972578 | — | 103.483331676 |
| | 11 | 104.321280076 | — | 102.485133898 | — | 102.516690762 | — | 105.084891895 |
| | 12 | 103.608899864 | — | 103.381455766 | — | 103.413959297 | — | 106.217617700 |

**Table 7.6:** Ground state energies in units of $\hbar\omega$ obtained with OpenFCI which implements the full configuration interaction method (with the maximum shell number $R = 5$). The ground state energy for each value of the confinement strength $\lambda = \{11, 12, 13, 15\}$ is boldfaced, showing the lowest energy configuration with respect to the total angular momentum $M$ and total spin $S$.
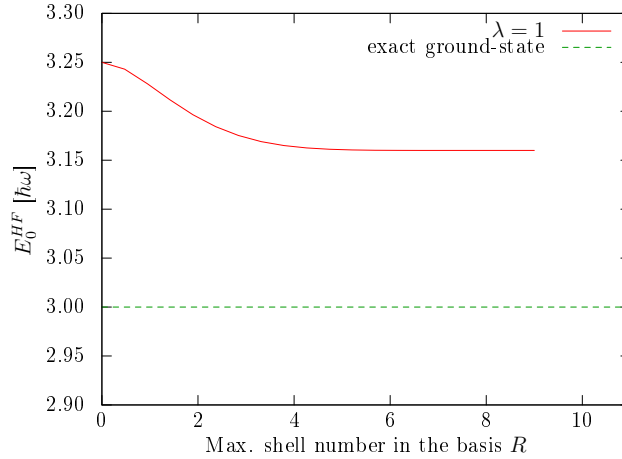
**Figure 7.9:** Hartree-Fock approximation to the ground state energy of a two-particle quantum dot, with a confinement strength $\lambda = 1$

The tables clearly show that the closed-shell model looks valid for a confinement strength in the range $\lambda = 0.1 \rightarrow 13$ and breaks at least for $\lambda \geq 15$. These values can be either translated into a possible range of the applied external magnetic field, or into the size of the quantum dot itself, or even into a combination of both the size of the quantum dot and the magnetic field. These results obviously predominate the ones obtained in section 7.2.1 which neglected the electron-electron interactions.

## 7.3 Convergence, stability and accuracy of the Hartree-Fock Algorithm

### 7.3.1 Importance of the model space

Figure 7.9 presents the results of the simulator, providing the Hartree-Fock approximation to the ground state energy of a two-particle quantum dot where the charge carriers are confined by a dimensionless confinement strength $\lambda = 1$. In two dimensions, the exact ground state energy of such a system is known to be equal to $E_0 = 3$ in units of $\hbar\omega$, as shown in chapter 4. Therefore we see easily that Hartree-Fock provides an approximation to the exact energy with a difference of 5.33%.

Figure 7.10 presents the convergence plots (left plots) of the Hartree-Fock approximation to the ground state energy for quantum dots with different numbers of particles (2, 6, 12 and 20 particles) as a function of the maximum shell number in the basis set $(R^b)$ and for different values of the confinement strength $\lambda$. We see from these results that the Hartree-Fock approximation converges to its best approximation with a basis set of a few shells above the Fermi level. For the case of a two-electron quantum dot (top of figure 7.10), we see that the Hartree-Fock approaximation has achieved its convergence limit with a basis set up to the $4^{th}$ shell. For a six-particle quantum dot, the limit seems to be achieved from the $5^{th}$ shell and from the $7^{th}$ shell for a 12-particle quantum dot.

**Figure 7.10:** (Left) Hartree-Fock approximation to the ground state energy of quantum dots with 2, 6, 12 and 20 trapped particles as a function of the size of the basis set, and for different values of the confinement strength $\lambda = 0, 0.5, 1$ or $2$. As the number of particles in the dot increases, the minimum model space includes all the shells occupied by particles. This explains for example why for 20 particles, the first energies are obtained only from $R^b = 3$.

(Right) Hartree-Fock relative error $(E^{HF}(R^b) - E^{HF}_{min})/E^{HF}_{min}$ as a function of the size of the basis set for the same quantum dots. An exponential dependence in $R^b$ can be observed in the cases where the relative error is not exactly zero.

When increasing the size of the quantum dot one shell at a time, the convergence limit $E^{HF}(R^b_{max})$ doesn't seem to be achieved with a linear increase in the size of the basis set. Then another interesting plot should show how the Hartree-Fock limit is scaled with the size of the basis set. This is displayed in the right plots of figure 7.10), where the relative error $\left(E^{HF}(R^b) - E^{HF}_{min}\right)/E^{HF}_{min}$ is given as a function of the maximum shell number in the basis set $(R^b)$. The plots display amost linear curves, implying a quasi-exponential dependence in $R^b$.

We also remark in the case of the 20-particle quantum dot (bottom of figure 7.10) that Hartree-Fock stops improving its limit when increasing the basis set in the case of the "high" confinement strength $\lambda = 2$. This is our first observation of the breakdown of the Hartree-Fock approach for a high number of particles within a strong confinement strength (i.e. for a GaAs quantum dot, $\lambda = 2$ would correspond to $\hbar\omega_0 = 2.96\,meV$).

## 7.3.2 Importance of the interaction strength

We discussed the ranges of the confinement strength $\lambda$ that would make sense physically through an experimental approximation using large scale diagonalization 7.2.2. From a computational point of view, it is also interesting to study the convergence of the Hartree-Fock algorithm with respect to the confinement strength and to observe how fast the iterative process is converging.

To do so we look at the "convergence history" of a simulation, meaning that we look at the improvement in the approximated energy as function of the number of iterations. This could be done by plotting the energy difference expressed by

$$\delta(iter) = |E^{HF}(iter) - E^{HF}(iter - 1)|.$$

However since the self-consistency in our simulator depends on the convergence of the eigenenergies and not on the total energy, it seems more natural to plot the following relative energy difference

$$\delta(iter) = \frac{1}{nbStates}\left(\sum_{n\,m_l}|\epsilon_{n\,m_l}(iter) - \sum_{n\,m_l}\epsilon_{n\,m_l}(iter - 1)|\right),$$

where $\epsilon_{n\,m_l}$ is the eigenenergy of the system of the single orbital $|n\,m_l\rangle$.

For a higher resolution than the machine resolution (e.g. $\epsilon \leq 2 \times 10^{-16}$), we may experience potential losses of numerical precision. We stopped the iterative process at the maximum number of iterations (here fixed to 1000).

Assuming the following form of the convergence over iterations

$$\delta(iter) \simeq 10^{-\beta\,iter},$$

a possibly more intuitive way to look at the "convergence history" would be to write:

$$\log\delta(iter) \simeq -\beta\,iter,$$

where $\beta$ is a constant depending on the parameters ($R^b$, $R^f$ and $\lambda$). In this case we can interpret the plot saying that, at this iteration, you improve the precision on the relative energy difference with $\beta$ digits compared to the previous iteration.

Figure 7.11 is therefore plotting the variations of the eigenenergies produced by the Hartree-Fock iterative process in a semilog form on the $y - axis$ as a function of iterations. From top to bottom are plotted different quantum dots composed of 2, 6, 12 and 20 particles respectively. Each plot compares different confinement strengths ($\lambda = \{1, 2, 5\}$) and different basis set ($R^b = \{4, 8\}$). For each dot the complete convergence history is given on the left and a zoom on the first iterations is plotted on the right. For each curve, $\beta$ is computed by linear regression and indicates the number of digits with which the precision is improved from one iteration to the next one. For the strange behaviour observed for some configurations of parameters, the linear regression is performed on the first iterations only where the iterative process is actually converging.

These plots show already several behaviours of the iterative process. First, increasing the confinement strength $\lambda$ always results in slower convergence steps between iterations.Finally, we note also the non-converging configurations ($\lambda = 5$, $R^b = 8$ for the 12-particle dot, but not for the 20-particle dot, $\lambda = 2$, $R^b = 8$ for the 20-particle dot while a higher confinement strength $\lambda = 5$, $R^b = 8$ seems to converge after two converging descents). We were looking for some limits of parameters from which Hartree-Fock would not converge anymore. However we see here that we can have a converging process for a given configuration, and a non-converging process with a lower confinement strength keeping other parameters fixed. This was not really expected and could be due to an implementation issue, rather difficult to identify.

Studying the "convergence history" also tells us about a phenomenon to take into account when dealing with the stability of the simulator. In most of the plots of figure 7.11 we observe a plateau with small oscillations for high iteration numbers. Since the simulations have been performed with a very high resolution of $\epsilon = 10^{-20}$, we expected to observe such a plateau around the machine precision (i.e. numerical precision $\simeq 2 \times 10^{-16}$). And we of course expect machine precision to prevent our results to be known up to a given number of digits.

However a closer look at these plateaux (figure 7.12) reveals that the limit of convergence will occur for much lower precision as the interaction strength is increased. In a sense, one could say that increasing the interaction strength will "lower the machine precision". It is difficult to see how this process happens in the iterative scheme. It seems that errors are added at each iteration proportionally to the interaction strength. Figure 7.12.

To comprehend this particular case might be complicated, but understanding this process could be helped by studying another problem: the "cancellation error" or "round-off error" in the finite difference method. Let us compute and compare the exact second derivative of $u(x) = e^x$ for $x = 1$, to the numerical second derivative of $u(x)$ using the finite difference method

$$u''(x) \longrightarrow (\delta^2 u)_j = \frac{u_{j+1} - u_j + u_{j-1}}{h^2}, \tag{7.8}$$

where $h$ is the spacing between discrete values of $x$. We note from figure 7.13 that the accuracy of the derivative improves from $h = 10^0$ to $2 \, 10^{-4}$ approximately. With values of $h$ lower than $h_{limit} = 2 \, 10^{-4}$, this simple scheme starts diverging. It can be
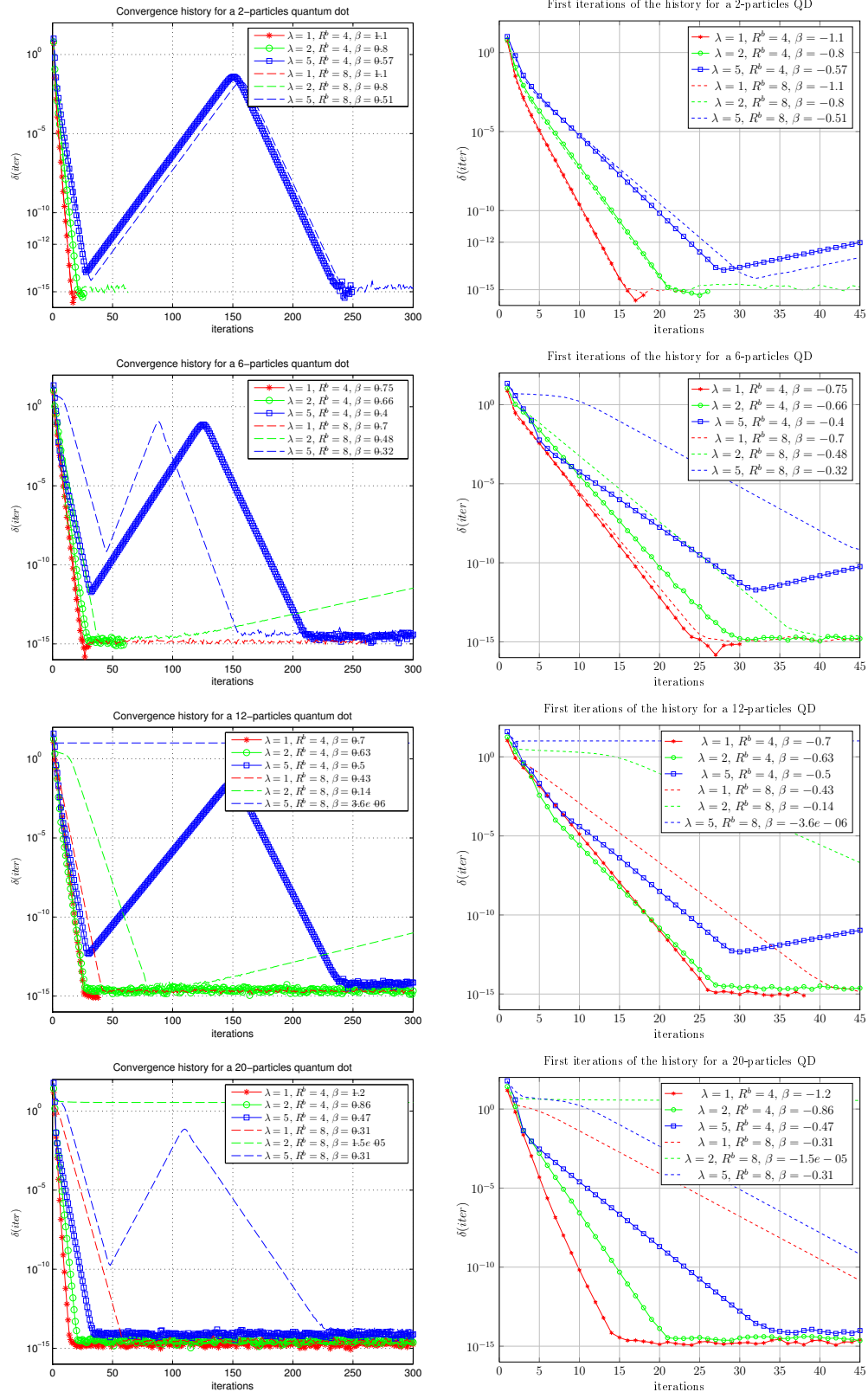
**Figure 7.11:** Convergence history of the Hartree-Fock iterative process. From top to bottom are plotted QDots with 2, 6, 12 and 20 particles respectively. Each plot compares different confinement strengths ($\lambda = \{1, 2, 5\}$) and different basis set ($R^b = \{4, 8\}$). For each dot the complete convergence history is given on the left and a zoom on the first iterations is plotted on the right. For each curve, $\beta$ is computed and indicates the number of digits that improves the precision from one iteration to the next one.
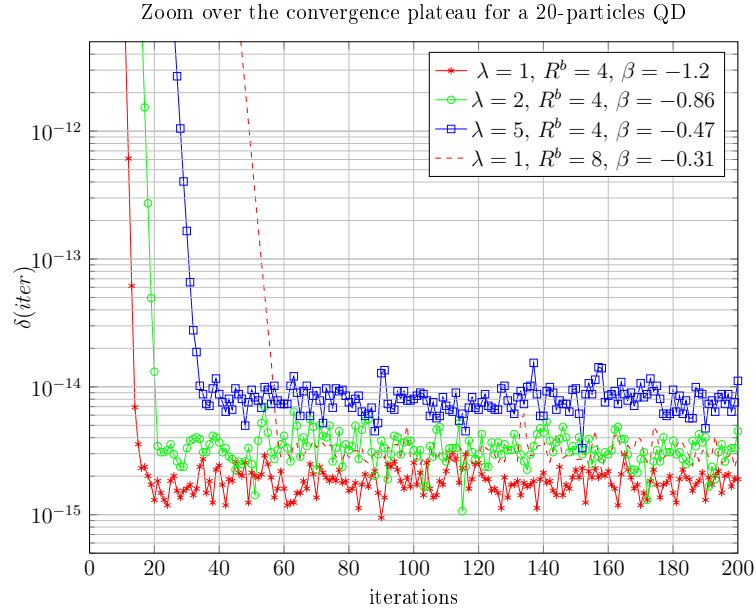
**Figure 7.12:** Zoom over the limit of convergence of the Hartree-Fock iterative process.
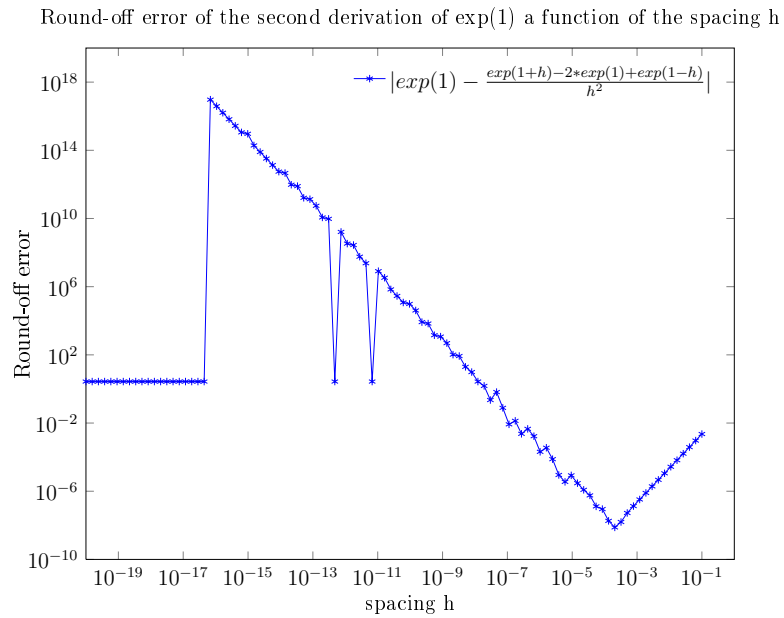


**Figure 7.13:** Round-off error of the second derivative of $e^{(}x)$ for $x = 1$ using the finite difference method.

shown that the finite difference method will not converge if $h \leq \sqrt{\epsilon}$ where $\epsilon$ is the machine precision [16]. If now we take a value of $h$ slightly below $h_{limit}$, we will add errors to the computation of the second derivative; an error which will be inversely proportional to $h$.

Our simulation can be affected in the same way when making a substraction, and according to the plots previously discussed, it might be related to the parameter $\lambda$.

Thinking of a substraction proportional to $\lambda$, the two-body interaction element $V_{\alpha\beta\gamma\delta}$, in which we substract the exchange term from the direct term, would logically appear to be responsible for the round-off error. Errors and growth of errors due to the iterative scheme will occur when the direct term is close in value to the exchange term. Since the interaction is directly proportional to the confinement strength $\lambda$, the error too will become proportional to $\lambda$. These errors then enter the eigenvalue solver of the Hartree-Fock algorithm in a non-trivial way which might be responsible for the strange behaviour we observed for some configurations of parameters.

It was important to look at the convergence history which tells us a lot about the convergence, the accuracy and the stability of the Hartree-Fock algorithm. Three parameters seem to dominate the behaviour of the simulator: the strength of the interaction which obviously dictates the choice of the precision and the maximum number of iterations imposed to the self-consistent scheme. Indeed we may get some wrong and unexpected behaviour of the simulator when asking for a too high precision in the self-consistent scheme. However one cannot fix these values once for all since the convergence speed and the final accuracy obviously depend on the confinement strength characterized by the dimensionless parameter $\lambda$.

## 7.4   Scaling of the simulator with parallelization

Our simulator is implemented in a way that it computes, writes to file and reads from file the two-body interaction matrices either in the harmonic oscillator basis (i.e. what we call here the Coulomb matrix), or in the Hartree-Fock basis (i.e. the basis made of the Hartree-Fock orbitals after the convergence of the self-consistent process).

We noticed above that building these big matrices is the weakest point of the simulator in terms of efficiency, just before the computation of the perturbation theory corrections. Using parallelization with MPI, the computation of the elements of these interaction matrices and the sum performed in the perturbation theory corrections have been equally shared among the number of processors and this section aims at studying the efficiency of this parallelization, or in other words, it observes the scaling of the complete simulator according to the number of processors used.

Table 7.7 compares the duration of different configurations as a function of the number of processors when the simulations were launched on the supercomputer of the University of Oslo called **TITAN**. The study has just been performed over 2 small sizes of quantum dots, respectively two-electron and six-electron dots. Therefore the effect of the size of the dot doesn't look significant here, but it seems negligible compared to the influence of the basis size. Moreover the duration is not completely

proportional to the number of processors, but not far to be. We did not expect to have a complete linear relationship between the number of processors used and the duration of the overall simulation since the Hartree-Fock algorithm itself is not parallelized. However it improves a lot the speed of the complete simulation and confirms the usefulness of parallelizing the code.

| $\sharp e^-$ | $\lambda$ | Basis size $(R^b)$ | Duration of the simulation (in minutes) wrt the nb. of processors below | | | | | | | | |
|---|---|---|---|---|---|---|---|---|---|---|---|
| | | | 1 | 9 | 19 | 49 | 99 | 199 | 299 | 399 | 499 |
| 2 | 1 | 2 | $\leq 0.01$ | $\leq 0.01$ | $\leq 0.01$ | $\leq 0.01$ | $\leq 0.01$ | 0.01 | $\leq 0.01$ | $\leq 0.01$ | 0.01 |
| | | 4 | 1.13 | 0.14 | 0.07 | 0.03 | 0.03 | 0.01 | 0.01 | 0.01 | 0.01 |
| | | 7 | 751.32 | 83.65 | 37.78 | 17.73 | 9.08 | 4.96 | 3.49 | 2.64 | 2.36 |
| | 10 | 2 | $\leq 0.01$ | $\leq 0.01$ | $\leq 0.01$ | $\leq 0.01$ | $\leq 0.01$ | $\leq 0.01$ | $\leq 0.01$ | $\leq 0.01$ | $\leq 0.01$ |
| | | 4 | 1.16 | 0.15 | 0.09 | 0.04 | 0.04 | 0.02 | 0.03 | 0.02 | 0.02 |
| | | 7 | 751.45 | 84.28 | 38.18 | 18.03 | 10.45 | 5.24 | 3.91 | 3.1 | 2.38 |
| 6 | 1 | 2 | $\leq 0.01$ | $\leq 0.01$ | $\leq 0.01$ | $\leq 0.01$ | $\leq 0.01$ | $\leq 0.01$ | $\leq 0.01$ | $\leq 0.01$ | 0 |
| | | 4 | 1.24 | 0.15 | 0.08 | 0.04 | 0.03 | 0.01 | 0.02 | 0.01 | 0.01 |
| | | 7 | 777.02 | 86.9 | 36.75 | 18.33 | 9.22 | 5.13 | 3.71 | 2.8 | 2.22 |
| | 10 | 2 | $\leq 0.01$ | $\leq 0.01$ | $\leq 0.01$ | $\leq 0.01$ | $\leq 0.01$ | $\leq 0.01$ | $\leq 0.01$ | $\leq 0.01$ | $\leq 0.01$ |
| | | 4 | 1.23 | 0.19 | 0.13 | 0.08 | 0.07 | 0.06 | 0.07 | 0.06 | 0.06 |
| | | 7 | 740.45 | 82.73 | 40.17 | 18.51 | 9.7 | 5.68 | 4.3 | 3.42 | 2.83 |

**Table 7.7:** Simulation duration (in minutes) for different configurations of parameters as a function of the number of processors used on the supercomputer `TITAN`.

## 7.5 Comparison of ab initio methods applied to quantum dots

In this section we discuss the reliability of two many-body techniques (Hartree-Fock and many-body perturbation theory) by comparing their approximations to the ground state energy of quantum dots with the "exact" ground state energy. Since it is not possible to compute an exact energy for any value of the confinement strength $\lambda$ and any number of particles trapped in the quantum dot, we will assume the results from configuration interaction as "exact" and we will therefore compute the relative error of each approximated ground state with respect to the CI energy. The relative error is simply defined by

$$\epsilon^{method} = \frac{E^{method} - E^{CI}}{E^{CI}}, \tag{7.9}$$

where $E^{CI}$ is the ground state energy obtained using full configuration interaction and computed thanks to OPENFCI. The quantity $E^{method}$ is the approximation to the ground state energy either using the Hartree-Fock method or many-body perturbation theory, or a combination of these techniques. The parameters used to compute the "exact" ground state are listed in tables 7.9, 7.10, 7.11, 7.12, 7.13 and 7.14 with the relative errors of each method, for each configuration of the parameters.

In order to simplify the notations, we introduce short keywords in the plots to denote the various techniques: **HF** refers to the Hartree-Fock method alone while MBPT(HF)-$2^{nd}$ order refers to the Hartree-Fock energy corrected with a $2^{nd}$ order many-body perturbation correction computed in the new Hartree-Fock (HF) basis set. Similarly MBPT(HF)-$3^{rd}$ order refers to the Hartree-Fock energy corrected with

the $2^{nd}$ and $3^{rd}$ order many-body perturbation corrections computed in the new Hartree-Fock basis set. When computing the ground state energy using the many-body perturbation theory directly from the Harmonic oscillator (HO) basis set, we denote by MBPT(HO)-$1^{st}$ order, MBPT(HO)-$2^{nd}$ order and MBPT(HO)-$3^{rd}$ order the MBPT energy correcting the non-interacting ground state energy respectively with up to the $1^{st}$, $2^{nd}$ and $3^{rd}$ order corrections.

### 7.5.1   Quadratic error growth for HF and MBPT

Figure 7.14 summarizes most of the simulations performed in order to compare the behaviour of all methods. It is difficult to compare the different methods from these first plots but it gives some ideas about the general trend of the techniques implemented.

We observe that all the methods exhibit approximately the same scaling with respect to the confinement strength. Since the data are plotted in logscale, we see clearly a power law. We denote by $\beta$ the slope of the logscale plot, which corresponds to the approximated error growth given by

$$\epsilon^{method} \propto \left( E^{method} \right)^{\beta}.$$
(7.10)

The different values of $\beta$ are valid only for the linear part of the logscale plots. For each configuration, $\beta$ is given on the plot itself, and for most of them indicates $\beta \simeq 2$, meaning that the error of the methods increases almost quadratically with $\lambda$.

If the error grows similarly among the different methods as a function of $\lambda^2$, each method display however a different accuracy for a given $\lambda$. Figure 7.15 zooms on the quadratic part for the same previous configurations and highlights the difference in accuracy between the methods.

### 7.5.2   Accuracy depending on the number of particles

Table 7.8 indicates the shifts in accuracy for each method with respect to the most accurate one. We see that the Hartree-Fock method corrected by second and third order perturbation correction obtains the best accuracy for two-electron and six-electron QD, but the order changes when it comes to a 12-electron QD, the same method exhibits the worst performance. This shows a clear dependence on the accuracy of the methods with respect to the number of particles in the system. Stated differently, HF gives a lower accuracy compared to MBPT as the number of particles increases in the dot.

### 7.5.3   Limit of validity or break of the methods

A quick study of the full configuration ground state of a two-electron QD, similar to the one done in section 7.2.2 reveals that the closed-shell model starts breaking in the range $\lambda \in [50; 100]$, since the lowest ground state energy for various total angular momentum $M = \{0 : 12\}$, $S = \{0, 2\}$ is achieved for $(M, S)^{2e^-}_{\lambda=100} = (1, 2)$ for $\lambda = 100$ while it is still $(M, S)^{2e^-}_{\lambda=50} = (0, 0)$ for $\lambda = 50$. Recall that the break of the closed-shell model of a six-electron dot occurs in the range $\lambda \in [13, 15]$. Unfortunately

**Figure 7.14:** Comparison of several *ab initio* methods for computing the ground state energy of quantum dots with 2, 6 and 12 electrons respectively from top to bottom. The plots display the error on the ground state energy performed with each method with respect to the configuration interaction energy obtained using OpenFCI, as a function of the confinement strength $\lambda$. Left plots are calculations performed with a basis size defined by $R^b = 4$, the right plots with $R^b = 8$.

**Figure 7.15:** Comparison of several *ab initio* methods for computing the ground state energy of quantums dots with 2, 6 and 12 electrons respectively from top to bottom. The plots display a zoom on the quadratic growth of the error when $\lambda$ is relatively small ($\lambda < 0.05$), showing different accuracies with respect to the method, the number of particles and the size of the basis.

| $\sharp\, e^-$ | Basis size $(R^b)$ | Relative error shift between each method ($\epsilon_{min}$ indicates the lowest relative error among the methods) | |
|---|---|---|---|
| 2 | 4 | MBPT(HF)-$2^{nd}$order and MBPT(HF)-$3^{rd}$order | $\rightarrow \epsilon_{min}$ |
| | | MBPT(H0)-$2^{nd}$order and MBPT(H0)-$3^{rd}$order | $\rightarrow 6.6\,\epsilon_{min}$ |
| | | HF | $\rightarrow 12.6\,\epsilon_{min}$ |
| | | MBPT(HO)-$1^{st}$ order | $\rightarrow 20.7\,\epsilon_{min}$ |
| | 8 | MBPT(HF)-$2^{nd}$order and MBPT(HF)-$3^{rd}$order | $\rightarrow \epsilon_{min}$ |
| | | MBPT(H0)-$2^{nd}$order and MBPT(H0)-$3^{rd}$order | $\rightarrow 2.5\,\epsilon_{min}$ |
| | | HF | $\rightarrow 8.5\,\epsilon_{min}$ |
| | | MBPT(HO)-$1^{st}$ order | $\rightarrow 12.7\,\epsilon_{min}$ |
| 6 | 4 | MBPT(HF)-$2^{nd}$order and MBPT(HF)-$3^{rd}$order | $\rightarrow \epsilon_{min}$ |
| | | HF | $\rightarrow 9.8\,\epsilon_{min}$ |
| | | MBPT(H0)-$2^{nd}$order and MBPT(H0)-$3^{rd}$order | $\rightarrow 40.9\,\epsilon_{min}$ |
| | | MBPT(HO)-$1^{st}$ order | $\rightarrow 54.1\,\epsilon_{min}$ |
| | 8 | MBPT(HF)-$2^{nd}$order and MBPT(HF)-$3^{rd}$order | $\rightarrow \epsilon_{min}$ |
| | | HF | $\rightarrow 1.3\,\epsilon_{min}$ |
| | | MBPT(H0)-$2^{nd}$order and MBPT(H0)-$3^{rd}$order | $\rightarrow 5.3\,\epsilon_{min}$ |
| | | MBPT(HO)-$1^{st}$ order | $\rightarrow 7.9\,\epsilon_{min}$ |
| 12 | 4 | MBPT(HO)-$2^{nd}$order and MBPT(HO)-$3^{rd}$order | $\rightarrow \epsilon_{min}$ |
| | | MBPT(HO)-$1^{st}$ order | $\rightarrow 1.3\,\epsilon_{min}$ |
| | | HF | $\rightarrow 1.8\,\epsilon_{min}$ |
| | | MBPT(HF)-$2^{nd}$order and MBPT(HF)-$3^{rd}$order | $\rightarrow 2\,\epsilon_{min}$ |
| | 8 | MBPT(HO)-$2^{nd}$order and MBPT(HO)-$3^{rd}$order | $\rightarrow \epsilon_{min}$ |
| | | MBPT(HO)-$1^{st}$ order | $\rightarrow 1.6\,\epsilon_{min}$ |
| | | HF | $\rightarrow 2.3\,\epsilon_{min}$ |
| | | MBPT(HF)-$2^{nd}$order and MBPT(HF)-$3^{rd}$order | $\rightarrow 2.8\,\epsilon_{min}$ |

**Table 7.8:** Classification of the methods with respect to their relative accuracy in the range of $\lambda$ that exhibits a quadractic error growth. The performance of each method shows a dependence to the number of particles in the dot. MBPT obtains a better accuracy than HF as the number of particles increases.

we don't know for which value of $\lambda$ the closed-shell model breaks in the case of the twelve-electron dot, but we know that this happens at least before the break of the six-electron QD, then before $\lambda = 15$. A similar study should be done for the 12-electron case, however it will require much more time and resources to compute it using full configuration interaction.

Therefore another interesting part to discuss on the plots of figure 7.14 concerns the behaviour of the methods while approaching large values of $\lambda$, e.g. approaching the limits of the closed shell. A zoom in the region $\lambda = [0.1, 50]$ is given in figure 7.16 and reports the error of each method.

It is only in this region that the $2^{nd}$ and $3^{rd}$ order perturbation corrections either in the Harmonic oscillator or in the basis set of Hartree-Fock orbitals start showing different accuracies. However they give results at the opposite of our expectations. Indeed while the $3^{rd}$ correction is supposed to improve the accuracy, we see that the error is here increasing compared to the $2^{nd}$ order correction in most of the cases. A possible explanation could be that this signals a slower convergence in terms of the interaction and that higher-order corrections are needed.

Other differences are based on the evolution of each method while $\lambda$ approaches critical values. We remark that the second (and third order) perturbation corrections blow up above $\lambda = 10$, while the first-order perturbation theory correction tends smoothly toward a linear error growth while all other methods starts oscillating more or less, showing signs of instability. We didn't expect the methods to get a lower error growth when approaching the limit of the closed-shell model. Since this
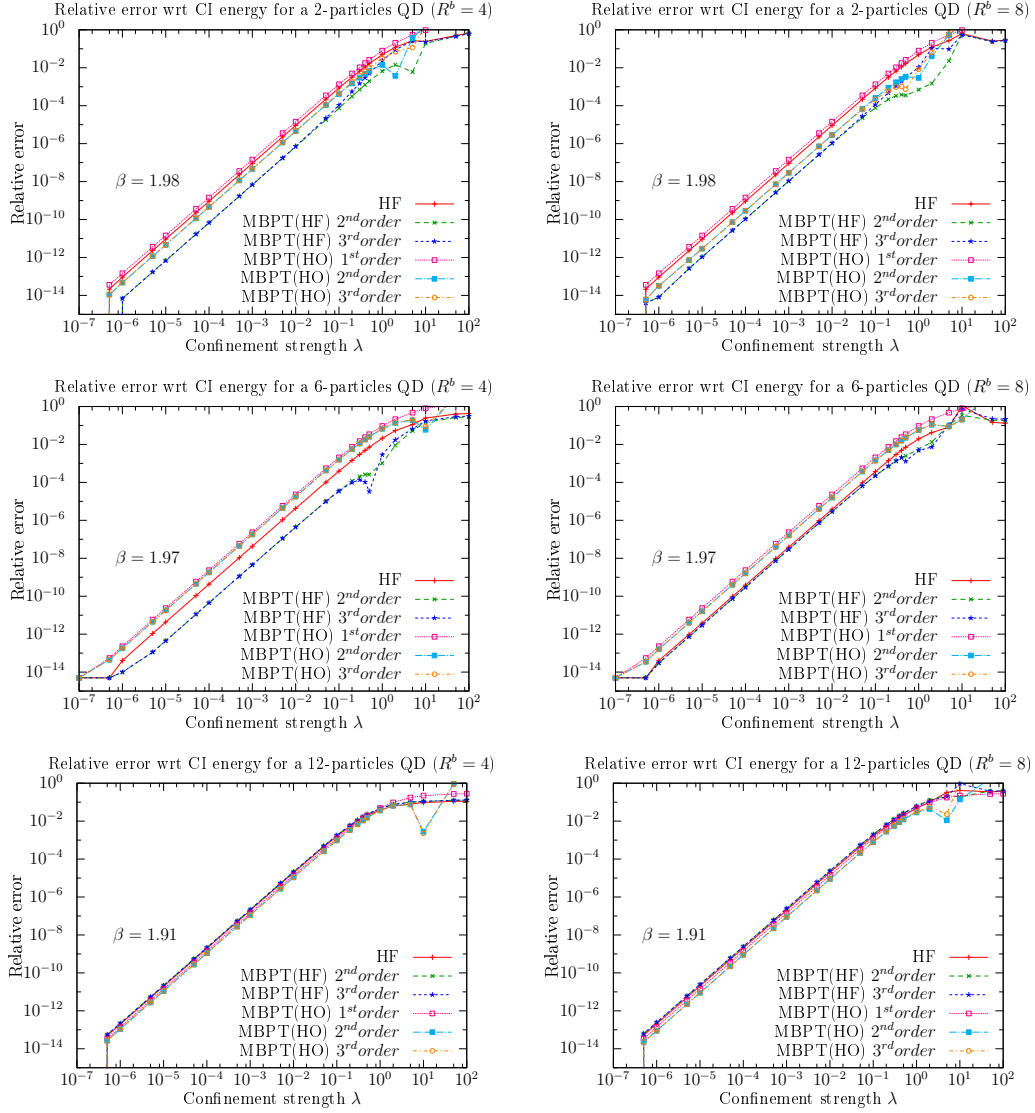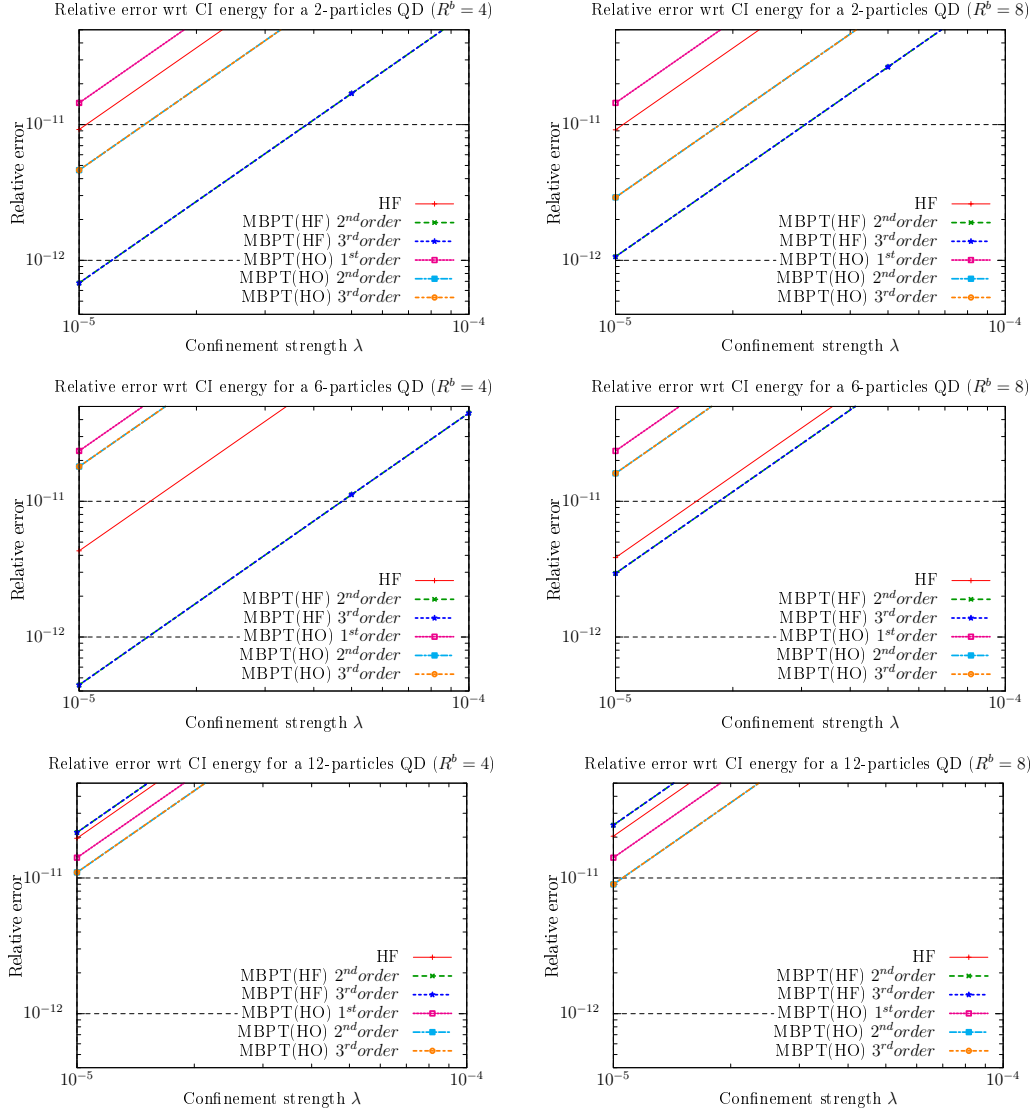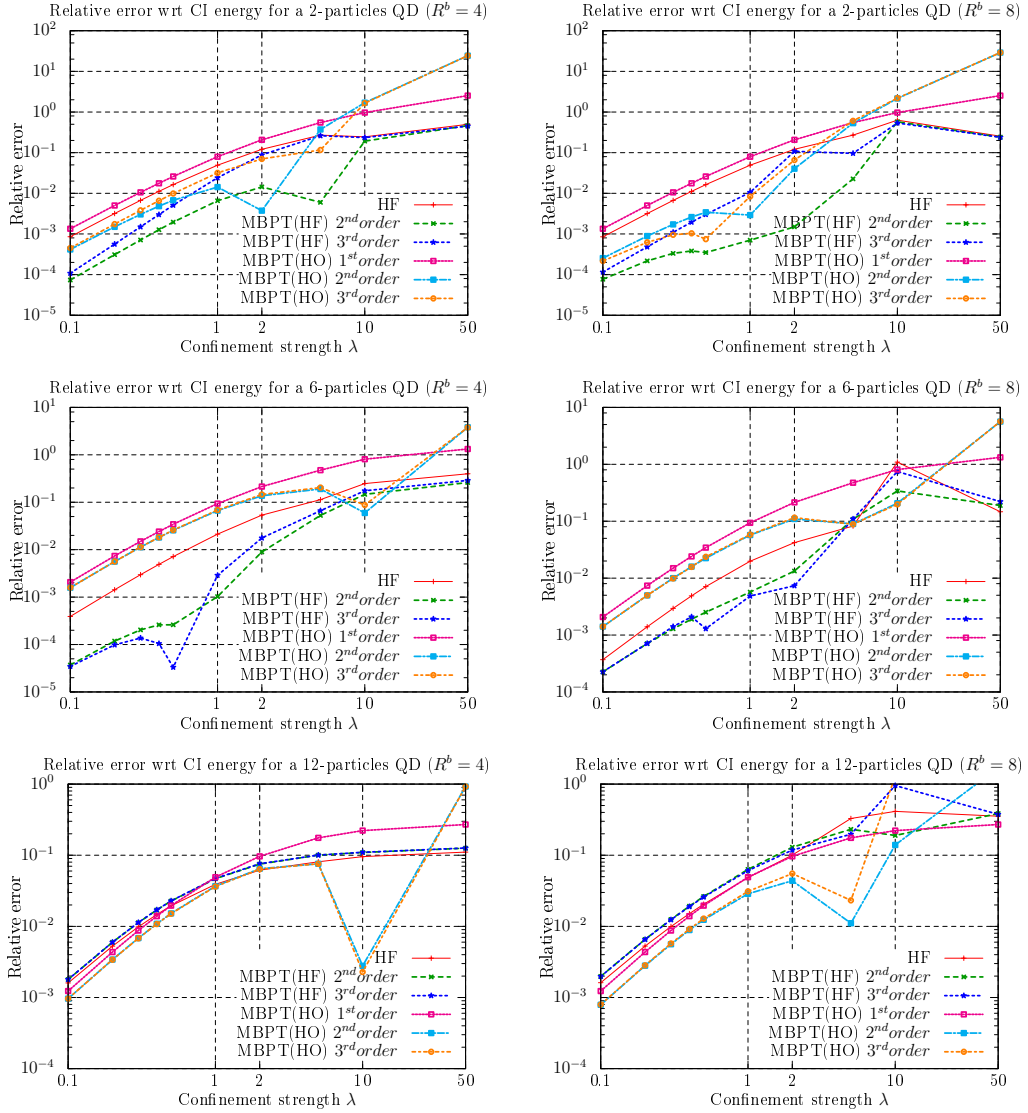
**Figure 7.16:** Comparison of several *ab initio* methods for computing the ground state energy of quantums dots with 2, 6 and 12 electrons respectively from top to bottom for large confinement strength $\lambda$. The plots display a zoom for $\lambda$ approaching the limit of the closed-shell model.

phenomenon seems more and more important as the number of electrons increases, this could be due to the smaller and smaller Hilbert space we used to compute the "exact" full configuration interaction energy in a short time ($R = 5$ for 2 electrons, $R = 4$ for 6 electrons and $R = 3$ for 12 electrons). On the contrary, an accurate study should include more and more shells as the size of the system increases.

While the instability of the $2^{nd}$ order correction has been predicted and discussed in the literature [47], we see here that up to $\lambda = 50$ which is already above the limit of the closed-shell model, the many-body perturbation corrections in the Hartree-Fock basis oscillates but does not blow up as with the harmonic oscillator basis. This may be due to the optimized eigenstates of the Hartree-Fock basis compared to the harmonic oscillator states, but this might not be true anymore as $\lambda$ further increases.

Finally we see that the Hartree-Fock approach as well as MBPT and the combinations of these methods actually give really high relative errors before they actually reach the limit of the closed-shell model. The relative errors are listed in tables 7.9, 7.10, 7.11, 7.12, 7.13 and 7.14. These errors are however underestimated; first because configuration interaction is also an approximation to the true ground state energy, and secondly, as we just mentioned, because our truncation of the Hilbert space was really rough, which translates into a bigger inaccuracy of our CI calculations.

| ♯ e⁻ | $R^b$ | λ | HF energy $(\hbar\omega)$ | HF rel. error | HF+MBPT(HF)-$2^{nd}$order energy $(\hbar\omega)$ | rel. error | HF+MBPT(HF)-$3^{rd}$order energy $(\hbar\omega)$ | rel. error | Full CI energy $(\hbar\omega)$ | parameters |
|---|---|---|---|---|---|---|---|---|---|---|
| 2 | 4 | 1E − 7 | 2.000000125331 | 0.00E + 00 | 2.000000125331 | 0.00E + 00 | 2.000000125331 | 0.00E + 00 | 2.000000125331 | |
| | | 1E − 7 | 2.000000125331 | 0.00E + 00 | 2.000000125331 | 0.00E + 00 | 2.000000125331 | 0.00E + 00 | 2.000000125331 | |
| | | 5E − 7 | 2.000000626657 | 2.00E − 14 | 2.000000626657 | 0.00E + 00 | 2.000000626657 | 0.00E + 00 | 2.000000626657 | |
| | | 1E − 6 | 2.000001253314 | 8.99E − 14 | 2.000001253314 | 4.88E − 15 | 2.000001253314 | 4.88E − 15 | 2.000001253314 | |
| | | 5E − 6 | 2.000006266568 | 2.30E − 12 | 2.000006266564 | 1.70E − 13 | 2.000006266564 | 1.70E − 13 | 2.000006266563 | |
| | | 1E − 5 | 2.000012533131 | 9.21E − 12 | 2.000012533114 | 6.80E − 13 | 2.000012533114 | 6.80E − 13 | 2.000012533112 | |
| | | 5E − 5 | 2.000062665444 | 2.30E − 10 | 2.000062665018 | 1.69E − 11 | 2.000062665018 | 1.70E − 11 | 2.000062664984 | |
| | | 1E − 4 | 2.000125330363 | 9.20E − 10 | 2.000125328658 | 6.78E − 11 | 2.000125328658 | 6.78E − 11 | 2.000125328523 | |
| | | 5E − 4 | 2.000626630801 | 2.30E − 08 | 2.000626588186 | 1.70E − 09 | 2.000626588196 | 1.70E − 09 | 2.000626584794 | |
| | | 1E − 3 | 2.001253209074 | 9.20E − 08 | 2.001253038639 | 6.79E − 09 | 2.001253038713 | 6.82E − 09 | 2.001253025058 | $(M,S)^{GS} = (0,0)$ for |
| | | 5E − 3 | 2.006263945539 | 2.29E − 06 | 2.006259689492 | 1.70E − 07 | 2.006259698750 | 1.75E − 07 | 2.006259347655 | $R = 5$, $M \in [0:12]$ and |
| | | 1E − 2 | 2.012522647963 | 9.13E − 06 | 2.012505647870 | 6.85E − 07 | 2.012505721857 | 7.22E − 07 | 2.012504269056 | $S \in [0:2]$ |
| | | 5E − 2 | 2.062404808005 | 2.22E − 04 | 2.061984602154 | 1.78E − 05 | 2.061993767625 | 2.22E − 05 | 2.061947942318 | |
| | | 1E − 1 | 2.124295000418 | 8.54E − 04 | 2.122637920311 | 7.38E − 05 | 2.122710367477 | 1.08E − 04 | 2.122481353547 | |
| | | 2E − 1 | 2.246574506683 | 3.19E − 03 | 2.240132733855 | 3.09E − 04 | 2.240697184146 | 5.61E − 04 | 2.239439975058 | |
| | | 3E − 1 | 2.366923700288 | 6.70E − 03 | 2.352838529008 | 7.11E − 04 | 2.354688569748 | 1.50E − 03 | 2.351166061395 | |
| | | 4E − 1 | 2.485425861700 | 1.12E − 02 | 2.461091716210 | 1.27E − 03 | 2.465339980045 | 3.00E − 03 | 2.457973187497 | |
| | | 5E − 1 | 2.602161579782 | 1.64E − 02 | 2.565209233355 | 1.96E − 03 | 2.573230325859 | 5.09E − 03 | 2.560187735597 | |
| | | 1E + 0 | 3.161921401726 | 4.92E − 02 | 3.033418457765 | 6.57E − 03 | 3.086386629747 | 2.41E − 02 | 3.013626129397 | |
| | | 2E + 0 | 4.185136950885 | 1.21E − 01 | 3.787264741771 | 1.44E − 02 | 4.063355183669 | 8.83E − 02 | 3.733597603174 | |
| | | 5E + 0 | 6.775965715485 | 2.70E − 01 | 5.365438495287 | 6.00E − 02 | 6.729277440105 | 2.62E − 01 | 5.333416434792 | |
| | | 1E + 1 | 9.192744506771 | 2.45E − 01 | 8.802994301904 | 1.92E − 01 | 9.120632575845 | 2.35E − 01 | 7.383537264058 | |
| | | 5E + 1 | 27.433561900391 | 4.98E − 01 | 26.776022625443 | 4.62E − 01 | 26.585406735688 | 4.52E − 01 | 18.314898304163 | |
| | | 1E + 2 | 49.760800203239 | 6.81E − 01 | 48.840671584843 | 6.50E − 01 | 48.142443831938 | 6.26E − 01 | 29.601244919262 | $(M,S)^{GS} = (1,2)$ |
| | 8 | 1E − 7 | 2.000000125331 | 0.00E + 00 | 2.000000125331 | 0.00E + 00 | 2.000000125331 | 0.00E + 00 | 2.000000125331 | |
| | | 5E − 7 | 2.000000626657 | 2.00E − 14 | 2.000000626657 | 5.11E − 15 | 2.000000626657 | 5.11E − 15 | 2.000000626657 | |
| | | 1E − 6 | 2.000001253314 | 8.99E − 14 | 2.000001253314 | 9.99E − 15 | 2.000001253314 | 9.99E − 15 | 2.000001253314 | |
| | | 5E − 6 | 2.000006266568 | 2.29E − 12 | 2.000006266563 | 2.65E − 13 | 2.000006266563 | 2.65E − 13 | 2.000006266563 | |
| | | 1E − 5 | 2.000012533131 | 9.16E − 12 | 2.000012533110 | 1.06E − 12 | 2.000012533110 | 1.06E − 12 | 2.000012533112 | |
| | | 5E − 5 | 2.000062665442 | 2.29E − 10 | 2.000062664931 | 2.66E − 11 | 2.000062664931 | 2.66E − 11 | 2.000062664984 | |
| | | 1E − 4 | 2.000125330354 | 9.16E − 10 | 2.000125328310 | 1.06E − 10 | 2.000125328310 | 1.06E − 10 | 2.000125328523 | |
| | | 5E − 4 | 2.000626630573 | 2.29E − 08 | 2.000626579481 | 2.66E − 09 | 2.000626579470 | 2.66E − 09 | 2.000626584794 | |
| | | 1E − 3 | 2.001253208163 | 9.15E − 08 | 2.001253008833 | 1.06E − 08 | 2.001253003743 | 1.07E − 08 | 2.001253025058 | |
| | | 5E − 3 | 2.006263922999 | 2.28E − 06 | 2.006258822370 | 2.62E − 07 | 2.006258811115 | 2.67E − 07 | 2.006259347655 | $(M,S)^{GS} = (0,0)$ for |
| | | 1E − 2 | 2.012522558992 | 9.09E − 06 | 2.012502194407 | 1.03E − 06 | 2.012502104834 | 1.08E − 06 | 2.012504269056 | $R = 5$, $M \in [0:12]$ and |
| | | 5E − 2 | 2.062402810851 | 2.21E − 04 | 2.061901184611 | 2.27E − 05 | 2.061890439468 | 2.79E − 05 | 2.061947942318 | $S \in [0:2]$ |
| | | 1E − 1 | 2.124288043470 | 8.51E − 04 | 2.122318018663 | 7.70E − 05 | 2.122236352485 | 1.15E − 04 | 2.122481353547 | |
| | | 2E − 1 | 2.246553680531 | 3.18E − 03 | 2.238953114069 | 2.17E − 04 | 2.238363039452 | 4.81E − 04 | 2.239439975058 | |
| | | 3E − 1 | 2.366889332103 | 6.69E − 03 | 2.350382041577 | 3.33E − 04 | 2.348581651218 | 1.10E − 03 | 2.351166061395 | |
| | | 4E − 1 | 2.485382115832 | 1.12E − 02 | 2.457033632929 | 3.82E − 04 | 2.453171703485 | 1.95E − 03 | 2.457973187497 | |
| | | 5E − 1 | 2.602114062463 | 1.64E − 02 | 2.559293672584 | 3.49E − 04 | 2.552460563728 | 3.02E − 03 | 2.560187735597 | |
| | | 1E + 0 | 3.161908943210 | 4.92E − 02 | 3.015743447990 | 7.03E − 04 | 2.981766772533 | 1.06E − 02 | 3.013626129397 | |
| | | 2E + 0 | 4.185004164083 | 1.21E − 01 | 3.739173812344 | 1.49E − 03 | 4.135774696713 | 1.08E − 01 | 3.733597603174 | |
| | | 5E + 0 | 6.775808076626 | 2.70E − 01 | 5.212459550317 | 2.27E − 02 | 4.820347271993 | 9.62E − 02 | 5.333416434792 | |
| | | 1E + 1 | 12.039973698080 | 6.31E − 01 | 11.622115727277 | 5.74E − 01 | 11.342226056905 | 5.36E − 01 | 7.383537264058 | |
| | | 5E + 1 | 22.966747273068 | 2.54E − 01 | 22.735888141372 | 2.41E − 01 | 22.696860293494 | 2.39E − 01 | 18.314898304163 | |
| | | 1E + 2 | 38.120267705447 | 2.88E − 01 | 37.780344127957 | 2.76E − 01 | 37.700193736724 | 2.74E − 01 | 29.601244919262 | $(M,S)^{GS} = (1,2)$ |

**Table 7.9:** Relative errors of several *ab initio* many-body techniques with respect to the full configuration interaction energy taken here as reference for the ground state energy of a two-particle dot. From left to right, we give the approximated ground state and the relative error respectively for: the Hartree-Fock method, the Hartree-Fock method corrected by a $2^{nd}$ and $3^{rd}$-order correction in the HF basis, the energy given by many-body perturbation theory in the harmonic oscillator basis up to first, second and third order, and finally the configuration interaction energy with the parameters used to compute them.

**Table 7.10:** Relative errors of several *ab initio* many-body techniques with respect to the full configuration interaction energy taken here as reference for the ground state energy of a six-particle dot. From left to right, we give the approximated ground state and the relative error respectively for: the Hartree-Fock method, the Hartree-Fock method corrected by a $2^{nd}$ and $3^{rd}$-order correction in the HF basis, the energy given by many-body perturbation theory in the harmonic oscillator basis up to first, second and third order, and finally the configuration interaction energy with the parameters used to compute them.

| $\sharp e^-$ | $R^b$ | $\lambda$ | HF energy ($\hbar\omega$) | HF rel. error | HF+MBPT(HF)-$2^{nd}$ order energy ($\hbar\omega$) | rel. error | HF+MBPT(HF)-$3^{rd}$ order energy ($\hbar\omega$) | rel. error | Full CI energy ($\hbar\omega$) | parameters |
|---|---|---|---|---|---|---|---|---|---|---|
| 6 | 4 | $1E-7$ | 10.000001221981 | $0.00E+00$ | 10.000001221981 | $0.00E+00$ | 10.000001221981 | $0.00E+00$ | 10.000001221981 | |
| | | $5E-7$ | 10.000006109906 | $0.00E+00$ | 10.000006109906 | $9.95E-15$ | 10.000006109906 | $9.95E-15$ | 10.000006109906 | |
| | | $1E-6$ | 10.000012219811 | $4.00E-14$ | 10.000012219810 | $1.01E-14$ | 10.000012219810 | $1.01E-14$ | 10.000012219811 | |
| | | $5E-6$ | 10.000061099016 | $1.08E-12$ | 10.000061099004 | $1.10E-13$ | 10.000061099004 | $1.10E-13$ | 10.000061099005 | |
| | | $1E-5$ | 10.000122197937 | $4.32E-12$ | 10.000122197889 | $4.40E-13$ | 10.000122197889 | $4.40E-13$ | 10.000122197893 | |
| | | $5E-5$ | 10.000610985844 | $1.08E-10$ | 10.000610984654 | $1.12E-11$ | 10.000610984654 | $1.12E-11$ | 10.000610984766 | |
| | | $1E-4$ | 10.001222196092 | $4.31E-10$ | 10.001221957331 | $4.48E-11$ | 10.001221957331 | $4.48E-11$ | 10.001221957779 | |
| | | $5E-4$ | 10.006109426662 | $1.08E-08$ | 10.006109307623 | $1.12E-09$ | 10.006109307626 | $1.12E-09$ | 10.006109318814 | |
| | | $1E-3$ | 10.012217893980 | $4.31E-08$ | 10.012217417803 | $4.47E-09$ | 10.012217417826 | $4.47E-09$ | 10.012217462554 | |
| | | $5E-3$ | 10.061051127218 | $1.07E-06$ | 10.061039218756 | $1.11E-07$ | 10.061039221609 | $1.11E-07$ | 10.061040334895 | Computations with only |
| | | $1E-2$ | 10.122006554490 | $4.27E-06$ | 10.121958901199 | $4.40E-07$ | 10.121958924256 | $4.37E-07$ | 10.121963352201 | $R = 4, (M, S) = (0, 0)$ |
| | | $5E-2$ | 10.606237585801 | $1.02E-04$ | 10.605043121040 | $1.02E-05$ | 10.605046227528 | $9.91E-06$ | 10.605151307825 | |
| | | $1E-1$ | 11.203164005504 | $3.90E-04$ | 11.198377948795 | $3.69E-05$ | 11.198404863749 | $3.45E-05$ | 11.198791644206 | |
| | | $2E-1$ | 12.370396017420 | $1.43E-03$ | 12.351280581510 | $1.18E-04$ | 12.351523995048 | $9.85E-05$ | 12.352740173584 | |
| | | $3E-1$ | 13.504544464008 | $2.97E-03$ | 13.461851176111 | $2.04E-04$ | 13.462746122656 | $1.37E-04$ | 13.464591945533 | |
| | | $4E-1$ | 14.608605661990 | $4.90E-03$ | 14.533634757963 | $2.60E-04$ | 14.535884428949 | $1.05E-04$ | 14.537409076271 | |
| | | $5E-1$ | 15.685501416282 | $7.14E-03$ | 15.570250047282 | $2.60E-04$ | 15.574818078556 | $3.32E-05$ | 15.574301411949 | |
| | | $1E+0$ | 20.748402254288 | $2.12E-02$ | 20.375253481742 | $1.02E-03$ | 20.375264152845 | $2.88E-03$ | 20.316754002510 | |
| | | $2E+0$ | 29.876173541426 | $5.35E-02$ | 28.614309748677 | $8.96E-03$ | 28.860853512576 | $1.77E-02$ | 28.360088424685 | |
| | | $5E+0$ | 53.691824552566 | $1.13E-01$ | 50.763459667051 | $5.27E-02$ | 51.415859614987 | $6.63E-02$ | 48.220896992378 | |
| | | $5E+1$ | 91.190697218117 | $2.48E-01$ | 83.796753131214 | $1.47E-01$ | 85.839785051119 | $1.75E-01$ | 73.067354457427 | lowest GS for $R = 5$, $(M, S) = (0, 0)$ |
| | | $5E+1$ | 373.166706573103 | $3.98E-01$ | 336.364762441183 | $2.61E-01$ | 343.866968316472 | $2.89E-01$ | 266.841126091951 | lowest GS for $R = 5$, |
| | | $5E+2$ | 723.570709199507 | $4.28E-01$ | 648.354721946766 | $2.80E-01$ | 665.070975971614 | $3.13E-01$ | 506.530170970484 | $(M, S) = (1, 4)$ |
| | 8 | $1E-7$ | 10.000001221981 | $0.00E+00$ | 10.000001221981 | $0.00E+00$ | 10.000001221981 | $0.00E+00$ | 10.000001221981 | |
| | | $5E-7$ | 10.000006109906 | $0.00E+00$ | 10.000006109906 | $9.95E-15$ | 10.000006109906 | $9.95E-15$ | 10.000006109906 | |
| | | $1E-6$ | 10.000012219811 | $4.00E-14$ | 10.000012219810 | $3.00E-14$ | 10.000012219810 | $3.00E-14$ | 10.000012219811 | |
| | | $5E-6$ | 10.000061099015 | $9.70E-13$ | 10.000061098998 | $7.30E-13$ | 10.000061098998 | $7.30E-13$ | 10.000061099005 | |
| | | $1E-5$ | 10.000122197932 | $3.85E-12$ | 10.000122197864 | $2.94E-12$ | 10.000122197864 | $2.94E-12$ | 10.000122197893 | |
| | | $5E-5$ | 10.000610985729 | $9.63E-11$ | 10.000610984030 | $7.36E-11$ | 10.000610984030 | $7.36E-11$ | 10.000610984766 | |
| | | $1E-4$ | 10.001222196130 | $3.85E-10$ | 10.001221954835 | $2.94E-10$ | 10.001221954835 | $2.94E-10$ | 10.001221957779 | |
| | | $5E-4$ | 10.006109415140 | $9.63E-09$ | 10.006109245263 | $7.35E-09$ | 10.006109245259 | $7.35E-09$ | 10.006109318814 | |
| | | $1E-3$ | 10.012217848026 | $3.85E-08$ | 10.012217168587 | $2.94E-08$ | 10.012217168558 | $2.94E-08$ | 10.012217462554 | |
| | | $5E-3$ | 10.061050005063 | $9.61E-07$ | 10.061033032599 | $7.26E-07$ | 10.061033029056 | $7.26E-07$ | 10.061040334895 | Computations with only |
| | | $1E-2$ | 10.122002197025 | $3.84E-06$ | 10.121934375205 | $2.86E-06$ | 10.121934347371 | $2.87E-06$ | 10.121963352201 | $R = 4, (M, S) = (0, 0)$ |
| | | $5E-2$ | 10.606152586930 | $9.44E-05$ | 10.604471080231 | $6.41E-05$ | 10.604468100180 | $6.44E-05$ | 10.605151307825 | |
| | | $1E-1$ | 11.202922249993 | $1.39E-03$ | 11.196270198560 | $2.25E-04$ | 11.196257347877 | $2.26E-04$ | 11.198791644206 | |
| | | $2E-1$ | 12.369986767796 | $2.94E-03$ | 12.343990196237 | $7.08E-04$ | 12.343859746947 | $7.11E-04$ | 12.352740173584 | |
| | | $3E-1$ | 13.504208965361 | $2.94E-03$ | 13.447246826392 | $1.29E-03$ | 13.445612822036 | $1.41E-03$ | 13.464591945533 | |
| | | $4E-1$ | 14.608357065775 | $4.88E-03$ | 14.509802433838 | $1.90E-03$ | 14.507104502585 | $2.08E-03$ | 14.537409076271 | |
| | | $5E-1$ | 15.684819018465 | $7.10E-03$ | 15.535086837586 | $2.52E-03$ | 15.554143298097 | $1.29E-03$ | 15.574301411949 | |
| | | $1E+0$ | 20.719248175282 | $1.98E-02$ | 20.201229212983 | $5.69E-03$ | 20.218329788077 | $4.84E-03$ | 20.316754002510 | |
| | | $2E+0$ | 29.553893712856 | $4.21E-02$ | 27.982294512087 | $1.33E-02$ | 28.151482969245 | $7.36E-03$ | 28.360088424685 | |
| | | $5E+0$ | 44.249048160124 | $8.24E-02$ | 42.999900804541 | $1.08E-01$ | 42.943908735317 | $1.09E-01$ | 48.220896992378 | |
| | | $5E+1$ | 152.918469535500 | $1.09E+00$ | 97.968877514451 | $3.41E-01$ | 207.568792185046 | $7.46E-01$ | 73.067354457427 | lowest GS for $R = 5$, $(M, S) = (0, 0)$ |
| | | $5E+1$ | 227.685682577638 | $1.47E-01$ | 216.399780989799 | $1.89E-01$ | 207.709314596807 | $2.22E-01$ | 266.841126091951 | lowest GS for $R = 5$, |
| | | $5E+2$ | 439.532217979911 | $1.32E-01$ | 413.447621224150 | $1.84E-01$ | 396.851566567381 | $2.17E-01$ | 506.530170970484 | $(M, S) = (1, 4)$ |

| # e⁻ | $R^b$ | $\lambda$ | HF energy ($\hbar\omega$) | rel. error | HF+MBPT(HF)-2$^{nd}$ order energy ($\hbar\omega$) | rel. error | HF+MBPT(HF)-3$^{rd}$ order energy ($\hbar\omega$) | rel. error | Full CI energy ($\hbar\omega$) | parameters |
|---|---|---|---|---|---|---|---|---|---|---|
| 12 | 4 | 1E − 7 | 28.000004576555 | 0.00E + 00 | 28.000004576555 | 0.00E + 00 | 28.000004576555 | 0.00E + 00 | 28.000004576555 | Computations with only $R = 3$, $(M, S) = (0, 0)$ |
| | | 5E − 7 | 28.0000228882772 | 5.00E − 14 | 28.0000228882772 | 5.71E − 14 | 28.0000228882772 | 5.71E − 14 | 28.000022882774 | |
| | | 1E − 6 | 28.000045765540 | 1.96E − 13 | 28.000045765539 | 2.18E − 13 | 28.000045765539 | 2.18E − 13 | 28.000045765545 | |
| | | 5E − 6 | 28.000228827509 | 4.91E − 12 | 28.000228827495 | 5.41E − 12 | 28.000228827495 | 5.41E − 12 | 28.000228827646 | |
| | | 1E − 5 | 28.000457654546 | 1.96E − 11 | 28.000457654489 | 2.16E − 11 | 28.000457654489 | 2.16E − 11 | 28.000457655095 | |
| | | 5E − 5 | 28.002288253834 | 4.91E − 10 | 28.002288252424 | 5.41E − 10 | 28.002288252424 | 5.41E − 10 | 28.002288267575 | |
| | | 1E − 4 | 28.004576460432 | 1.96E − 09 | 28.004576454794 | 2.16E − 09 | 28.004576454794 | 2.16E − 09 | 28.004576515396 | |
| | | 5E − 4 | 28.022880412872 | 4.90E − 08 | 28.022880271860 | 5.41E − 08 | 28.022880271853 | 5.41E − 08 | 28.022881786724 | |
| | | 1E − 3 | 28.045756103306 | 1.96E − 07 | 28.045755538941 | 2.16E − 07 | 28.045755538888 | 2.16E − 07 | 28.045761597478 | |
| | | 5E − 3 | 28.228591777300 | 4.86E − 06 | 28.228577605242 | 5.36E − 06 | 28.228577598505 | 5.36E − 06 | 28.228728882585 | |
| | | 1E − 2 | 28.456712525178 | 1.92E − 05 | 28.456655526319 | 2.12E − 05 | 28.456654471930 | 2.12E − 05 | 28.457259680513 | |
| | | 5E − 2 | 30.264911808725 | 4.43E − 04 | 30.263429009206 | 4.92E − 04 | 30.263421756722 | 4.92E − 04 | 30.278318327442 | |
| | | 1E − 1 | 32.484376480755 | 1.60E − 03 | 32.478202624544 | 1.79E − 03 | 32.478141067399 | 1.79E − 03 | 32.536480931004 | |
| | | 2E − 1 | 36.797055408932 | 5.27E − 03 | 36.771062499380 | 5.97E − 03 | 36.770542250789 | 5.99E − 03 | 36.992010607447 | |
| | | 3E − 1 | 40.961183077452 | 9.84E − 03 | 40.901512484210 | 1.13E − 02 | 40.899775842855 | 1.13E − 02 | 41.368445666447 | |
| | | 4E − 1 | 45.000567680461 | 1.47E − 02 | 44.894701107258 | 1.70E − 02 | 44.890807609895 | 1.71E − 02 | 45.670810879121 | |
| | | 5E − 1 | 48.936365417564 | 1.94E − 02 | 48.773724150896 | 2.27E − 02 | 48.766733218374 | 2.28E − 02 | 49.905865978617 | |
| | | 1E + 0 | 67.569930222732 | 3.90E − 02 | 67.024444698457 | 4.68E − 02 | 66.992675350455 | 4.72E − 02 | 70.312502175757 | |
| | | 2E + 0 | 102.292196585864 | 6.16E − 02 | 100.826554465561 | 7.51E − 02 | 100.737427532380 | 7.59E − 02 | 109.010808418516 | |
| | | 5E + 0 | 200.826644244514 | 8.08E − 02 | 196.562566888881 | 1.00E − 01 | 196.552202980407 | 1.00E − 01 | 218.488098056035 | |
| | | 1E + 1 | 359.443501215690 | 9.56E − 02 | 353.978643401936 | 1.09E − 01 | 353.780127476716 | 1.10E − 01 | 397.443249829703 | |
| | | 5E + 1 | 1,621.747795925120 | 1.11E − 01 | 1,594.575953000710 | 1.26E − 01 | 1,593.293295115500 | 1.26E − 01 | 1,823.602313382110 | |
| | | 5E + 2 | 3,198.533123735590 | 1.13E − 01 | 3,144.658909324040 | 1.28E − 01 | 3,142.089310529960 | 1.29E − 01 | 3,605.813353473020 | |
| | 8 | 1E − 7 | 28.000004576555 | 0.00E + 00 | 28.000004576555 | 0.00E + 00 | 28.000004576555 | 0.00E + 00 | 28.000004576555 | Computations with only $R = 3$, $(M, S) = (0, 0)$ |
| | | 5E − 7 | 28.0000228882772 | 5.35E − 14 | 28.0000228882772 | 6.43E − 14 | 28.0000228882772 | 6.43E − 14 | 28.000022882774 | |
| | | 1E − 6 | 28.000045765539 | 2.04E − 13 | 28.000045765538 | 2.46E − 13 | 28.000045765538 | 2.46E − 13 | 28.000045765545 | |
| | | 5E − 6 | 28.000228827504 | 5.08E − 12 | 28.000228827475 | 6.13E − 12 | 28.000228827475 | 6.13E − 12 | 28.000228827646 | |
| | | 1E − 5 | 28.000457654526 | 2.03E − 11 | 28.000457654409 | 2.45E − 11 | 28.000457654409 | 2.45E − 11 | 28.000457655095 | |
| | | 5E − 5 | 28.002288253339 | 5.08E − 10 | 28.002288250403 | 6.13E − 10 | 28.002288250403 | 6.13E − 10 | 28.002288267575 | |
| | | 1E − 4 | 28.004576458452 | 2.03E − 09 | 28.004576446710 | 2.45E − 09 | 28.004576446710 | 2.45E − 09 | 28.004576515396 | |
| | | 5E − 4 | 28.022880363596 | 5.08E − 08 | 28.022880070043 | 6.13E − 08 | 28.022880070061 | 6.13E − 08 | 28.022881786724 | |
| | | 1E − 3 | 28.045755907335 | 2.03E − 07 | 28.045754733030 | 2.45E − 07 | 28.045754733171 | 2.45E − 07 | 28.045761597478 | |
| | | 5E − 3 | 28.228587100883 | 5.02E − 06 | 28.228557742903 | 6.06E − 06 | 28.228557742903 | 6.06E − 06 | 28.228728882585 | |
| | | 1E − 2 | 28.456694897827 | 1.98E − 05 | 28.456577306641 | 2.40E − 05 | 28.456577450118 | 2.40E − 05 | 28.457259680513 | |
| | | 5E − 2 | 30.264652314968 | 4.51E − 04 | 30.261697622438 | 5.49E − 04 | 30.261716167559 | 5.48E − 04 | 30.278318327442 | |
| | | 1E − 1 | 32.483931929728 | 1.62E − 03 | 32.472063225263 | 1.98E − 03 | 32.472219432147 | 1.98E − 03 | 32.536480931004 | |
| | | 2E − 1 | 36.796754408665 | 5.28E − 03 | 36.749159304656 | 6.56E − 03 | 36.750303251535 | 6.53E − 03 | 36.992010607447 | |
| | | 3E − 1 | 40.957264235247 | 9.94E − 03 | 40.850593827221 | 1.25E − 02 | 40.856383632075 | 1.24E − 02 | 41.368445666447 | |
| | | 4E − 1 | 44.981509722895 | 1.51E − 02 | 44.793359760008 | 1.92E − 02 | 44.805605335578 | 1.89E − 02 | 45.670810879121 | |
| | | 5E − 1 | 48.883234063775 | 2.05E − 02 | 48.593529883188 | 2.63E − 02 | 48.617043675475 | 2.58E − 02 | 49.905865978617 | |
| | | 1E + 0 | 66.912244170015 | 4.84E − 02 | 65.870798169807 | 6.32E − 02 | 66.038258669640 | 6.08E − 02 | 70.312502175757 | |
| | | 2E + 0 | 98.067797155616 | 1.00E − 01 | 94.893535047153 | 1.30E − 01 | 96.145512858464 | 1.18E − 01 | 109.010808418516 | |
| | | 5E + 0 | 290.237582802627 | 3.28E − 01 | 269.034180902363 | 2.31E − 01 | 261.549657366640 | 1.97E − 01 | 218.488098056035 | |
| | | 1E + 1 | 561.833857484633 | 4.14E − 01 | 472.763584640851 | 1.90E − 01 | 18.347844959507 | 9.54E − 01 | 397.443249829703 | |
| | | 5E + 1 | 1,178.795947280830 | 3.54E − 01 | 1,120.256010293640 | 3.86E − 01 | 1,139.154117277190 | 3.75E − 01 | 1,823.602313382110 | |
| | | 5E + 2 | 2,279.692075613080 | 3.68E − 01 | 2,160.771693088170 | 4.01E − 01 | 2,201.068248999480 | 3.90E − 01 | 3,605.813353473020 | |

**Table 7.11:** Relative errors of several *ab initio* many-body techniques with respect to the full configuration interaction energy taken here as reference for the ground state energy of a 12-particle dot. From left to right, we give the approximated ground state and the relative error respectively for: the Hartree–Fock method, the Hartree–Fock method corrected by a 2$^{nd}$ and 3$^{rd}$-order correction in the HF basis, the energy given by many-body perturbation theory in the harmonic oscillator basis up to first, second and third order, and finally the configuration interaction energy with the parameters used to compute them.

| # e⁻ | $R^b$ | λ | MBPT(HO)-$1^{st}$ order energy ($\hbar\omega$) | rel. error | MBPT(HO)-$2^{nd}$ order energy ($\hbar\omega$) | rel. error | MBPT(HO)-$3^{rd}$ order energy ($\hbar\omega$) | rel. error | Full CI energy ($\hbar\omega$) | parameters |
|---|---|---|---|---|---|---|---|---|---|---|
| 2 | 4 | 1E−7 | 2.000000125331 | 0.00E+00 | 2.000000125331 | 0.00E+00 | 2.000000125331 | 0.00E+00 | 2.000000125331 | |
| | | 5E−7 | 2.000000626657 | 3.49E−14 | 2.000000626657 | 9.99E−15 | 2.000000626657 | 9.99E−15 | 2.000000626657 | |
| | | 1E−6 | 2.000001253314 | 1.45E−13 | 2.000001253314 | 4.51E−14 | 2.000001253314 | 4.51E−14 | 2.000001253314 | |
| | | 5E−6 | 2.000006266568 | 3.61E−12 | 2.000006266566 | 1.15E−12 | 2.000006266566 | 1.15E−12 | 2.000006266563 | |
| | | 1E−5 | 2.000012533131 | 1.45E−11 | 2.000012533122 | 4.62E−12 | 2.000012533122 | 4.62E−12 | 2.000012533112 | |
| | | 5E−5 | 2.000062665444 | 3.61E−10 | 2.000062665215 | 1.15E−10 | 2.000062665215 | 1.15E−10 | 2.000062664984 | $(M,S)^{GS} = (0,0)$ for |
| | | 1E−4 | 2.000125330363 | 1.45E−09 | 2.000125329446 | 4.62E−10 | 2.000125329446 | 4.62E−10 | 2.000125328523 | $R = 5$, $M \in [0:12]$ and |
| | | 5E−4 | 2.000626630801 | 3.61E−08 | 2.000626607881 | 1.15E−08 | 2.000626607890 | 1.15E−08 | 2.000626584794 | $S \in [0:2]$ |
| | | 1E−3 | 2.001253209074 | 1.44E−07 | 2.001253117385 | 4.61E−08 | 2.001253117459 | 4.62E−08 | 2.001253025058 | |
| | | 5E−3 | 2.006263945539 | 3.60E−06 | 2.006261651873 | 1.15E−06 | 2.006261661131 | 1.15E−06 | 2.006259347655 | |
| | | 1E−2 | 2.012522647963 | 1.43E−05 | 2.012513466119 | 4.57E−06 | 2.012513540105 | 4.61E−06 | 2.012504269056 | |
| | | 5E−2 | 2.062404808005 | 3.48E−04 | 2.062173825512 | 1.10E−04 | 2.062182990983 | 1.14E−04 | 2.061947942318 | |
| | | 1E−1 | 2.124295000418 | 1.34E−03 | 2.123363888315 | 4.16E−04 | 2.123436335481 | 4.50E−04 | 2.122481353547 | |
| | | 2E−1 | 2.246574506683 | 5.01E−03 | 2.242792725798 | 1.50E−03 | 2.243357176090 | 1.75E−03 | 2.239439975058 | |
| | | 3E−1 | 2.366923700288 | 1.06E−02 | 2.358286512449 | 3.03E−03 | 2.360136553189 | 3.82E−03 | 2.351166061395 | |
| | | 4E−1 | 2.485425861700 | 1.76E−02 | 2.469845248267 | 4.83E−03 | 2.474093512102 | 6.56E−03 | 2.457973187497 | |
| | | 5E−1 | 2.602161579782 | 2.60E−02 | 2.577468933253 | 6.75E−03 | 2.585490025756 | 9.88E−03 | 2.560187735597 | |
| | | 1E+0 | 3.161921401726 | 7.95E−02 | 3.056561595695 | 1.42E−02 | 3.109529767677 | 3.18E−02 | 3.013626129397 | |
| | | 2E+0 | 4.185136950885 | 2.07E−01 | 3.719618108148 | 3.74E−02 | 3.995708550047 | 7.02E−02 | 3.733597603174 | |
| | | 5E+0 | 6.775965715485 | 5.50E−01 | 3.347757146059 | 3.72E−01 | 4.711596090878 | 1.17E−01 | 5.333416434792 | |
| | | 1E+1 | 9.192744506771 | 9.68E−01 | −5.142127788917 | 1.70E+00 | −4.824474514976 | 1.65E+00 | 7.383537264058 | |
| | | 5E+1 | 27.433561900391 | 2.53E+00 | −427.215647186034 | 2.43E+01 | −427.406263075788 | 2.43E+01 | 18.314898304163 | |
| | | 5E+2 | 49.760800203239 | 3.30E+00 | −1,840.194002475680 | 6.32E+01 | −1,840.892230228590 | 6.32E+01 | 29.601244919262 | $(M,S)^{GS} = (1,2)$ |
| | 8 | 1E−7 | 2.000000125331 | 0.00E+00 | 2.000000125331 | 0.00E+00 | 2.000000125331 | 0.00E+00 | 2.000000125331 | |
| | | 5E−7 | 2.000000626657 | 3.49E−14 | 2.000000626657 | 4.88E−15 | 2.000000626657 | 4.88E−15 | 2.000000626657 | |
| | | 1E−6 | 2.000001253314 | 1.45E−13 | 2.000001253314 | 3.00E−14 | 2.000001253314 | 3.00E−14 | 2.000001253314 | |
| | | 5E−6 | 2.000006266568 | 3.61E−12 | 2.000006266565 | 7.25E−13 | 2.000006266565 | 7.25E−13 | 2.000006266563 | |
| | | 1E−5 | 2.000012533131 | 1.45E−11 | 2.000012533118 | 2.91E−12 | 2.000012533118 | 2.91E−12 | 2.000012533112 | |
| | | 5E−5 | 2.000062665442 | 3.61E−10 | 2.000062665130 | 7.28E−11 | 2.000062665130 | 7.28E−11 | 2.000062664984 | $(M,S)^{GS} = (0,0)$ for |
| | | 1E−4 | 2.000125330354 | 1.45E−09 | 2.000125329105 | 2.91E−10 | 2.000125329105 | 2.91E−10 | 2.000125328523 | $R = 5$, $M \in [0:12]$ and |
| | | 5E−4 | 2.000626630573 | 3.61E−08 | 2.000626599343 | 7.27E−09 | 2.000626599331 | 7.27E−09 | 2.000626584794 | $S \in [0:2]$ |
| | | 1E−3 | 2.001253208163 | 1.44E−07 | 2.001253083234 | 2.91E−08 | 2.001253083143 | 2.90E−08 | 2.001253025058 | |
| | | 5E−3 | 2.006263922999 | 3.60E−06 | 2.006260786846 | 7.23E−07 | 2.006260786846 | 7.17E−07 | 2.006259347655 | |
| | | 1E−2 | 2.012522558992 | 1.43E−05 | 2.012510051031 | 2.87E−06 | 2.012509961457 | 2.83E−06 | 2.012504269056 | |
| | | 5E−2 | 2.062402810851 | 3.48E−04 | 2.062088448305 | 6.81E−05 | 2.062077703161 | 6.29E−05 | 2.061947942318 | |
| | | 1E−1 | 2.124288043470 | 1.34E−03 | 2.123022947487 | 2.55E−04 | 2.122940713309 | 2.16E−04 | 2.122481353547 | |
| | | 2E−1 | 2.246553680531 | 5.01E−03 | 2.241426690483 | 8.87E−04 | 2.240836615866 | 6.24E−04 | 2.239439975058 | |
| | | 3E−1 | 2.366889332103 | 1.06E−02 | 2.355212932990 | 1.72E−03 | 2.353412542631 | 9.55E−04 | 2.351166061395 | |
| | | 4E−1 | 2.485382115832 | 1.76E−02 | 2.464381107007 | 2.61E−03 | 2.460519177563 | 1.04E−03 | 2.457973187497 | |
| | | 5E−1 | 2.602114062463 | 2.60E−02 | 2.568931212534 | 3.42E−03 | 2.562098103678 | 7.46E−04 | 2.560187735597 | |
| | | 1E+0 | 3.161908943210 | 7.95E−02 | 3.022410712821 | 2.91E−03 | 2.988434037364 | 8.36E−03 | 3.013626129397 | |
| | | 2E+0 | 4.185004164083 | 2.07E−01 | 3.583014576652 | 4.03E−02 | 3.979615461021 | 6.59E−02 | 3.733597603174 | |
| | | 5E+0 | 6.775808076626 | 5.50E−01 | 2.493985074207 | 5.32E−01 | 2.101872795883 | 6.06E−01 | 5.333416434792 | |
| | | 1E+1 | 12.039973698080 | 9.68E−01 | −8.557201076326 | 2.16E+00 | −8.837090746698 | 2.20E+00 | 7.383537264058 | |
| | | 5E+1 | 22.966747273068 | 2.53E+00 | −512.592854371255 | 2.90E+01 | −512.631882219133 | 2.90E+01 | 18.314898304163 | |
| | | 1E+2 | 38.120267705447 | 3.30E+00 | −2,181.702831216570 | 7.47E+01 | −2,181.782981607800 | 7.47E+01 | 29.601244919262 | $(M,S)^{GS} = (1,2)$ |

**Table 7.12:** Relative errors of several *ab initio* many-body techniques with respect to the full configuration interaction energy taken here as reference for the ground state energy of a two-particle dot. From left to right, we give the approximated ground state and the relative error respectively for: the Hartree–Fock method, the Hartree–Fock method corrected by a $2^{nd}$ and $3^{rd}$-order correction in the HF basis, the energy given by many-body perturbation theory in the harmonic oscillator basis up to first, second and third order, and finally the configuration interaction energy with the parameters used to compute them.

| ♯ e⁻ | $R^b$ | $\lambda$ | MBPT(HO)-$1^{st}$ order energy ($\hbar\omega$) | rel. error | MBPT(HO)-$2^{nd}$ order energy ($\hbar\omega$) | rel. error | MBPT(HO)-$3^{rd}$ order energy ($\hbar\omega$) | rel. error | Full CI energy ($\hbar\omega$) | parameters |
|---|---|---|---|---|---|---|---|---|---|---|
| 6 | 4 | 1E−7 | 10.000001221981 | 0.00E+00 | 10.000001221981 | 0.00E+00 | 10.000001221981 | 0.00E+00 | 10.000001221981 | |
| | | 5E−7 | 10.000006109906 | 4.99E−14 | 10.000006109906 | 4.00E−14 | 10.000006109906 | 4.00E−14 | 10.000006109906 | |
| | | 1E−6 | 10.000012219811 | 2.30E−13 | 10.000012219812 | 1.80E−13 | 10.000012219812 | 1.80E−13 | 10.000012219811 | |
| | | 5E−6 | 10.000061099016 | 5.88E−12 | 10.000061099051 | 4.51E−12 | 10.000061099051 | 4.51E−12 | 10.000061099005 | |
| | | 1E−5 | 10.000122197937 | 2.35E−11 | 10.000122198074 | 1.80E−11 | 10.000122198074 | 1.80E−11 | 10.000122197893 | |
| | | 5E−5 | 10.000610985844 | 5.88E−10 | 10.000610989272 | 4.51E−10 | 10.000610989272 | 4.51E−10 | 10.000610984766 | |
| | | 1E−4 | 10.001221962092 | 2.35E−09 | 10.001221975805 | 1.80E−09 | 10.001221975805 | 1.80E−09 | 10.001221957779 | |
| | | 5E−4 | 10.006109426662 | 5.87E−08 | 10.006109769452 | 4.50E−08 | 10.006109769455 | 4.50E−08 | 10.006109318814 | |
| | | 1E−3 | 10.012217893980 | 2.35E−07 | 10.012219264969 | 1.80E−07 | 10.012219264992 | 1.80E−07 | 10.012217462554 | |
| | | 5E−3 | 10.061051127218 | 5.84E−06 | 10.061085367457 | 4.48E−06 | 10.061085370310 | 4.48E−06 | 10.061040334895 | Computations with only $R=4$, $(M,S)=(0,0)$ |
| | | 1E−2 | 10.122006554490 | 2.32E−05 | 10.122143334441 | 1.78E−05 | 10.122143364498 | 1.78E−05 | 10.121963352201 | |
| | | 5E−2 | 10.606237585801 | 5.51E−04 | 10.609620968271 | 4.21E−04 | 10.609624074760 | 4.22E−04 | 10.605151307825 | |
| | | 1E−1 | 11.203164005504 | 2.07E−03 | 11.216502589201 | 1.58E−03 | 11.216529504155 | 1.58E−03 | 11.198791644206 | |
| | | 2E−1 | 12.370396017420 | 7.38E−03 | 12.422047789038 | 5.61E−03 | 12.422291202576 | 5.63E−03 | 12.352740173584 | |
| | | 3E−1 | 13.504544464008 | 1.50E−02 | 13.616635599511 | 1.13E−02 | 13.617530546057 | 1.14E−02 | 13.464591945533 | |
| | | 4E−1 | 14.608606661990 | 2.41E−02 | 14.800266020621 | 1.81E−02 | 14.802515691607 | 1.82E−02 | 14.537409076271 | |
| | | 5E−1 | 15.685501416282 | 3.44E−02 | 15.972939052367 | 2.56E−02 | 15.977507083641 | 2.59E−02 | 15.574301411949 | |
| | | 1E+0 | 20.748402254288 | 9.37E−02 | 21.671943370641 | 6.67E−02 | 21.709654041743 | 6.86E−02 | 20.316754002510 | |
| | | 2E+0 | 29.876173541426 | 2.14E−01 | 32.248147804911 | 1.37E−01 | 32.494691568810 | 1.46E−01 | 28.360088424685 | |
| | | 5E+0 | 53.691824552566 | 4.74E−01 | 57.402327489498 | 1.90E−01 | 58.054727437434 | 2.04E−01 | 48.220896992378 | |
| | | 1E+1 | 91.190697218117 | 8.09E−01 | 77.411181569731 | 5.94E−02 | 79.454213489636 | 8.74E−02 | 73.067354457427 | lowest GS for $R=5$, $(M,S)=(0,0)$ |
| | | 5E+1 | 373.166706573103 | 1.33E+00 | −748.683028521954 | 3.81E+00 | −741.180822646665 | 3.78E+00 | 266.841126091951 | lowest GS for $R=5$, |
| | | 1E+2 | 723.570709199507 | 1.43E+00 | −4,246.713397970430 | 9.38E+00 | −4,229.997143945580 | 9.35E+00 | 506.530170970484 | $(M,S)=(1,4)$ |
| | 8 | 1E−7 | 10.000001221981 | 0.00E+00 | 10.000001221981 | 0.00E+00 | 10.000001221981 | 0.00E+00 | 10.000001221981 | |
| | | 5E−7 | 10.000006109906 | 4.99E−14 | 10.000006109906 | 3.00E−14 | 10.000006109906 | 3.00E−14 | 10.000006109906 | |
| | | 1E−6 | 10.000012219811 | 2.30E−13 | 10.000012219812 | 1.60E−13 | 10.000012219812 | 1.60E−13 | 10.000012219811 | |
| | | 5E−6 | 10.000061099015 | 5.88E−12 | 10.000061099046 | 4.02E−12 | 10.000061099046 | 4.02E−12 | 10.000061099005 | |
| | | 1E−5 | 10.000122197932 | 2.35E−11 | 10.000122198054 | 1.61E−11 | 10.000122198054 | 1.61E−11 | 10.000122197893 | |
| | | 5E−5 | 10.000610985729 | 5.88E−10 | 10.000610988786 | 4.02E−10 | 10.000610988786 | 4.02E−10 | 10.000610984766 | |
| | | 1E−4 | 10.001221961630 | 2.35E−09 | 10.001221973859 | 1.61E−09 | 10.001221973859 | 1.61E−09 | 10.001221957779 | |
| | | 5E−4 | 10.006109415140 | 5.87E−08 | 10.006109720789 | 4.02E−08 | 10.006109720785 | 4.02E−08 | 10.006109318814 | |
| | | 1E−3 | 10.012217848026 | 2.35E−07 | 10.012219070316 | 1.61E−07 | 10.012219070288 | 1.61E−07 | 10.012217462554 | |
| | | 5E−3 | 10.061050005063 | 5.84E−06 | 10.061080050129 | 3.99E−06 | 10.061080497586 | 3.99E−06 | 10.061040334895 | Computations with only $R=4$, $(M,S)=(0,0)$ |
| | | 1E−2 | 10.122002197025 | 2.32E−05 | 10.122123876129 | 1.59E−05 | 10.122123848295 | 1.59E−05 | 10.121963352201 | |
| | | 5E−2 | 10.606152586930 | 5.51E−04 | 10.609134335466 | 3.76E−04 | 10.609131355414 | 3.75E−04 | 10.605151307825 | |
| | | 1E−1 | 11.202922249993 | 2.07E−03 | 11.214556057981 | 1.41E−03 | 11.214543207298 | 1.41E−03 | 11.198791644206 | |
| | | 2E−1 | 12.369968767796 | 7.38E−03 | 12.414261664157 | 4.98E−03 | 12.414231214867 | 4.98E−03 | 12.352740173584 | |
| | | 3E−1 | 13.504208965361 | 1.50E−02 | 13.599116818529 | 9.99E−03 | 13.597482814172 | 9.87E−03 | 13.464591945533 | |
| | | 4E−1 | 14.608357065775 | 2.41E−02 | 14.769121512097 | 1.59E−02 | 14.766442358843 | 1.58E−02 | 14.537409076271 | |
| | | 5E−1 | 15.684819018465 | 3.44E−02 | 15.924275771860 | 2.25E−02 | 15.943332232371 | 2.37E−02 | 15.574301411949 | |
| | | 1E+0 | 20.719248175282 | 9.37E−02 | 21.477290248615 | 5.71E−02 | 21.494390914709 | 5.80E−02 | 20.316754002510 | |
| | | 2E+0 | 29.553893712856 | 2.14E−01 | 31.469535316807 | 1.10E−01 | 31.638723773964 | 1.16E−01 | 28.360088424685 | |
| | | 5E+0 | 44.249048160124 | 4.74E−01 | 52.545599438849 | 8.95E−02 | 52.480007369626 | 8.83E−02 | 48.220896992378 | |
| | | 1E+1 | 152.918469535500 | 8.09E−01 | 57.945869367135 | 2.07E−01 | 87.545784037730 | 1.98E−01 | 73.067354457427 | lowest GS for $R=5$, $(M,S)=(0,0)$ |
| | | 5E+1 | 227.685682577638 | 1.33E+00 | −1,235.315833586860 | 5.63E+00 | −1,244.006299979860 | 5.66E+00 | 266.841126091951 | lowest GS for $R=5$, |
| | | 1E+2 | 439.532217979911 | 1.43E+00 | −6,193.244618230070 | 1.32E+01 | −6,209.840672886840 | 1.33E+01 | 506.530170970484 | $(M,S)=(1,4)$ |

**Table 7.13:** Relative errors of several *ab initio* many-body techniques with respect to the full configuration interaction energy taken here as reference for the ground state energy of a six-particle dot. From left to right, we give the approximated ground state and the relative error respectively for: the Hartree-Fock method, the Hartree-Fock method corrected by a $2^{nd}$ and $3^{rd}$-order correction in the HF basis, the energy given by many-body perturbation theory in the harmonic oscillator basis up to first, second and third order, and finally the configuration interaction energy with the parameters used to compute them.

| # e⁻ | $R^b$ | λ | MBPT(HO)-$1^{st}$order energy ($\hbar\omega$) | rel. error | MBPT(HO)-$2^{nd}$order energy ($\hbar\omega$) | rel. error | MBPT(HO)-$3^{rd}$order energy ($\hbar\omega$) | rel. error | Full CI energy ($\hbar\omega$) | parameters |
|---|---|---|---|---|---|---|---|---|---|---|
| 12 | 4 | 1E−7 | 28.00004576555 | 0.00E+00 | 28.00004576555 | 0.00E+00 | 28.00004576555 | 0.00E+00 | 28.00004576555 | |
| | | 5E−7 | 28.00002882772 | 3.21E−14 | 28.00002882774 | 2.50E−14 | 28.00002882774 | 2.50E−14 | 28.00002882774 | |
| | | 1E−6 | 28.00045765540 | 1.39E−13 | 28.00045765548 | 1.11E−13 | 28.00045765548 | 1.11E−13 | 28.00045765545 | |
| | | 5E−6 | 28.00228827509 | 3.53E−12 | 28.00228827724 | 2.75E−12 | 28.00228827724 | 2.75E−12 | 28.00228827646 | |
| | | 1E−5 | 28.000457654546 | 1.41E−11 | 28.000457655403 | 1.10E−11 | 28.000457655403 | 1.10E−11 | 28.000457655095 | |
| | | 5E−5 | 28.002288253834 | 3.53E−10 | 28.002288275275 | 2.75E−10 | 28.002288275275 | 2.75E−10 | 28.002288275575 | |
| | | 1E−4 | 28.004576460432 | 1.41E−09 | 28.004576546194 | 1.10E−09 | 28.004576546194 | 1.10E−09 | 28.004576515396 | |
| | | 5E−4 | 28.022880412872 | 3.52E−08 | 28.022882556758 | 2.75E−08 | 28.022882556751 | 2.75E−08 | 28.022881786724 | |
| | | 1E−3 | 28.045756103306 | 1.41E−07 | 28.045764677986 | 1.10E−07 | 28.045764677933 | 1.10E−07 | 28.045761597478 | |
| | | 5E−3 | 28.228591777300 | 3.50E−06 | 28.228805968749 | 2.73E−06 | 28.228805962013 | 2.73E−06 | 28.228728882585 | |
| | | 1E−2 | 28.45671251 25178 | 1.39E−05 | 28.457568384542 | 1.08E−05 | 28.457568330153 | 1.08E−05 | 28.457259680513 | |
| | | 5E−2 | 30.26491808725 | 3.29E−04 | 30.26099804477 | 2.57E−04 | 30.26009255 1993 | 2.57E−04 | 30.278318327442 | |
| | | 1E−1 | 32.484376480755 | 1.23E−03 | 32.567844313365 | 9.64E−04 | 32.567782756221 | 9.62E−04 | 32.536480931004 | Computations with only |
| | | 2E−1 | 36.797055408932 | 4.35E−03 | 37.118267444379 | 3.41E−03 | 37.117747195788 | 3.40E−03 | 36.992010607447 | $R = 3$, $(M,S) = (0,0)$ |
| | | 3E−1 | 40.961183077452 | 8.73E−03 | 41.651269393041 | 6.84E−03 | 41.649532751687 | 6.79E−03 | 41.368445666447 | |
| | | 4E−1 | 45.000567680461 | 1.39E−02 | 46.168501593352 | 1.09E−02 | 46.162956661990 | 1.08E−02 | 45.670810879121 | |
| | | 5E−1 | 48.936365417564 | 1.96E−02 | 50.665009743311 | 1.52E−02 | 50.658018810789 | 1.51E−02 | 49.905865978617 | |
| | | 1E+0 | 67.569930222732 | 4.91E−02 | 72.894489927834 | 3.67E−02 | 72.862718779832 | 3.63E−02 | 70.312502175757 | |
| | | 2E+0 | 102.2921968585864 | 9.65E−02 | 116.0468611620514 | 6.45E−02 | 115.9577336 87333 | 6.37E−02 | 109.010808418516 | |
| | | 5E+0 | 200.826644244514 | 1.75E−01 | 235.0512672 87627 | 7.58E−02 | 235.0409033 79153 | 7.58E−02 | 218.48098056035 | |
| | | 1E+1 | 359.443501215690 | 2.22E−01 | 398.5495786 96396 | 2.78E−02 | 398.3510627 71176 | 2.28E−03 | 397.44324982 9703 | |
| | | 5E+1 | 1,621.747795925120 | 2.70E−01 | 138.629658327638 | 9.24E−01 | 137.346034838477 | 9.25E−01 | 1,823.60231338210 | |
| | | 1E+2 | 3,198.5331237735590 | 2.77E−01 | −4,106.036271230580 | 2.14E+00 | −4,108.605870024660 | 2.14E+00 | 3,605.81335473020 | |
| 12 | 8 | 1E−7 | 28.00004576555 | 0.00E+00 | 28.00004576555 | 0.00E+00 | 28.00004576555 | 0.00E+00 | 28.00004576555 | |
| | | 5E−7 | 28.00002882772 | 3.21E−14 | 28.00002882774 | 2.14E−14 | 28.00002882774 | 2.14E−14 | 28.00002882774 | |
| | | 1E−6 | 28.00045765539 | 1.39E−13 | 28.00045765548 | 8.93E−14 | 28.00045765548 | 8.93E−14 | 28.00045765545 | |
| | | 5E−6 | 28.00228827504 | 3.53E−12 | 28.00228827724 | 2.25E−12 | 28.00228827709 | 2.25E−12 | 28.00228827646 | |
| | | 1E−5 | 28.004576545 26 | 1.41E−11 | 28.00045765 5347 | 8.98E−12 | 28.00045765 5347 | 8.98E−12 | 28.00045765 5095 | |
| | | 5E−5 | 28.002288253339 | 3.53E−10 | 28.002288273860 | 2.24E−10 | 28.002882 73860 | 2.24E−10 | 28.002882675575 | |
| | | 1E−4 | 28.004576458452 | 1.41E−09 | 28.004576540536 | 8.98E−10 | 28.004576540536 | 8.98E−10 | 28.004576515396 | |
| | | 5E−4 | 28.022880363596 | 3.52E−08 | 28.022882415312 | 2.24E−08 | 28.022882415329 | 2.24E−08 | 28.022881786724 | |
| | | 1E−3 | 28.045755907335 | 1.41E−07 | 28.045764112201 | 8.97E−08 | 28.045764112342 | 8.97E−08 | 28.045761597478 | |
| | | 5E−3 | 28.228587100883 | 3.50E−06 | 28.228791824108 | 2.23E−06 | 28.228791841925 | 2.23E−06 | 28.228728882585 | |
| | | 1E−2 | 28.456694897827 | 1.39E−05 | 28.457511805978 | 8.86E−06 | 28.457511949455 | 8.86E−06 | 28.457259680513 | |
| | | 5E−2 | 30.264652314968 | 3.29E−04 | 30.284683540374 | 2.10E−04 | 30.284703885494 | 2.11E−04 | 30.278318327442 | |
| | | 1E−1 | 32.483931929728 | 1.23E−03 | 32.562346456954 | 7.90E−04 | 32.562342663839 | 7.95E−04 | 32.536480931004 | Computations with only |
| | | 2E−1 | 36.796754408665 | 4.35E−03 | 37.095636018735 | 2.80E−03 | 37.096779965614 | 2.83E−03 | 36.992010607447 | $R = 3$, $(M,S) = (0,0)$ |
| | | 3E−1 | 40.957264235247 | 8.73E−03 | 41.600348685342 | 5.61E−03 | 41.606138490195 | 5.75E−03 | 41.368445666447 | |
| | | 4E−1 | 44.981509722895 | 1.39E−02 | 46.08332192345 | 8.88E−03 | 46.08332192345 | 9.14E−02 | 45.670810879121 | |
| | | 5E−1 | 48.883234063775 | 1.96E−02 | 50.523563333035 | 1.24E−02 | 50.547077125322 | 1.28E−02 | 49.905865978617 | |
| | | 1E+0 | 66.912244170015 | 4.91E−02 | 72.328704286727 | 2.87E−02 | 72.496164786560 | 3.11E−02 | 70.312502175757 | |
| | | 2E+0 | 98.067797155616 | 9.65E−02 | 113.783719056084 | 4.38E−02 | 115.035696867396 | 5.53E−02 | 109.010808418516 | |
| | | 5E+0 | 290.237582802627 | 1.75E−01 | 220.906626259943 | 1.11E−01 | 213.42210272 4219 | 2.32E−02 | 218.48098056035 | |
| | | 1E+1 | 561.833857484633 | 2.22E−01 | 341.97101458 5657 | 1.40E−01 | −112.44472509 5687 | 1.28E+00 | 397.44324982 9703 | |
| | | 5E+1 | 1,178.795947280830 | 2.70E−01 | −1,275.834444440860 | 1.70E+00 | −1,256.930937457310 | 1.69E+00 | 1,823.60231338210 | |
| | | 1E+2 | 2,279.692075613080 | 2.77E−01 | −9,763.892682304570 | 3.71E+00 | −9,723.596126393260 | 3.70E+00 | 3,605.81335473020 | |

**Table 7.14:** Relative errors of several *ab initio* many-body techniques with respect to the full configuration interaction energy taken here as reference for the ground state energy of a 12-particle dot. From left to right, we give the approximated ground state and the relative error respectively for: the Hartree-Fock method, the Hartree-Fock method corrected by a $2^{nd}$ and $3^{rd}$-order correction in the HF basis, the energy given by many-body perturbation theory in the harmonic oscillator basis up to first, second and third order, and finally the configuration interaction energy with the parameters used to compute them.

## 7.5.4   Short comparison to the variational Monte Carlo method

We briefly compare our previous results with a few runs of the variational Monte Carlo (VMC) simulator developed by Rune Albrigtsen. The details of the simulations performed are given in appendix C. The idea is to compare (even for a few simulations) the approximated energy of VMC to the FCI ground state and to the other methods. Table 7.15 indicates that the energies computed with VMC are lower than the FCI ground state for quantum dots with 2, 6 and 12 electrons and with a confinement strength $\lambda = 1$.

These VMC calculations, as our Hartree-Fock implementation, use the closed-shell Slater determinant as an ansatz for the ground state. The lower energy obtained with VMC could be due to a breakdown of the method considering $\lambda = 1$ as a large interaction strength. However we have seen in section 7.2.2 that $\lambda = 1$ is still far from the breaking limit ($\lambda_{limit}^{2e^-} \geq 50$, $\lambda_{limit}^{6e^-} \geq 13$), and that increasing the model space of FCI usually increases this limit.

Therefore, FCI calculations should be run over a much larger space in order to decide the nature of the ground state and study the breaking of the VMC calculations according to the new "exact" energies.

|  | 2-electron QD energy ($\hbar\omega$) | 6-electron QD energy ($\hbar\omega$) | 12-electron QD energy ($\hbar\omega$) |
|---|---|---|---|
| Full CI | 3.013626 | 20.316754 | 70.312502 |
| VMC | 3.0025 $\pm 1.2\,10^{-4}$ | 20.1909 $\pm 3.6\,10^{-4}$ | 65.79 $\pm 1.9\,10^{-3}$ |
| HF | 3.16908 | 20.744840 | 66.912244 |
| HF+MBPT(HF)-$2^{nd}$order | 3.015743 | 20.337553 | 65.870798 |
| MBPT(HO)-$1^{st}$order | 3.253314 | 22.219812 | 73.765549 |
| MBPT(HO)-$2^{nd}$order | 3.022410 | 21.477290 | 72.328704 |

**Table 7.15:** Comparison of approximation to the ground state energy of quantum dots with $\lambda = 1$.

This short comparison with the VMC results let us think that some of our previous conclusions may be altered by the accuracy of the FCI calculations within a too small Hilbert space. If the FCI method in a very small space becomes less accurate than the Hartree-Fock method, and closer to the MBPT results, we would conclude wrongly that MBPT performs better than Hartree-Fock (which we may have done in section 7.5.2).

This shows the importance of the FCI accuracy with respect to the size of the model space.

# Chapter 8

# Conclusion

## 8.0.5 Critical discussion of the method and results

In this thesis we performed a computional study of a quantum dot in two dimensions where the electrons are trapped in a harmonic oscillator potential and repel each other with a Coulomb interaction. The main objective was to compare the efficiency and the limits of convergence/accuracy of several *ab-inito* many-body techniques to approximate the ground state energy of the quantum dot with respect to the confinement strength. For this purpose, we developed a simulator for computing the Hartree-Fock (HF) and many-body perturbation theory (MBPT) energies. The many-body perturbation corrections were implemented up to third order, however our results (section 7.5.3) showed that the third order never really improved the accuracy over the second order corrected energy.

The implemented model and the origin of the dimensionless confinement strength $\lambda$ are discussed in chapter 4, where $\lambda$ shows to be proportional to the natural oscillator length of the host semiconductor. However the confinement strength can also be modified by applying an external magnetic field which will squeeze the electrons in smaller regions of space. We derived the Hamiltonian of quantum dots in a magnetic field also in chapter 4 where we show that the interaction with the magnetic field can simply be reformulated as a new harmonic oscillator confinement potential with a modified oscillator frequency $\omega$, to which one should add a shift in energy due to the interaction of the magnetic field with the angular and spin parts of the system. For a typical quantum dot made of Gallium arsenide (GaAs), we show that the dimensionless confinement strength should vary in the range $\lambda \in [0, 1.6]$, decreasing as the magnetic field increases. However as the magnetic field increases, our simple model may fail since it does not take into account the modification in the physical length of the quantum dot when forcing the electrons to get closer to each other. It does also not include the modification in the type of interaction that models the repulsion between the electrons. From a computational point of view, it was interesting anyway to observe the behaviour of the various computational techniques for a bigger range of $\lambda$ ($\lambda \in [0, 100]$), and keeping our electron interaction in the form of a Coulomb repulsion.

If our model relies on an arbitrary form of the electron interaction, its implementation is also restricted to a closed-shell model in which the wave function of

the system is approximated by a unique Slater determinant. This closed-shell model implies that the particles of the system occupies all the shells up to the Fermi level. We made an attempt to study the limit of this model by neglecting the electron interactions. This is done in section 7.2.1 while observing the level crossing of the Fock-Darwin orbitals as a function of the magnetic field. It shows that the model actually breaks for $B = 2.1\,T$ (i.e. $\lambda = 1.54$ in GaAs) in a six-particles quantum dot and $B = 1.2\,T$ (i.e. $\lambda = 1.58$ in GaAs) in a twelve-particles quantum dot, giving some upper bound in magnetic field and lower bound in $\lambda$. Again this theoretical case completely neglects the effect of the repulsion between the electrons while the magnetic field increases, which should in reality results in a much lower limit for B, but in a non-trivial change in $\lambda$. As mentionned in 7.2.1 this range of magnetic field are easily achievable today in laboratories. Therefore the closed-shell model could not potentially be used to investigate any possible magnetic strength.

Anyway, introducing the electron interaction and sticking to the Coulomb interaction model, a numerical computation is clearly the only way to find an upper bound for $\lambda$ indicating the limit of the closed-shell model. The study was performed using full configuration interaction (FCI) on a six-electrons quantum dot (section 7.2.2). We observed a change in total angular momentum $M$ and total spin $S$ from $(0,0) \rightarrow (1,2)$ indicating a break of the closed-shell model for an increase of the confinement strength from $\lambda = 13$ to $\lambda = 15$. A similar study done for the two-electrons dot (section 7.5.3) shows a breakdown of the closed-shell model between $\lambda = 50$ and $\lambda = 100$. However these findings regarding the limitations of the shell model should be taken with great care, or as a preliminary study for a more accurate investigation, since our FCI calculations were performed in a very restricted Hilbert space. For example we noticed that for a six-electrons dot, FCI calculations indicate a breakdown between $\lambda = 5$ and $\lambda = 10$ for a maximum shell number $R = 4$ since the lowest ground states respectively correspond to $(M,S)_{\lambda=5}^{R=4} = (0,0)$ and $(M,S)_{\lambda=5}^{R=4} = (1,4)$. Therefore one might conclude (wrongly) that this marks the limit of the shell model. However the same calculations were done with a maximum shell number $R = 5$, the ground state obtained for the configuration indicates $(M,S)^{R=5} = (0,0) \leq (M,S)^{R=4} = (1,4)$, meaning that the closed-shell model is actually still valid for a six-electrons dot when $\lambda = 10$. Therefore restricting the Hilbert space too much in FCI calculations could lead to wrong interpretations. It also means that our current observations could lead to higher limits while running FCI simulations in a bigger model space.

After studying the limits of the shell model, it was interesting to know if the computational techniques would actually break or not before the shell model. Since Hartree-Fock theory, perturbation theory and combinations of these techniques are in essence lower approximations to the exact ground state than FCI, we also observed how fast the different methods will diverge from the FCI calculation taken here as reference with respect to the interaction strength $\lambda$ and the number of particles in the dot. The implementation of a simulator based on the Hartree-Fock method and many-body perturbation theory allowed us to investigate the approximated ground states for $\lambda = 0 \rightarrow 100$ and different sizes of our model space characterized by the maxmum shell number $R^b$. The results are summarized and analyzed in section( 7.5).

It shows that HF, MBPT and the combinations of these methods display an error growing quadratically with $\lambda$ when compared to the "exact" FCI energies. It also show some linear difference in the relative error between the methods themselves. For example, a two-electrons dot will be better approximated by HF+MBPT(HF)-$2^{nd}$order with a much smaller error than MBPT(HO)-$1^{st}$order (Results are summarized in table 7.8). Finally this linear difference in accuracy appears to change with the size of the dot, which indicates that the Hartree-Fock method becomes less accurate compared to many-body perturbation theory as the number of electrons in the dot increases.

### 8.0.6 Perspectives for future works

When investigating the performance of our simulator (section 7.3) we observed an exponential scaling of the method with respect to the size of the model space (given by $R^b$). More specifically the duration of the simulation and the complexity of the Hartree-Fock approach increase exponentially with the size of the basis. A first issue in the implementation was to optimize the resolution of the huge eigenvalue problem performed at each Hatree-Fock iteration. This has been done by splitting the huge matrix to diagonalize into much smaller matrices , making use of symmetry properties of the system, particularly due to invariance of the two-body interaction matrix with respect to the total angular momentum. Once this new implementation improved the efficiency, the second bottleneck occurs when computing the matrix elements of the same two-body interaction matrix. We saw that the parallelization of the code with MPI improves almost linearly the performance of the simulator with respect to the number of processors used (discussed in section 7.4). Moreover, the first interaction matrix computed in the harmonic oscillator basis can be computed once for all and reused for any simulation requiring the same basis size (i.e. same $R^b$), which saves already a lot of time before entering the Hartree-Fock algorithm itself. Our simulator includes this improvement and reads the matrix from file if it exists. However a new interaction matrix has to be computed at the end of Hartree-Fock calculation, and this depends on several input parameters. The construction of this second matrix is actually not optimized yet. However a way to do it would be to compute each matrix element using a center-of-mass transformation, as it is done in OPENFCI [32]. This would of course require the implementation of numerical integration whereas our simple simulator currently works within the energy basis, relying on nice properties of Harmonic oscillator orbitals. Once numerical integration is implemented, this will also allow us to compute the matrix elements in three-dimension and to change the shape of the confining potential.

We already discussed a lot about the limitation of the closed-shell model and how it might affect the reliability of our results. A more accurate comparison of the method should include FCI results with a much bigger model space, which could lead to an interesting study of the shell model break while plotting variational Monte-Carlo (VMC) results which exhibits much better accuracy than HF or MBPT. Of course a way to overcome the restriction due to the closed-shell model would be to implement an open-shell model. Despite the more complex implementation (mainly

combinatorics) for including the combinations of Slater determinants, it would be interesting to compare the efficiency and the convergence of an open-shell HF compared to our current closed-shell implementation. This would also give us many insights on the electronic structure responsible for this inaccuracy of the correlation effects.

Combining the techniques is usually a good tradeoff between convergence and accuracy. We did it for example by correcting the HF energy with a second order perturbation correction which improves the results, at least for small systems. We could either use the two-body interaction matrix computed in the basis set of Hartree-Fock orbitals as input of the FCI calculation, or use the FCI method to produce an effective interaction that would serve of starting point in our HF simulation instead of the bare Coulomb interaction computed in the harmonic oscillator basis.

### 8.0.7   Further extensions

This simple numerical study of quantum dots opens many questions on how to improve the performance of computational techniques, how the same problem scales with other techniques, and also how does it improves our understanding of quantum dots themselves. Therefore it would be interesting to compare approximations to the ground state of quantum dots with other techniques such as couple cluster (CC) theory or density functional theory (DFT).

Moreover, a time-dependent study of quantum dots would give us more information on their interaction with the environment which would be very instructive for improving their current applications in modern electronics or in biology.

# Appendix A

# Analytical expression of the two-body Coulomb interaction

This function computes the exchange part in the anti-symmetrized Coulomb matrix element $\langle \alpha\beta|V|\gamma\delta\rangle_{as} = \langle \alpha(\boldsymbol{r_i})\beta(\boldsymbol{r_j})|V(\boldsymbol{r_{ij}})|\gamma(\boldsymbol{r_i})\delta(\boldsymbol{r_j})\rangle_{as}$ where the $\alpha$, $\beta$, $\gamma$ and $\delta$ are four state indices and $\mathbf{r_i}$, $\mathbf{r_j}$ the positions of particle $i$ and $j$. Each state $|k\rangle$ can be rewritten in terms of its quantum numbers. In two dimensions, it reads $|k\rangle = |n_k m_k s_k\rangle$. For simplicity the angular momentum projection quantum number $m_l$ will just be written as $m$ in the following equations.

The complete anti-symmetrized Coulomb matrix element reads

$$\langle\alpha\beta|V|\gamma\delta\rangle_{as} = \underbrace{\langle\alpha\beta|V|\gamma\delta\rangle}_{\substack{\text{direct} \\ \text{term}}} - \underbrace{\langle\alpha\beta|V|\gamma\delta\rangle}_{\substack{\text{exchange} \\ \text{term}}}, \tag{A.1}$$

The exchange term $\langle\alpha\beta|V|\gamma\delta\rangle$ expands as follow

$$\langle\alpha\beta|V|\gamma\delta\rangle = \delta_{m_{s1},m_{s4}}\,\delta_{m_{s2},m_{s3}}\,\langle(n_1,m_1),(n_2,m_2)|V|(n_3,m_3),(n_4,m_4)\rangle \tag{A.2}$$

$$= \delta_{m_{s1},m_{s4}}\,\delta_{m_{s2},m_{s3}}\,V_{\alpha\beta\gamma\delta}, \tag{A.3}$$

where we separate the spin part from the spatial part $V_{\alpha\beta|V|\gamma\delta}$.

Note that in our simulator, the function `Anisimovas(n1,m1,n2,m2,n3,m3,n4,m4)` only computes $V_{1234}$ where the numbers $1 \rightarrow 4$ are state indices similar to $\alpha$, $\beta$, $\gamma$, $\delta$.

According to Anisimovas [3] (the detail of the derivation is also reviewed by Rontani [49]), the spatial part can be solved analytically when the basis set is built upon the single harmonic oscillator orbitals.

$$V_{1234} = \delta_{m_1+m_2,m_3+m_4} \sqrt{\left[ \prod_{i=1}^{4} \frac{n_i!}{(n_i + |m_i|!)} \right]}$$

$$\times \sum_{j_1=0,\ldots,j_4=0}^{n_1,\ldots,n_4} \left[ \frac{(-1)^{j_1+j_2+j_3+j_4}}{j_1!j_2!j_3!j_4!} \left[ \prod_{k=1}^{4} \binom{n_k + |m_k|}{n_k - j_k} \right] \frac{1}{2^{\frac{G+1}{2}}} \right.$$

$$\times \sum_{l_1=0,\ldots,l_4=0}^{\gamma_1=0,\ldots,\gamma_4=0} \left. \left( \delta_{l_1,l_2} \, \delta_{l_3,l_4} \, (-1)^{\gamma_2+\gamma_3-l_2-l_3} \left[ \prod_{t=1}^{4} \binom{\gamma_t}{l_t} \right] \Gamma\left(1 + \frac{\Lambda}{2}\right) \Gamma\left(\frac{G - \Lambda + 1}{2}\right) \right) \right],$$

$$\text{(A.4)}$$

where

$$\gamma_1 = j_1 + j_4 + \frac{|m_1| + m_1}{2} + \frac{|m_4| - m_4}{2},$$

$$\gamma_2 = j_2 + j_3 + \frac{|m_2| + m_2}{2} + \frac{|m_3| - m_3}{2},$$

$$\gamma_3 = j_3 + j_2 + \frac{|m_3| + m_3}{2} + \frac{|m_2| - m_2}{2},$$

$$\gamma_4 = j_4 + j_1 + \frac{|m_4| + m_4}{2} + \frac{|m_1| - m_1}{2},$$

$$G = \gamma_1 + \gamma_2 + \gamma_3 + \gamma_4,$$

$$\Lambda = l_1 + l_2 + l_3 + l_4.$$

As a note, our implementation of the function `Anisimovas(...)` which computes the spatial part of the exchange term, includes the following subfunctions:

- `minusPower(int k)` which computes $(-1)^k$,

- `LogFac(int n)` which computes $log_e(n!)$,

- `LogRatio1(int j_1,int j_2,int j_3,int j_4)` which computes the $log_e$ of $\frac{1}{j_1!j_2!j_3!j_4!}$,

- `LogRatio2(int G)` which computes the $log_e$ of $\frac{1}{2^{\frac{G+1}{2}}}$,

- `Product1 (int n_1,int m_1,int n_2,int m_2, int n_3,int m_3,int n_4,int m_4)` which computes the explicit (not the $log_e$) product $\sqrt{\left[ \prod_{i=1}^{4} \frac{n_i!}{(n_i+|m_i|!)} \right]}$,

- `LogProduct2(int n_1,int m_1,int n_2,int m_2, int n_3,int m_3,int n_4,int m_4, int j_1,int j_2,int j_3,int j_4 )` which computes the $log_e$ of $\prod_{k=1}^{4} \binom{n_k + |m_k|}{n_k - j_k}$,

- `LogProduct3(int l_1,int l_2,int l_3,int l_4, int \gamma_1,int \gamma_2,int \gamma_3,int \gamma_4)` which computes the $log_e$ of $\prod_{t=1}^{4} \binom{\gamma_t}{l_t}$,

- `lgamma(double x)` which computes the $log_e[\Gamma(x)]$.

# Appendix B

# The method of Lagrange Multipliers

In mathematical optimization, the method of Lagrange multipliers (named after Joseph Louis Lagrange) provides a strategy for finding the stationnary points of a function (and among them maxima/minima if the derivative of the function is defined for those points) subject to some constraints.

## B.0.8  General approach of the method

For example (see figure B.1), consider the following optimization problem:

- maximize the **functional** $f(x, y)$,

- subject to the **constraint** $g(x, y) = c$.

We introduce a new variable ($\lambda$) called a Lagrange multiplier, and study the **Lagrange function** (or *Lagrangian*) defined by

$$\Lambda(x, y, \lambda) = f(x, y) - \lambda \left( g(x, y) - c \right). \tag{B.1}$$

If $(x, y)$ is a maximum for the original constrained problem, then there exists a $\lambda$ such that $(x, y, \lambda)$ is a stationary point for the Lagrange function (stationary points are those points where the partial derivatives of $\Lambda$ are zero). However, not
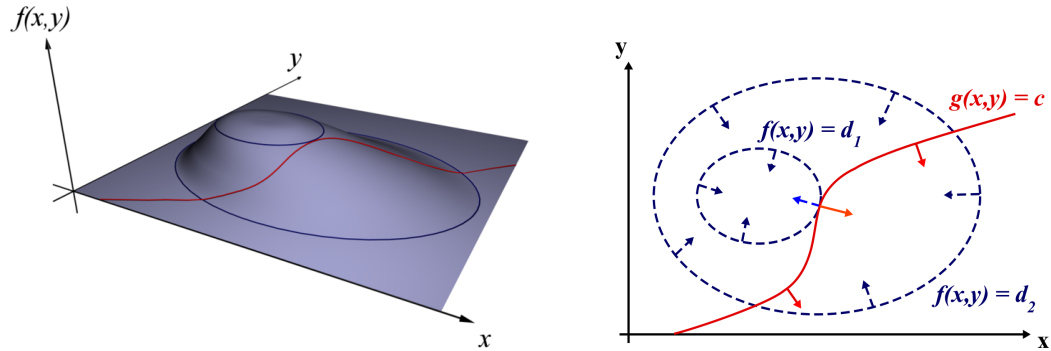


**Figure B.1:** Find $x$ and $y$ to maximize $f(x, y)$ subject to a constraint (shown in red) $g(x, y) = c$.
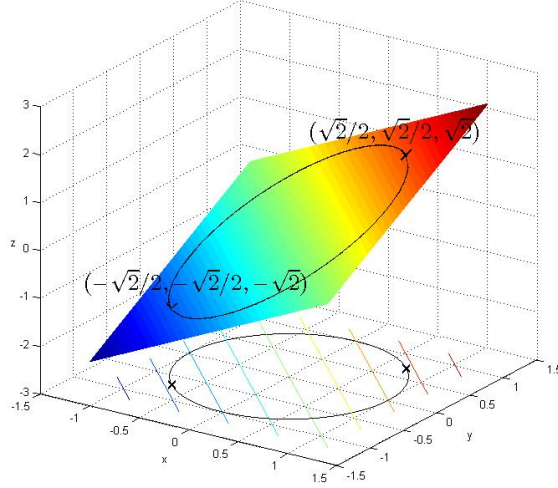
**Figure B.2:** Illustration of the constrained optimization problem.

all stationary points yield a solution of the original problem. Thus, the method of Lagrange multipliers yields a necessary condition for optimality in constrained problems.

## B.0.9   Example

Let's use the method for a simple example:

Suppose you wish to maximize $f(x, y) = x + y$ subject to the constraint $x^2 + y^2 = 1$. The constraint is the unit circle as shown on figure B.2, and the level sets of $f$ are diagonal lines (with slope $-1$), so one can see graphically that the maximum occurs at $(\sqrt{2}/2, \sqrt{2}/2)$ (and the minimum occurs at $(-\sqrt{2}/2, -\sqrt{2}/2)$)

Formally, we get from the constraint that $g(x, y) - c = x2 + y2 - 1$, and the Lagrange function reads

$$\Lambda(x, y, \lambda) = f(x, y) + \lambda(g(x, y) - c) = x + y + \lambda(x^2 + y^2 - 1). \qquad \text{(B.2)}$$

Set the derivative $\partial \Lambda = 0$, which yields the system of equations:

$$\begin{cases} \dfrac{\partial \Lambda}{\partial x} = 1 + 2\lambda x = 0, & \text{(i)} \\[2ex] \dfrac{\partial \Lambda}{\partial y} = 1 + 2\lambda y = 0, & \text{(ii)} \\[2ex] \dfrac{\partial \Lambda}{\partial \lambda} = x^2 + y^2 - 1 = 0, & \text{(iii)} \end{cases} \qquad \text{(B.3)}$$

As always, the $\partial \lambda$ equation is the original constraint.

Combining the first two equations yields $x = y$ (explicitly, $\lambda \neq 0$, otherwise $(i)$ yields $1 = 0$, so one has $x = -1/(2\lambda) = y$).

Substituting into $(iii)$ yields $2x^2 = 1$, so $x = \pm\sqrt{2}/2$ and the stationary points are $(\sqrt{2}/2, \sqrt{2}/2)$ and $(-\sqrt{2}/2, -\sqrt{2}/2)$. Evaluating the objective function $f$ on these yields $f(\sqrt{2}/2, \sqrt{2}/2) = \sqrt{2}$ and $f(-\sqrt{2}/2, -\sqrt{2}/2) = -\sqrt{2}$,

thus the maximum is $\sqrt{2}$, which is attained at $(\sqrt{2}/2, \sqrt{2}/2)$ and the minimum is $-\sqrt{2}$, which is attained at $(-\sqrt{2}/2, -\sqrt{2}/2)$.

# Appendix C

# Results of variational Monte-Carlo simulations

In order to produce the variational Monte Carlo energies for different quantum dots, we used the simulator developed by R. Albrigtsen detailled in his thesis [2]. The simulator is able to compute the energy of a system in two or three dimension of quantum dots modelled by an harmonic oscillator confining potential identical in two dimension to our potential. Several parameters can be tuned in order to get accurate results in a reasonnable amount of time, and it is possible to use an optimizer that will find the best input parameters ($\alpha$ and $\beta$) before launching the production run.

| Input parameters for optimization | | | | | Output parameters | | |
|---|---|---|---|---|---|---|---|
| nb. electrons | $\alpha_{\{xyz\}}$ | $\beta$ | nb. therma. cycles | nb. Monte Carlo cycles | nb. iterations | $\alpha_{\{xyz\}}$ | $\beta$ |
| 2 | 0.9 | 0.5 | $10^4$ | $10^4$ | 100 | 0.990855 | 0.403824 |
| 6 | 0.9 | 0.6 | $10^4$ | $10^4$ | 100 | 0.927269 | 0.565266 |
| 12 | 0.9 | 0.6 | $10^4$ | $10^4$ | 100 | 0.878028 | 0.653256 |

**Table C.1:** Results of the optimizaton of the VMC parameters for quantum dots with 2, 6 and 12 particles in two dimensions ($dt = 0.01$).

| Input parameters for production run | | | | | | Blocking param. | | Results | |
|---|---|---|---|---|---|---|---|---|---|
| nb. electrons | $\alpha_{\{xyz\}}$ | $\beta$ | nb. therma. cycles | nb. Monte Carlo cycles | nb. proc. | block size | block sample | Energy [a.u.] | $\sigma^2$ [a.u.] |
| 2 | 0.99086 | 0.40382 | $10^6$ | $10^7$ | 3 | 20000 | 5000 | 3.00025 | $\pm 1.2\,10^{-4}$ |
| 6 | 0.92727 | 0.56527 | $10^6$ | $10^7$ | 3 | 20000 | 5000 | 20.19099 | $\pm 1.2\,10^{-3}$ |
| 6 | 0.92727 | 0.56527 | $10^7$ | $10^8$ | 3 | 20000 | 5000 | 20.1909 | $\pm 3.6\,10^{-4}$ |
| 12 | 0.87803 | 0.65326 | $10^6$ | $10^7$ | 3 | 20000 | 5000 | 65.79 | $\pm 1.9\,10^{-3}$ |

**Table C.2:** Approximations to the ground state energy of quantum dots with 2, 6 and 12 particles using the variational Monte-Carlo method with $dt = 0.01$.

# Bibliography

[1] *Electron transport in quantum dots*, Proceedings of the Advanced Study Institute, 1997.

[2] R. Albrigtsen. Computational environment for many-electron systems. Master's thesis, University of Oslo, 2009.

[3] E. Anisimovas and A. Matulis. Energy spectra of few-electron quantum dots. *J. Phys.*, 10:601–615, 1998.

[4] G. Baardsen. Spin effects in circular quantum dots. Master's thesis, Helsinki University of Technology, 2009.

[5] B. H. Bransden and C. J. Joachain. *Physics of Atoms and Molecules; 2nd ed.* Prentice-Hall, Harlow, 2003.

[6] L. Brey, N. F. Johnson, and B. I. Halperin. Optical and magneto-optical absorption in parabolic quantum wells. *Phys. Rev. B*, 40:10647–10649, 1989.

[7] M. Bruchez, M. Moronne, P. Gin, S. Weiss, and P. A. Alivisatos. Semiconductor nanocrystals as fluorescent biological labels. *Science*, 281:2013–2016, 1998.

[8] W. C. W. Chan and S. Nie. Quantum dot bioconjugates for ultrasensitive nonisotopic detection. *Science*, 281:2016–2018, 1998.

[9] D. Chaney and P. A. Maksym. Size-dependent suppression of spin relaxation in electrostatic quantum dots. *Phys. Rev. B*, 75:035323, 2007.

[10] M. Ciorga, A. S. Sachrajda, P. Hawrylak, C. Gould, P. Zawadzki, S. Jullian, Y. Feng, and Z. Wasilewski. Addition spectrum of a lateral dot from coulomb and spin-blockade spectroscopy. *Phys. Rev. B*, 61:R16315–R16318, 2000.

[11] C. J. Cramer. *Essentials of computational chemistry : theories and models.* John Wiley & Sons, 2008.

[12] J. Dempsey, N. F. Johnson, L. Brey, and B. I. Halperin. Collective modes in quantum-dot arrays in magnetic fields. *Phys. Rev. B*, 42:11708–11713, 1990.

[13] P. J. Ellis and E. Osnes. An introductory guide to effective operators in nuclei. *Rev. Mod. Phys.*, 49:777–832, 1977.

[14] V. Fock. Bemerkung zur quantelung des harmonischen oszillators im magnetfeld. *Zeitschrift für Physik A Hadrons and Nuclei*, 47:446–448, 1928.

[15] X. Gao, Y. Cui, R. M. Levenson, L. W. Chung, and S. Nie. In vivo cancer targeting and imaging with semiconductor quantum dots. *Nat Biotech*, 22:969–976, 2004.

[16] D. Goldberg. What every computer scientist should know about floating-point arithmetic. *ACM Computing Surveys*, 23:5–48, 1991.

[17] M. B. Haider, J. L. Pitters, G. A. DiLabio, L. Livadaru, J. Y. Mutus, and R. A. Wolkow. Controlled coupling and occupation of silicon atomic quantum dots at room temperature. *Phys. Rev. Lett.*, 102:046805, 2009.

[18] W. A. Harrison. *Electronic Structure and the Properties of Solids: The Physics of the Chemical Bond*. Dover Publications, 1989.

[19] O. Heinonen, E. Gross, and E. Runge. *Many-Particle Theory*. Hilger, 1991.

[20] T. Heinzel. *Mesoscopic Electronics in Solid State Nanostructures*. Wiley-VCH, Weinheim, 2003.

[21] D. Heitmann. Far infrared spectroscopy of quantum-dots and antidot arrays. *Physica B*, 212:201 – 206, 1995. Proceedings of the Workshop on Novel Physics in Low-Dimensional Electron Systems.

[22] D. Heitmann and J. P. Kotthaus. The spectroscopy of quantum dot arrays. *Physics Today*, 46:56–63, 1993.

[23] A. Hoshino, K. ichi Hanaki, K. Suzuki, and K. Yamamoto. Applications of t-lymphoma labeled with fluorescent quantum dots to cell tracing markers in mouse body. *Biochemical and Biophysical Research Communications*, 314:46 – 53, 2004.

[24] N. Johnson and M. Payne. Exactly solvable model of interacting particles in a quantum dot. *Phys. Rev. Lett.*, 67:1157, 1991.

[25] N. Johnson and M. Reina. The accuracy of the hartree-fock approximation for quantum dots. *J. Phys.*, 4:623–628, 1992.

[26] K. Kalyanasundaram. Cleavage of water by visible-light irradiation of colloidal cds solutions; inhibition of photocorrosion by $ruo_2$. *Angewandte Chemie International Edition in English*, 20:987–988, 2003.

[27] W. Kohn. Cyclotron resonance and de haas-van alphen oscillations of an interacting electron gas. *Phys. Rev.*, 123:1242–1244, 1961.

[28] L. P. Kouwenhoven, D. G. Austing, and S. Tarucha. Few-electron quantum dots. *Reports on Progress in Physics*, 64:701–736, 2001.

[29] M. Kralj and K. Pavelic. Medicine on a small scale. *EMBO reports*, 4:1008âĂŞ1012, 2003.

[30] A. Kumar, S. Laux, and F. Stern. Electron states in a gaas quantum dot in a magnetic field. *Phys. Rev. B*, 42:5166–5175, 1990.

[31] W. Kutzelnigg. Diamagnetism in relativistic theory. *Phys. Rev. A*, 67:032109+, 2003.

[32] S. Kvaal. Open source fci code for quantum dots and effective interactions. *arXiv.org*, 2008.

[33] S. Kvaal. Openfci home page at: `http://folk.uio.no/simenkva/`, 2009.

[34] A. Kwasniowski and J. Adamowski. Effect of confinement potential shape on exchange interaction in coupled quantum dots. *J. Phys.*, 20:215208, 2008.

[35] C. S. Lent, P. D. Tougaw, W. Porod, and G. H. Bernstein. Quantum cellular automata. *Nanotechnology*, 4:49–57, 1993.

[36] Q. P. Li, K. Karraï, S. K. Yip, S. Das Sarma, and H. D. Drew. Electrodynamic response of a harmonic atom in an external magnetic field. *Phys. Rev. B*, 43:5151–5154, 1991.

[37] M. Macucci, K. Hess, and G. J. Iafrate. Electronic energy spectrum and the concept of capacitance in quantum dots. *Phys. Rev. B*, 48:17354–17363, 1993.

[38] M. Macucci, K. Hess, and G. J. Iafrate. Numerical simulation of shell-filling effects in circular quantum dots. *Phys. Rev. B*, 55:R4879–R4882, 1997.

[39] I. L. Medintz, T. H. Uyeda, E. R. Goldman, and H. Mattoussi. Quantum dot bioconjugates for imaging, labelling and sensing. *Nat Mater*, 4:435–446, 2005.

[40] Y. Meir, N. S. Wingreen, and P. A. Lee. Transport through a strongly interacting electron system: Theory of periodic conductance oscillations. *Phys. Rev. Lett.*, 66:3048–3051, 1991.

[41] P. Merlot. The code can be downloaded at: `http://folk.uio.no/patrime/src/master.php`, 2009.

[42] H. Mizuta, H.-O. Muller, K. Tsukagoshi, D. Williams, Z. Durrani, A. Irvine, G. Evans, S. Amakawa, K. Nakazato, and H. Ahmed. Nanoscale coulomb blockade memory and logic devices. *Nanotechnology*, 12:155–159, 2001.

[43] M. Moshinsky and Y. F. Smirnov. *The Harmonic Oscillator in Modern Physics: From Atoms to Quarks*. Taylor & Francis, 1996.

[44] F. M. Peeters. Magneto-optics in parabolic quantum dots. *Phys. Rev. B*, 42:1486–1487, 1990.

[45] D. Pfannkuche, V. Gudmundsson, and P. A. Maksym. Comparison of a hartree, a hartree-fock, and an exact treatment of quantum-dot helium. *Phys. Rev. B*, 47:2244–2250, 1993.

[46] S. Rahman. Applications of quantum dots in the biological sciences. Simula Research Laboratory, Lysaker, Norway, 2008.

[47] S. Raimes. *Many-electron Theory*. North-Holland Publishing, 1972.

[48] S. M. Reimann and M. Manninen. Electronic structure of quantum dots. *Rev. Mod. Phys.*, 74:1283–1342, 2002.

[49] M. Rontani. *Electronic States in Semiconductor Quantum Dots*. PhD thesis, Universita degli Studi di Modena e Reggio Emilia, 1999.

[50] R. Rossetti, S. Nakahara, and L. E. Brus. Quantum size effects in the redox potentials, resonance raman spectra, and electronic spectra of cds crystallites in aqueous solution. *J. Phys. Chem.*, 79:1086–1088, 1983.

[51] C. Sikorski and U. Merkt. Spectroscopy of electronic states in insb quantum dots. *Phys. Rev. Lett.*, 62:2164–2167, 1989.

[52] H. Soo Choi, W. Liu, P. Misra, E. Tanaka, J. P. Zimmer, B. Itty Ipe, M. G. Bawendi, and J. V. Frangioni. Renal clearance of quantum dots. *Nat Biotech*, 25:1165–1170, 2007.

[53] M. Stopa. Quantum dot self-consistent electronic structure and the coulomb blockade. *Phys. Rev. B*, 54:13767–13783, 1996.

[54] M. Taut. Two electrons in an external oscillator potential: Particular analytic solutions of a coulomb correlation problem. *Phys. Rev. A*, 48:3561–3566, 1993.

[55] M. Taut. Two electrons in a homogeneous magnetic field: particular analytical solutions. *J. Phys. A*, 27:1045–1055, 1994.

[56] M. B. Tavernier, E. Anisimovas, F. M. Peeters, B. Szafran, J. Adamowski, and S. Bednarek. Four-electron quantum dot in a magnetic field. *Phys. Rev. B*, 68:205305, 2003.

[57] J. Thijssen. *Computational Physics*. Cambridge University Press, Cambridge, UK, 2007.

[58] E. B. Voura1, J. K Jaiswal1, H. Mattoussi, and S. M. Simon. Tracking metastatic tumor cell extravasation with quantum dot nanocrystals and fluorescence emission-scanning microscopy. *Nature Medicine*, 10:993 – 998, 2004.

[59] E. Waltersson and E. Lindroth. Many-body perturbation theory calculations on circular quantum dots. *Phys. Rev. B*, 76:045314, 2007.

[60] C. Weisbuch and H. Benisty. Overview of fundamentals and applications of electrons, excitons and photons in confined structures. *Journal of Luminescence*, 85:271 – 293, 2000.

[61] H. Weller, H. M. Schmidt, U. Koch, and A. Fojtik. Photochemistry of colloidal semiconductors. onset of light absorption as a function of size of extremely small cds particles. *Chem. Phys. Lett.*, 124:557–560, 1986.

[62] R. K. Willardson and A. C. Beer. *Semiconductors and semimetals*. Academic Press, 1971.

[63] J. O. Winter. *Development and optimization of quantum dot-neuron interfaces.* PhD thesis, The University of Texas at Austin, 2004.

[64] S. K. Yip. Magneto-optical absorption by electrons in the presence of parabolic confinement potentials. *Phys. Rev. B*, 43:1707–1718, 1991.